



HAL
open science

Theoretical study of fluid adsorption in porous materials

Chongzhi Qiao

► **To cite this version:**

Chongzhi Qiao. Theoretical study of fluid adsorption in porous materials. Material chemistry. Université de Lyon; East China University of science and technology (Shanghai, Chine), 2019. English. NNT : 2019LYSEN051 . tel-02445898

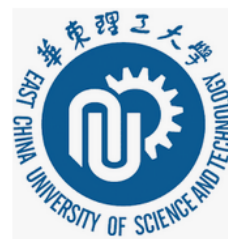
HAL Id: tel-02445898

<https://theses.hal.science/tel-02445898>

Submitted on 20 Jan 2020

HAL is a multi-disciplinary open access archive for the deposit and dissemination of scientific research documents, whether they are published or not. The documents may come from teaching and research institutions in France or abroad, or from public or private research centers.

L'archive ouverte pluridisciplinaire **HAL**, est destinée au dépôt et à la diffusion de documents scientifiques de niveau recherche, publiés ou non, émanant des établissements d'enseignement et de recherche français ou étrangers, des laboratoires publics ou privés.



Numéro National de Thèse : 2019LYSEN051

THESE de DOCTORAT DE L'UNIVERSITE DE LYON

opérée par

l'Ecole Normale Supérieure de Lyon

en cotutelle avec

l'East China University of Science and Technology

Ecole Doctorale N° 206

Ecole Doctorale de Chimie (Chimie, procédés, environnement)

Spécialité de doctorat : Chimie Théorique

Discipline : Chimie

Soutenue publiquement le 20/10/2019, par :

Chongzhi QIAO

Theoretical study of fluid adsorption in porous materials

Etude théorique de l'adsorption de fluide dans des matériaux poreux

Sous la direction de :

Pr. Wei DONG	ENS de Lyon	Directeur de thèse
Pr. Shuangliang ZHAO	East China University of Science and Technology	Co-tuteur de thèse

Devant le jury composé de :

Myroslav HOLOVKO	Directeur de recherche National Academy of Sciences of Ukraine	Rapporteur
Xiaosong CHEN	Professeur des universités Beijing Normal University	Rapporteur
Jacques MERCADIER	Professeur des universités Université de Pau et des Pays de l'Adour	Examineur
Jing XU	Professeure des universités East China University of Science and Technology	Examinatrice
Yuanhui JI	Professeure des universités Southeast University	Examinatrice
Honglai LIU	Professeur des universités East China University of Science and Technology	Examineur
Wei DONG	Directeur de Recherche CNRS ENS de Lyon	Directeur de thèse

分类号: 064 密级: _____

U D C: _____

华东理工大学

学位论文

多孔材料中流体热力学性质的理论研究

乔 崇 智

指导教师姓名: 赵双良 教授 华东理工大学

Wei DONG 教授 法国里昂高师

申请学位级别: 博士 专业名称: 化学工程

论文定稿日期: 2019.09.04 论文答辩日期: 2019.10.20

学位授予单位: 华东理工大学

学位授予日期: _____

答辩委员会主席: 陈晓松 教授

评 阅 人: 路小华 教授

张现仁 教授

吉远辉 教授

陈晓松 教授

刘洪来 教授

作 者 声 明

我郑重声明：本人恪守学术道德，崇尚严谨学风。所呈交的学位论文，是本人在导师的指导下，独立进行研究工作所取得的结果。除文中明确注明和引用的内容外，本论文不包含任何他人已经发表或撰写过的内容。论文为本人亲自撰写，并对所写内容负责。

论文作者签名：

年 月 日

Acknowledgement

First, I would like to express my sincere appreciation to those who have contributed to this thesis and supported me during my five-year Ph.D. journey. This thesis cannot be done without accompany and support from these nice people.

I would like to express the extremely appreciation to my two supervisors, Prof. Wei Dong of Ecole Normale Supérieure de Lyon (ENS-Lyon, France) and Prof. Shuangliang Zhao of East China University of Science and Technology (ECUST, China). I am deeply grateful to Prof. Wei Dong, who led me to the field of statistical thermodynamics. He gave me many useful suggestions not only about research but also about my daily life, and future career. I have been greatly benefited from his wide knowledge, physical intuition, and keen analytical ability. As a foreign student in France, I also appreciate his care during my stay in Lyon. I feel lucky that I have been Wei's student. I would also like to express my gratitude to my supervisor, Prof. Shuangliang Zhao, for his same firm support, insightful guidance, and earnest help.

I would like to thank Prof. Vincent Krakoviack and Prof. Ralf Everaers for their helpful discussion; David, Carine, and Ivan for their warmhearted help; Emmanuelle, Sigismund, Rodrigo, Elsheref, Santos, and Ruben for the accompany as my office roommates; Tao and Christian for solving computer problem; Edwige, Marie-Francoise, and Damien for the administrative affairs of the lab; and all the members in Laboratoire de Chimie, ENS-Lyon. I would like take this opportunity to thank my friends in Lyon, Zheng Zheng, Dawei Zhang, Tao Wang, Qingyi Gu, Ling Zhang, Junqing Gong, Xinnan Lu, Chen-hui Chan, and Xin Zhu, et al. Merci pour tout.

I would also like to express my sincere gratitude to Prof. Honglai Liu for giving me the chance to study in ECUST as a Ph.D. student. I would also like to thank Cheng Lian, Xiaochen Yu, Cheng Cai, Jiawei Zhang, Bingxu Chen, and Xiejun Xu for their help both in my daily life and research. I would also like to acknowledge all the members in Interface and Thermodynamics group, ECUST. By the way, I would like to

thank my friends, Xuezheng Zhao, Kaihang Shi, Zhengrui Li, Yuxiao Zhang, Hengbo Lv, Enyang Wang, and Lin Yu.

I would like to thank my Ph. D. committee members, Prof. Myroslav Holovko, Prof. Xiaosong Chen Prof. Jacques Mercadier, Prof. Jing Xu, Prof. Yuanhui Ji, and Prof. Honglai Liu for their contributions. Their discussion, ideas, and feedback have been absolutely invaluable.

I would also like to acknowledge to Campus France for an Eiffel scholarship, to Région Rhône-Alpes (France) for a CMIRA scholarship, and to the Chinese Scholarship Council for the visiting fellowship.

In the final place, I would like to thank my parents, Liang Qiao and Yan Wang, my uncle Si Wang, Limin Sun, and my aunt Kui Chen for their moral support.

In memory of my dearest grandparents, Yinghua Wang and Huijun Zhou.

Abstract

Porous materials are strategically important in chemical engineering, e.g., sustainable developments based on new clean energies, capturing Greenhouse gas, etc. The development and application of porous materials involve studies of the thermodynamics and dynamics of fluids in porous materials. In last decades, plenty of experimental and theoretical studies have been reported. However, due to the variety of porous materials, and thermodynamic properties of confined fluid are affected by so many materials and fluid properties, e.g., pore size distribution, pore connectivity, etc., studies are still on a case-by-case way. The case-by-case study is hard to offer neither the control variables of confined fluid nor the common relation among the different confined fluids. The development of thermodynamic theories that can accurately describe the thermodynamic properties of confined fluids becomes more and more important. This thesis investigates the relation between confined fluid and the corresponding bulk fluid, interfacial properties of fluids at a curved surface, the general equation of state for confined fluids, and quench effect. This thesis is composed of following several parts:

(1) With the help of scaled particle theory (SPT) and molecular simulation, we studied the thermodynamic properties of the confined fluid, e.g., pressure, chemical potential. A general scale relation has been found, which links the chemical potential, free energy density, and the pressure, from the confined fluids to that of the fluid in the homogeneous phase. This scale relation shows that the difference in thermodynamic properties between a confined fluid and a homogeneous fluid can be described solely by the porosity, the excess adsorption amount. The intrinsic relation between scaling relation and Gibbs adsorption theory is also revealed. This scaling relation provides a new method to measure the thermodynamic properties of confined fluid that are experimentally difficult to measure directly.

(2) By introducing a higher order curvature term into the SPT theory, we have developed a new, fully analytical approach called ASPT (augmented scaled particle theory). ASPT significantly improves the accuracy of SPT and gives excellent results for both the homogeneous phase and the surface tension of fluids at a spherical surface.

(3) Although morphological thermodynamics is supposed to be a general approach for studying confined fluids, it has never been tested in complicated systems, such as

fluids in porous materials. We proposed an equation of state based on morphological thermodynamics for fluids confined in various situations. It turns out that this approach makes it possible to obtain excellent results for the thermodynamics of these confined fluids.

(4) The size of a medium is described by the chemical potential to insert a new particle. Using SPT theory and Monte-Carlo simulations, we have demonstrated that a quench-annealed system is more congested than a system without such disorders (e.g., binary mixture).

With the help of theoretical study and molecular simulation, this thesis studies the thermodynamic properties of confined fluids, clarifies the control variables of confined fluids, and discovers the common law of thermodynamics properties among different confined fluids. A scaling relation and two new equations of state were reported, they will deepen the understanding of confined fluid, and will advance the development of the thermodynamics for confined fluids.

Keywords: confined fluids; porous materials; statistical thermodynamics; adsorption; morphological thermodynamics

Résumé

Les matériaux poreux ont une importance stratégique dans de nombreux domaines, par exemple, des développements durables basés sur de nouvelles énergies propres, des capteurs des gaz à effet de serre. Le développement et l'application de matériaux poreux impliquent des études sur la thermodynamique et la dynamique des fluides adsorbés dans des matériaux poreux. Au cours des dernières décennies, de nombreuses études expérimentales et théoriques ont été effectuées. Cependant, en raison de la diversité des matériaux poreux, les propriétés thermodynamiques des fluides confinés peuvent être affectées par de nombreux paramètres caractérisant les matériaux poreux, tels que la distribution de la taille des pores, la connectivité des pores, les interactions fluide-matériau, etc. Jusqu'à présent, les études théoriques des fluides confinés ont été menées au cas par cas. Cette situation ne permet pas de voir clairement les caractéristiques communes des fluides confinés, encore moins les éventuels liens entre les fluides confinés et ceux en phase homogène. Lors de cette thèse, nous avons mené des études sur les quatre problèmes suivants :

(1) Nous avons étudié les propriétés thermodynamiques (potentiel chimique et la pression) d'un nombre important de fluides confinés dans divers milieux poreux. Une relation d'échelle générale a été trouvée, qui relie le potentiel chimique ainsi que la pression, des fluides confinés au celui du fluide en phase homogène. Cette relation d'échelle montre que la différence de propriétés thermodynamiques entre un fluide confiné et un fluide homogène peut être décrite uniquement par la porosité, la quantité d'adsorption en excès. Cette relation d'échelle a avancé significativement notre compréhension de la thermodynamique des fluides confinés et ouvre des perspectives très intéressantes pour déterminer les propriétés thermodynamiques de fluides confinés à partir des celles des fluides homogènes.

(2) En introduisant un terme de courbure d'ordre supérieur dans la théorie SPT, nous avons développé une nouvelle approche totalement analytique, baptisée ASPT (augmented scaled particle theory). ASPT améliore significativement la précision de la SPT et donne des excellents résultats à la fois pour la phase homogène et pour les la tension superficielle au voisinage d'une surface sphérique.

(3) Bien que la thermodynamique morphologique est sensée d'être une approche générale pour traiter des systèmes hétérogène dans lesquels une interface morphologiquement compliquée est présente, elle n'a jamais été testée dans des systèmes compliqués, comme par exemple des fluides confinés en milieux poreux.

Nous avons mis au point une approche basée sur la thermodynamique morphologique pour des fluides confinés dans de diverses situations. Il s'avère que cette approche permet d'obtenir d'excellents résultats pour la thermodynamique de ces fluides confinés.

(4) L'encombrement d'un milieu est décrit par le potentiel chimique pour insérer une nouvelle particule. A l'aide de la théorie SPT et des simulations Monte-Carlo, nous avons démontré que un système avec des désordres figés (« quench-annealed » système) est plus encombré qu'un système sans tels désordres (par exemple, mélange binaire).

À travers les études décrites ci-dessus, nous avons réussi, à la fois, à développer certaines nouvelles méthodes théoriques pour des fluides confinés et à apporter des nouveaux éléments de réponse à quelques questions fondamentales qui étaient ouvertes auparavant.

Mots clés: fluides confinés; matériaux poreux; thermodynamique statistique; adsorption; thermodynamique morphologique

摘要

多孔材料在化学工程多个领域有着重要应用，如新能源电极材料，温室气体的捕集，混合物分离与提纯，高效催化，传感器设计等。多孔材料的开发与应用涉及到流体在多孔材料中的热力学与动力学性质研究。在过去几十年中，针对受限流体的性质开展了大量实验和理论研究工作。但由于多孔材料种类丰富，受限流体性质还受孔径大小、孔隙率、流体与材料的相互作用、流体密度、温度、压强等诸多因素影响，且这些因素之间往往还相互关联，因此统计力学方法如分子模拟、经典密度泛函理论等常常只能对受限流体性质进行逐案分析 (case-by-case study)。这种逐案分析既难以给出某类受限流体性质的关键调控变量从而提供调控思路，也不能分析不同受限流体热力学性质之间的关联及共同规律。基于此，面向受限流体的普适规律研究，发展能够准确描述受限流体性质的热力学理论显得日益迫切。本论文围绕受限流体与体相流体关联，流体在弯曲表面的界面性质，普适受限流体状态方程和冻结效应的影响开展了研究，主要内容包括以下几方面：

(1) 以受限流体的化学势，压强等热力学性质为对象，通过结合定标粒子理论 (Scaled Particle Theory, SPT) 和分子模拟，研究了受限流体与体相流体直接的关联。发现了一个普适的对应态原理，表明仅使用孔隙率，过剩吸附量和与之平衡的均相流体压强即可描述受限流体与均相流体热力学性质的区别。揭示了与吉布斯吸附理论的内在关系。该发现加深了对受限流体的理解，也为实验提供了测量难以直接测量的受限流体热力学性质的新方法。

(2) 以探究流体在弯曲表面的界面性质为目标，通过结合形态热力学 (Morphological Thermodynamics) 与研究均相流体的 SPT，提出了一个改进的 SPT 理论。该理论首次将 SPT 与形态热力学相结合，通过引入高阶曲率项的方法给出了更为精确的描述流体在球形表面界面张力的表达式，该表达式具有相比于现有理论更高的精度及简洁的表达式。同时，也给出了具有高精度的描述均相流体的状态方程。将加深对于流体在弯曲表面界面性质的理解。

(3) 以构建适用于不同受限流体的普适状态方程为目标，通过结合形态热力学与 SPT，探究了影响受限流体热力学的变量。通过将多孔材料的孔隙率，表

面积和两个曲率项作为关键变量，以化学势为自变量，提出了第一个不依赖于多孔材料结构的受限流体状态方程，其结果在不同条件下均与分子模拟相符。为工业中分析流体状态提供了理论基础。

(4) 流体进入多孔材料的阻力跟其化学势相关，通过 SPT 和分子模拟研究了流体密度，孔隙率等受限条件对化学势的影响。结果表明降低孔隙率，提高流体密度及增大固液界面，均会导致化学势增加，即流体阻力的增大。为工业应用中减小流体阻力提供了思路。

本文通过理论研究和分子模拟的结合，分析了受限流体的热力学性质，明确了调控受限流体的关键变量，发现了不同受限流体热力学性质之间的共同规律，基于此，提出了一个对应态原理和两个状态方程，加深了对于受限流体的理解，将推动受限流体热力学的发展。

关键字：受限流体，多孔材料，统计热力学，吸附，形态热力学

Contents

Acknowledgement	I
Abstract	III
Résumé.....	V
摘 要.....	VII
1. Introduction.....	1
1.1 Porous material and its application	1
1.2 Experimental study on porous material.....	3
1.3 Theoretical Model	4
A. Models of the pair potential	5
B. Models of porous material.....	6
1.4 Theoretical approach	10
A. SPT for confined fluid.....	10
B. Morphological thermodynamics	12
C. Other theoretical approaches.....	14
1.5 Simulation method	15
1.6 Current problem and the objective of the present work	16
2. A confinement-adsorption scaling relation	19
2.1 Introduction	19
2.2 Model and method.....	20
A. Model	20
B. Method	22
C. Conditions of considered systems	23
2.3 Results and discussion.....	27
2.4 Conclusion.....	34
3. Development of augmented scaled particle theory	37
3.1 Introduction	37

3.2 Original SPT.....	39
3.3 Augmented SPT.....	42
A. Single-point matching formulation	42
B. Double-point matching formulation.....	47
3.4 Results and discussion.....	53
A. Determination of the adjustable parameter in ASPT1	53
B. Pressure.....	54
C. Surface tension.....	56
D. Non-Hadwiger coefficient	62
E. Multi-component system	63
3.5 Concluding remarks	64
4. A general equation of state for confined fluid: morphological thermodynamics.....	67
4.1 Introduction	67
4.2 Theory	69
A. A brief introduction of Morphological thermodynamics	69
B. A new general equation of state.....	72
4.3 Results and discussion.....	74
A. Madden Glandt disorder porous medium	74
B. Hard sponge disordered porous medium.....	76
C. Ordered porous medium.....	79
D. Slit pore system.....	80
4.4 Concluding remarks	86
5. Quench effect on the chemical potential.....	87
5.1 Introduction	87
5.2 Model and methods	88
A. Model	88
B. Theory	89
C. Application of scaled particle theory.....	90

D. Simulation	92
5.3 Results and discussion.....	93
A. Strictly vanishing quench effect.....	93
B. Small quench effect.....	97
C. Turning point for the change from small to large quench effects.....	99
D. Strong quench effect	101
5.4 Concluding remarks	105
6. Final remarks	107
Appendix A. Some results for other versions of ASPT1	113
A.1. Single-point matching formulation with $n = 1$	113
A.2. Single-point matching formulation with $n = 2$	117
Appendix B. Invalidation of morphological thermodynamics	123
B.1. Fluid around two spherical solutes	123
B.2 Non-Hadwiger term.....	124
A. A brief review of Hansen-Goos' work	124
B. Non-Hadwiger coefficient in convex system.....	127
Appendix C. The summary of dissertation in Chinese	131
Appendix D. Publication during the doctoral study.....	141
Bibliography	143

1. Introduction

1.1 Porous material and its application

High-performance functionalized materials have strategic importance for many societal issues, e.g., sustainable developments based on new clean energies. Hydrogen is one of possible future clean energies. Scientific research has been actively undertaken to find a viable material for hydrogen storage ¹. In the late 1990s, carbon nanotubes generated excitement for hydrogen storage while it turned out later that they do not attain the viable adsorption capacity, (more than 6% of the system's total weight). Currently, the searching of such a storage system is directed toward new synthetic porous materials. ²

Besides fluid storage, porous materials also have many other important applications. Various zeolites have been used as molecular sieves and catalysts. Due to the specific pore size and topology, high selectivity is imparted to the zeolite-based catalysts. Such selectivity is extensively exploited in various chemical processes, e.g., catalytic cracking in the oil industry. When chiral building blocks are used for elaborating porous materials, the selectivity can be pushed to a higher level and thus enantioselective porous materials have been synthesized³, which can have important applications in pharmaceutical industry.

Now, material engineering allows for bestowing various interesting properties on porous materials. For example, magnetic porous materials have been synthesized ⁴ and some can have the transition temperature well above room temperature⁵. One attractive feature offered by the porous magnetic materials is their module ability. On one hand, the magnetic property can be modulated by choosing the appropriate building blocks for the synthesis. On the other hand, it can also be tuned, even after the materials being fabricated, by guest molecules adsorbed in the pores⁶. There is also considerable interest in the optical properties of some porous materials on account of their tunability and the possibility to incorporate a wide range of metal ions and organic ligand chromophores.

Such materials are of potential application as phosphors or fluorescent probes, particularly in chemical sensors⁷. Another very interesting example is aerogel. Aerogels are synthesized by using a gas to replace the liquid in the pores of gel. Aerogels have many interesting properties, such as very large surface area, low density, large porosity, and very low thermal conductivity. Thus, the aerogel is an ideal thermal insulation material and has a potential application in aeronautics and astronautics.⁸⁻¹⁰ Due to the large porosity and the very large surface area, aerogels are also widely used in catalysis.¹¹⁻¹³ The aerogel is a typically random porous material. With the development of synthesis technique, the ordered porous material such as Metal-organic frameworks (MOFs) and Zeolite imidazolate frameworks (ZIFs) have attracted more and more attention in both fundamental study and industry applications. For instance, MOFs is a coordination compound with a three-dimensional pore structure: organic struts link metal-containing clusters. MOFs were first synthesized in the late 1990s. Young¹⁴, Fujita¹⁵, Venkataraman¹⁶ reported the applications of MOFs in catalysis of coordination polymers and gas adsorption. MOFs have many attractive properties i.e., low density, high solid-liquid interface area, and the controllable functionality.¹⁷⁻¹⁹ The most interesting property of MOF is its flexibility.²⁰⁻²² Normally, the supramolecular host-guest interaction leads to the flexibility of porous material. However, recent study found that the framework flexibility is also presented without the guest molecule and the phenomenon of adsorption or desorption. The framework flexibility of MOFs may be caused by some external stimulus in general (by guests and external force fields i.e., mechanical stress, photoresponse, thermoresponsivity, host-guest interaction, electrical and magnetic interaction). Due to the framework flexibility of MOFs, it has potential application in many industrial fields, such as gas separation, biomedical application, catalysis, and sensor. The MOFs sensor is based on the framework flexibility can cause a reversible color change. For instance, DUT-8(Ni) changes its color from yellow to green during the adsorption of CO₂, *n*-butane, N₂, etc.²³ Another example is based on the host-guest interactions, Yanai et al. were proposed that the composite material

DSB@[Zn₂(bdc)₂dabco]_n (DSB – distyrylbenzene) can be used to detect CO₂ and C₂H₂.²⁴

Another very important application of porous materials is controlled releasing process of drugs.^{25,26} Considerable efforts devoted to developing methods for controlled drug-release to satisfy the ever-increasing demand for prolonged and better control of drug administration. The capability of continuous drug delivery over a specific period can assure an optimized therapeutic efficiency and a better patient's comfort for various chronic diseases, e.g., diabetes, cancers, AIDS, etc. A long release time requires a large capacity to store drug molecules. The controlled delivery necessitates some adaptability of the porous materials according to the drug content inside. New hybrid flexible porous materials opened some attractive perspectives for controlled drug delivery.

Above examples showed the strategic roles played by porous materials in a large variety of domains ranging from catalysis, separation, sensor technology to the pharmaceutical industry. It is estimated that porous solids represent more than 20% of the Gross Domestic Product of the industrial countries for the applications they imply directly or indirectly.²⁷

1.2 Experimental study on porous material

Since the porous materials have been used in many new areas, more precise control over the pore geometric properties is required. The templating-fabrication strategy is the most popular technique for control the pore size distribution and creates a variety of porous networks with a wide range of pore sizes from the micropore to macropore.^{28–33} In this method, Organic-bases molecules, polymer, and emulsion are normally considered as template species. The template species will be removed by heat treatment (soft template), acid or alkali solution (hard template) than the controllable pore scales can match the needs of different applications. Templating-fabrication strategy has widely used to synthesize ordered microporous material, such as MCM-48 and SBA-16, ordered mesoporous materials like MCM-41. Those materials are widely considered

as catalysis, sensor, and capacitor. Another very interesting new synthesis technique is Pekala's method. In this method, a gas replaced the liquid in the pores of gel. Hence, aerogels have a network structure of interconnected nanosized primary particles and have a wide range pore size from micropores, which are related to the intra-particle structure, to macropores, which are produced by the inter-particle structure. Those two synthesis methods introduce how to control the pore structure, now, how to characterize the pore structure of random porous material will be introduced.

To characterize and reconstruct the morphologies of porous material, the statistical geometric properties obtained from two-dimensional images of microstructure, i.e. porosity, interfacial surface area, and the two-point correlation function are widely used.³⁴ More recently the chord length distribution³⁵ has been employed in the generation of 3D microstructural models.^{36,37} These methods have been very instructive in understanding the general properties of complex media, however, direct prediction of transport properties^{38,39} from reconstructed samples have been in only fair agreement with experimental data. These standard methods base characterization and reconstruction primarily on geometrical information; there is no attempt to match the genesis of the material. Understanding how morphologies of porous material influence the properties of fluids in the porous material is important not only for a fundamental point of view but also for conceiving innovative and sustainable industrial processes. Unfortunately, some thermodynamic properties of fluid in porous material still can not be obtained from the experiment, such as pressure and the free energy of the confined fluid. Hence, the theoretical study of the properties of fluids in porous material is still needed. In next section, some theoretical models will be introduced.

1.3 Theoretical Model

Although a large literature exists on the study of confined fluids by both experimental and theoretical methods.⁴⁰⁻¹⁷⁵ Today, we do not have yet a precise idea about the respective roles played by pore-connectivity, pore-size distribution, the

morphologies of pore space, or quench disorder. The confined fluid particles feel not only the interaction with other fluid particles but also from solid ones. The interaction between fluid particles and porous materials can also make the confined fluid behave very differently from the bulk one. In this section, the models of pair potential and the models for porous material are introduced.

A. Models of the pair potential

Generally, the pair potential can be divided into two parts, the short-range repulsive part, which is derived from the overlap of outer electron shells, and the long-range attractive part, which comes from the spontaneous fluctuations of the electronic charge distribution. Due to the harsh repulsive part built the short-range order of fluid, which lead to the structure of fluid, the repulsive part is the most important property of the fluid. Hence, the first interaction model only considered the repulsion between fluid particles and the attraction is ignored, which is hard sphere potential. The pair potential, $v(r)$, of hard sphere model is

$$v(r) = \begin{cases} \infty, & r < \sigma \\ 0, & r \geq \sigma \end{cases}, \quad (1.1)$$

where σ is the diameter of the fluid particle, and r is the distance between two fluid particles. Since only the repulsive part is considered in this model, which means the fluid only has one fluid phase, the vapor-liquid phase transition cannot be found in hard sphere fluid. And the freezing transition can be found in hard sphere fluid at high fluid density, $\rho\sigma^3 \approx 0.945$. If the diameter, d , is equal to zero, the ideal gas model is obtained. In ideal gas model, the pair interaction is ignored, this model can be used to study the dilute system. Although this model is very simple, it still can offer many important features of confined fluid, as presented by Dong.¹⁷³ A simple pair potential model that can be used to describe the vapor-liquid phase transition can be proposed based on hard sphere model with an additional attraction, named square-well potential,

$$v(r) = \begin{cases} \infty, & r < \sigma \\ \varepsilon, & \sigma \leq r < d, \\ 0 & r \geq d \end{cases} \quad (1.2)$$

where ε is the depth of the well, and d is the width of the well. Since the attractive part is from the spontaneous fluctuation, which means it should have a very smooth form. The Lennard-Jones potential offers a continuous function to describe the pair potential,

$$v(r) = 4\varepsilon \left[\left(\frac{\sigma}{r} \right)^{12} - \left(\frac{\sigma}{r} \right)^6 \right], \quad (1.3)$$

where σ is the collective diameter, ε is the depth of the well. This model is widely used in molecular simulation. One should mention that this potential has a very long tail. To accelerate molecular simulation, a cut-off technique is widely used. To keep the continuity of the Lennard-Jones potential, it can be rewritten as

$$v(r) = 4\varepsilon \left[\left(\frac{\sigma}{r} \right)^{12} - \left(\frac{\sigma}{r} \right)^6 \right] - v(r_c). \quad (1.4)$$

And the Lennard-Jones potential always is divided by a reference hard sphere part and an attractive part, as Weeks-Chandler-Andersen theory¹⁷⁶ and Barker-Henderson theory¹⁷⁷. From the above models of pair potential, one can found that the pair potential can always separate into two parts. This idea is from Van der Waals. In addition, perturbation theories, which is formed based on this idea, is a powerful tool for studying thermodynamic properties of fluids.

B. Models of porous material

Generally, the porous material can be divided into two parts, the ordered porous medium, and the disordered porous medium. The ordered porous medium like MOF or ZIF can be described by a repeatable unit cell. The disordered porous medium, random porous medium, are always built with the help of fixed particles. However, recent studies found that the structure of porous material might have changed, during the fluid adsorbed in, such as swelling, or contracting.^{17-19,22,178-192} In some cases, this behavior

cannot be ignored like in MOF or ZIF.^{18,182,186} Most of models of disordered porous medium assumed that the structure of porous medium is a rigid one, which will not be modified by the behavior of fluid. This assumption makes the porous material can be considered as an external potential field, which is very convenient for theoretical approaches, such as, integral equations and density functional theory (DFT), and computer simulation. Although the structural change of porous medium is ignored, the description of the disorder of random porous material is still very complicated. The properties of fluid in random porous material must be taken two ensemble average. The first ensemble average is over all fluid configurations. And the second ensemble average is over all material configuration. Although the structure of random porous medium is a disordered and inhomogeneous one, after the ensemble average, it can be considered as an isotropic one. This concept is the fundamental basis of theoretical studies of Madden-Glandt model such as, Ornstein-Zernike equation^{114,149,157,163}, Density Functional Theory^{60,151,161,167,172}, and Scaled Particle Theory^{61,66,84,193–202}.

The first random porous medium model was proposed by W. G. Madden and E. D. Glandt in 1988.⁴⁰ In this model, the porous medium, also called matrix, is generated by fixing an equilibrium fluid, and the matrix particles are considered as an obstacle. The void among matrix particles is considered as pore. The interaction between matrix particles can be ideal gas potential or the hard sphere potential. And the porous medium is called an overlapping hard sphere (OHS) matrix and hard sphere (HS) matrix, respectively. And the interaction between fluid and matrix can be any pairwise additive potential. During the fluid adsorbed in porous medium, the fluid-matrix interaction will not modify the matrix structure. The matrix particle distribution is same as an equilibrium fluid distribution. With powerful theoretical tools, such as Ornstein-Zernike equation, density functional theory, numerous studies of confined fluid are carried out. The behavior of fluids confined in random porous medium, such as, phase behavior^{59,80,145–147,150}, adsorption^{76,82,104,105,110,124}, diffusivity^{48,158}, were systematically studied.

However, many works of confined fluid are based on Madden-Glandt model, some fundamental questions are still unsolved. For instance, how to calculate the pressure of fluids in Madden-Glandt matrix is still questioned. Rosinberg et al. used a replica technique to calculate the pressure of fluid confined in Madden-Glandt matrix.⁵³ And a complicated Virial expression for pressure was obtained. To obtain a simple expression of pressure in Madden-Glandt matrix, Dong also reported a simple expression of pressure which was obtained by considering the mechanic equilibrium.⁸⁹ In this same year, Kierlik et al. also proposed a so-called thermodynamics pressure, and found that this pressure and mechanical pressure are not identical.⁹⁵ In Kierlik's work, the Madden-Glandt matrix was obtained from Grand canonical ensemble. It should be mentioned that only mechanical pressure can be used in molecular simulation. In 2005, Dong and Chen first proposed a Virial equation for the thermodynamic pressure which can be used in molecular simulation and an exact relation between the pressure of fluids confined in porous material and the pressure of the corresponding bulk fluid.¹⁶⁴ This relation provides, for the first time, the basis of an experimental method for measuring the fluid pressure inside a random porous material. Also, the definition of the system volume may cause the difference among those pressure results. From an ideal gas system, one can find that if the system volume contains the volume occupied by matrix particle, the pressure equilibrium between the confined system and the corresponding bulk system will be broken. Hence, choosing the accessible volume as system volume seems more reasonable. However, the accessible volume is difficult to measure in experiment.

The morphology of some real porous materials like MCM-41 are sponge-like²⁰³, which is significantly different from the Madden-Glandt matrix. Hence, Zhao et al.¹⁷¹ proposed a new matrix model, named hard sponge matrix model. In this model, the matrix particle is considered as the pore, which is not like the previous model where the matrix particle is considered as obstacle. This model can be considered as the opposite of overlapping hard sphere matrix. The Ornstein-Zernike equations of fluids

confined in hard sponge model were proposed by Zhao et al. by using both diagram expansion and replica method. An analytical equation of state of fluid confined in hard sponge matrix was reported by Holovko et al.⁷⁹ In this work, the strict derivation of this equation of state is leaked. Here, it should be noted that, in Madden-Glandt model, from the viewpoint of fluid, the interface between fluid and matrix is a concave one, in hard sponge model, the interface between them is a convex one. How this difference will change the thermodynamic properties of confined fluid will be discussed in **Chapter 4**. Based on this model, Dong et al.⁴⁶ developed a new random porous model, called soft-sponge model, and the only difference from hard sponge model is when the fluid particle overlapped with material the interaction potential does not tend to be infinity, but finite positive value.

Above two porous medium models can describe some fundamental features of fluids in porous medium, such as disorder effect, the pore size distribution, and pore connectivity. In experiment, the templating-fabrication strategy skill is widely used in the synthesis of porous materials for controlling the pore size distribution. The template components are removed by heat treatment, acid or alkali solution. The pore size of this kind of material can be from micropore to macropore, two models cannot describe. The first templated matrices model is reported by Van Tassel. The Van Tassel matrix model is generated by fixing a two-component equilibrium fluid one component is considered as matrix species and the other component is the template species. After fixing, the template component will be removed. The pores in this model are generated from two parts, the first one is the voids between matrix particles, the primitive one, and the second one is from the removed template species. This model is very similar to the process of fabricating the templated porous material in experiments. However, this process is hard to describe in theoretical study. Even for an ideal gas fluid in Van Tassel matrix model, the expressions of the thermodynamics properties are not entirely analytically.¹⁷³ Zhao et al. also reported a templated porous medium.¹⁷⁵ In Zhao's template matrix model, the template pore is generated by piercing some cavities in the

Madden-Glandt matrix. This process can simplify the description of the structure of templated porous materials. The Ornstein-Zernike equations of fluids confined in Zhao's template matrix model were proposed by Zhao et al. by using both diagram expansion and replica method. Normally, there are two methods for studying the properties and the behavior of fluid confined in porous medium, simulation, and theoretical approach.

1.4 Theoretical approach

Many interesting studies of the properties and phase behavior of confined fluids are based on some numerical methods, i.e., molecular simulation, density functional theory, and Ornstein-Zernike equations. In this section, two general methods which have potential to offer totally analytical results of fluids confined in different porous materials will be introduced in next two subsections. Some numerical methods for confined fluid will be also introduced in the last subsection.

A. SPT for confined fluid

Scaled particle theory (SPT) was first reported by Reiss et al.^{204,205} in more than a half century ago. It provides a powerful tool to determine the equation of state of a bulk hard sphere (HS) fluid. SPT is not just limited to calculating the thermodynamical properties, i.e, pressure, chemical potential. It can also provide many surface and structural properties, i.e. surface tension, Tolman length, and radial distribution function. Many extensions and applications have been reported, e.g. Dong and his coworkers^{66,193,195} extend SPT to HS fluids confined in some random porous matrices.

Patsahan et al. first extended SPT to fluids confined in Madden-Glandt matrix model and obtained an accurate analytical equation of state. The basic idea of SPT is to insert an additional scaled particle into a fluid, this is equivalent to creating a spherical cavity. The excess chemical potential of inserting a point scaled particle can be obtained exactly. And a thermodynamical consideration can be used to describe the work of creating a finite size spherical cavity. Patsahan et al. introduced the exact analytical

results of a point scaled particle in hard sphere or overlapping hard sphere matrix, and the first equation of state for confined fluids, SPT1, was carried out. However, in SPT1, when the matrix density tends to zero and the matrix size tends to infinity, the expression of SPT1 cannot reduce to the original bulk SPT result. Later, with the help of a new formulation of SPT, this inconsistency was eliminated in SPT2. In this formulation, the morphology of porous materials is only presented by four parameters, packing fraction of matrix species, the ratio of the radius of fluid particle to matrix particle, and two porosities. The first porosity (geometrical porosity, ϕ_0) is only about the geometry of porous materials which the probing particle is a point scaled particle. The second porosity (probe particle porosity, ϕ) measures the accessible volume of the center of fluid, and the probing particle is a fluid particle. The SPT2b shows a great agreement with the molecular simulation results. However, a divergence was found in SPT2b when the packing fraction of fluid is higher than the value of probe particle porosity. Based on the study of one-dimensional hard rod fluid in random porous materials⁷⁷, an expansion of the term which contains probe particle porosity was used in SPT2b1 to eliminate this divergence. This expansion also improved the accuracy of the SPT prediction. However, it was found that when the fluid particle size is larger than matrix particle size, all versions of SPT significantly overestimated the thermodynamics properties of confined fluids even in fluid with a low density. Comparing the expressions of SPT2, SPT2b, and SPT2b1, one can find that probe fluid particle porosity leads to this overestimation. The essence of those improvements of SPT is to reduce the influence of probe fluid particle porosity. Also, if we just use geometry porosity to replace probe particle porosity as SPT2a, the prediction of SPT will significantly underestimate the properties of confined fluid. Hence, find a more suitable porosity to describe the accessible volume of fluid is the key point to improve SPT. It should be mentioned that only four parameters are used for describing the porous material in SPT. We can assume that once those four parameters of porous material are obtained, the SPT can be used for describing the thermodynamic properties of fluid

confined in such porous material. Based on this, the SPT can be easily extended to other random porous materials, such as hard sponge matrices, and hard convex body matrices.^{196,202} Later, the SPT was extended to study the thermodynamic properties and phase behavior of the hard-convex body fluid in random porous materials.^{196,206} With the help of perturbation method, the phase behavior of network-forming fluid and ionic fluid.^{194,201} Hence, the SPT can be considered as a general framework for fluids confined in different porous materials.

B. Morphological thermodynamics

Here, I introduce another general framework for confined fluid, morphological thermodynamics, which was proposed by Mecke and his co-works.^{207–210} This method is from a beautiful mathematics theorem, Hadwiger's volume theorem.^{211,212} It is not only a beautiful mathematics theorem but also offers a very powerful way to study confined fluid. Initially, Mecke and Wagner used this theorem to analyze the spatial patterns of galaxy distribution.²¹³ And then they found that this method can also be contributed to studies in microemulsions^{214,215}, composite media^{207,208}, complex molecule²¹⁶. They named this method as morphological thermodynamics. In 2003, Bryk²¹⁷ derived an analytical equation to calculate the surface tension of a hard sphere fluid close to curved substrates by morphological thermodynamics. The result showed that the expression of surface tension of fluid close to arbitrary convex substrates does not include a logarithmic term of curvature. In 2004, König²⁰⁹ derived a morphological thermodynamic form grand potential expression. This grand potential expression is used to calculate the solvation free energy of a cylindrical or a spherical hard sphere particle solute in hard sphere fluid.

$$F_{sol} = pV + \sigma A + \kappa_1 C + \kappa_2 X \quad (1.5)$$

where p is the pressure and σ is the interfacial tension near a planar wall, κ_1 and κ_2 are the properties of the fluid. the volume, V , the surface area, A , the integrated mean curvature, C , and the Euler characteristic, X , are the geometric properties of

solute. The result obtained from the equation above has a good agreement with the result from Rosenfeld's fundamental measure theory. In 2009, Oettel²¹⁸ calculated the depletion potential between two hard sphere particles among the small hard sphere solvent using morphological thermodynamics and density functional theory (DFT). The result showed that morphological thermodynamics is invalidated when the distance between two hard sphere particles is greater than one solvent particle's diameter and smaller than a few of solvent particle's diameters, since the additivity restriction of Hadwiger's volume theorem is broken down in this situation. In 2012, Jin²¹⁹ studied the shape effect on solvation using morphological thermodynamics and DFT, the solvation free energy of solute with different shapes was calculated. Comparing with DFT result, it showed that when the solvent correlation length is smaller than the solute particle diameter, morphological thermodynamics is valid.

Recently, some studies²²⁰⁻²²⁴ showed that the morphological thermodynamics is an approximate method but an exact one. Laird²²³ used molecular dynamics simulation (MD) to calculate the interfacial tension, γ , between spherical or cylindrical particle and hard sphere fluid. They fitted the MD result to determine a polynomial of $1/R$. This result showed that the morphological thermodynamics is valid in low packing fraction ($\eta < 0.42$), while in a high packing fraction, the first non-Hadwiger coefficient showed a significant increase. Hansen-Goos²²¹ used Virial expansion to determine an exact surface tension expression, and this expression implied the existence of non-Hadwiger coefficient. To quantify the first non-Hadwiger coefficient, some simulations were carried out, the numerous results showed that the first non-Hadwiger coefficient is smaller than the smallest morphological thermodynamics coefficient in one order of magnitude. In those articles, they did not prove that the non-Hadwiger term coefficients with higher order are always in the same sign. In this case, the sum of non-Hadwiger terms may be equal to zero. In fact, their studies considered a fluid near spherical or cylindrical particle, it means that the interface between fluid and the obstacle particle is concave from fluid view, while the Hadwiger's volume theorem is only valid in the

convex interface. Although morphological is questioned recently, it is still considered as a potential tool for building a general framework for describing the fluid confined in different porous materials.

C. Other theoretical approaches

The Ornstein-Zernike equations and density functional theory are also the very popular theoretical methods for studying the thermodynamic properties of confined fluids. The two-body correlation functions are the basic quantities of Ornstein-Zernike equations. Since the replica Ornstein-Zernike equations of fluids in Madden-Gladnt random porous medium were reported by Given and Stell,⁷⁵ substantial effort has been focused on the study of the properties of a fluid confined in random porous materials using replica Ornstein-Zernike equations theory. For instance, Kierlik¹⁰⁶ used replica Ornstein-Zernike equations to investigate the phase diagrams of fluids in the random porous material, they found, in most cases, vapor-liquid coexistence curve of fluids in the random porous material is similar to the bulk ones, although it is narrowed. With the help of replica method, Zhao et. al. also proposed the Ornstein-Zernike equations for Hard-sponge and Templated random porous medium. However, the suitable closer for those Ornstein-Zernike equations is still not clear. Density functional theory is also a classical theoretical method for studying the inhomogeneous fluids, the porous material is generally considered as an external potential. For ordered porous material, density functional theory is widely used. For instance, Liu et. al.²²⁵ used density functional theory to predict the behavior of H₂ adsorbed in different kinds of MOFs. They found that the saturated pressure increases along with temperature in the low temperature region but a decrease in the high temperature region. For random porous material, if the material is still treated as an external potential, lots of configurations of material must be included in averaging procedure and the computation cost must be very expensive. Recently, Schmidt et al.^{151,167} treated the random porous material on the level of one-body density distribution rather than as an external field and derived a so-called replica density functional theory.

1.5 Simulation method

Molecular simulation is a powerful and robust statistical mechanics method for confined fluid.^{226–228} The basic idea of molecular simulation is to attain a set of configurations distributed according to some statistical distribution function, or statistical ensemble. There are two classical molecular simulation approaches for confined fluid: Monte Carlo method and molecular dynamics method. The molecular dynamics is based on the classical equations of motion or Langevin equation. Therefore, molecular dynamics can be used to study the time-dependent processes like diffusivity. The Monte Carlo method is an essential stochastic method, where the configurations are generated by moving or inserting and removing particles. Therefore, to study the static properties of confined fluid, the Monte Carlo method will be more efficient. Many interesting studies of confined fluid are based on molecular simulation. For instance, the chemical reaction in porous medium, Turner^{229–232} used Reaction ensemble Monte Carlo method to study reactions confined in porous material, they found the confinement effect is significantly improved the chemical reaction yield which almost cannot be observed in bulk system. Another interesting example is about phase transitions of fluids adsorbed in random porous material. Many experimental evidences support that the confinement effect can influence the liquid-vapor phase transitions. Such as comparing with the bulk vapor-liquid coexistence curve, the vapor-liquid coexistence curve of confined fluid is remarkably narrowed, and the critical temperature and density are lower. Since the properties of confined fluid are affected by many characteristics of porous material, such as porosity, pore size distribution, pore connectivity, how those characteristics of porous material will affect phase behavior had carried out a series of simulation studies. To accelerate the efficiency of the simulation of confined fluid, two powerful simulation techniques, the Gibbs-ensemble method, and the Gibbs-Duhem integration, were adapted by Brennan and Dong¹⁵³.

In molecular simulation, the ordered porous medium like MOF and ZIF can be described by a repeatable unit cell. Since the disordered porous medium is always built

with the help of fixed particles, for describing the structure of disordered porous material, lots of configurations (usually, about 5-20) of disordered porous medium are generated from the canonical ensemble Monte Carlo simulation, and the average over the material configurations was taken. Hence, the computation cost of computer simulation is expensive. In porous material, the pores can be divided into two parts, the open pores, and the closed (dead) pores. The open pores mean the fluid particle can access via diffusion process, while the dead pores are isolated from the outside fluid. In Monte Carlo simulation, the fluid particle can appear in closed pores via the random inserting operation, or via a large displacement operation.

1.6 Current problem and the objective of the present work

Although a large number of experimental and theoretical investigations have been made during the last decades, our understanding of confined fluids is still incomplete. Currently, we do not really know which extend thermodynamics can be applied at the scale of nanopores. Different aspects of confined fluids are being studied in a case-by-case way. In [Chapter 2](#), we first time presented a general scaling relation between the confined fluid and bulk one-component fluid, which allows for connecting some thermodynamic properties of a confined fluid to bulk ones. Upon rescaling adsorbed fluid density, the adsorption-isotherms for many different confining environments collapse to the corresponding bulk curve. We also revealed the intimate connection of the reported scaling relation to Gibbs theory of inhomogeneous fluids.

As we mentioned before, morphological thermodynamics are questioned recently. The existence of non-Hadwiger term has been confirmed by both theoretical study and molecular simulation. In the scaled particle theory, the formulation of the work for creating a spherical cavity in a fluid is identical to the morphological thermodynamics, and the scaled particle theory for the bulk system is not as accurate as other equation of state such as Carnahan-Starling equation of state. This indicated that the scaled particle theory can be improved by adding a non-Hadwiger term. In [Chapter 3](#), we set up two

new versions of SPT. The first one contains an adjustable parameter. The second one uses two Laurent series to describe the chemical potential for inserting a scaled particle. Both new versions of SPT significantly improved the accuracy of not only thermodynamic properties, i.e. pressure and chemical potential, but also surface properties, i.e. surface tension and Tolman length. We also first time obtained a self-consistency expression of non-Hadwiger term. Moreover, the same idea can be used to treat the multi-components system, and the improvement is significant.

Morphological thermodynamics offered a tool for building a general framework to describe the thermodynamic properties of fluids confined in different porous materials. However, how to use this tool is still unclear. In [Chapter 4](#), by considering the chemical potential as the independent variable, we derived, for first time, a new general equation of state by using morphological thermodynamic. In this equation of state, the porous material is described by only four geometric properties, i.e., the geometry porosity, fluid-solid interface area, integrated Gaussian curvature, and integrated mean curvature. To our best knowledge, this is the first equation of state for confined fluid which is irrelevant to the model of porous medium. Our new equation of state has a great agreement with molecular simulation results in a large range.

Madden-Glandt model is the first model of random porous material. In this model, the disordered porous material is mimicked by random matrix configuration that can be generated by fixing a relevant fluid system at its equilibrium state. Thus, the quenched “fluid” particles constitute the matrix (thereafter called matrix particles), and the voids among them are pores. In [Chapter 5](#), we proposed a quantitative measure of quench effect for the adsorption of fluids in random porous materials. With the help of scaled particle theory and molecular simulation, we find when matrix particles are larger than fluid particles, the confined fluid shows the same behavior, i.e., chemical potential, as the binary mixture bulk system.

2. A confinement-adsorption scaling relation

2.1 Introduction

Accompanying the elaboration of high-performance functionalized nanoporous materials, a large number of experimental and theoretical investigations have been made during the last decades. Nevertheless, our understanding of confined fluids is still incomplete. Currently, we do not really know to which extent thermodynamics can be still applied at the scale of nanopores. Different aspects of confined fluids are being studied in a case-by-case way. It can be readily admitted that the fluid-solid interface and the fluid inhomogeneity near it have to be taken into account. For fluid adsorption in the real porous material, the fluid-solid interfaces are generally curved ones. It might appear surprising that the thermodynamics for dealing with curved interfaces is not so well established although early investigations go back to Tolman.²³³ Mecke and co-workers have made efforts to develop a general framework, named as morphological thermodynamics, to account for more complex surface morphology.^{209,210,217,220,234} The foundation of morphological thermodynamics has been questioned recently.^{221–224} To our best knowledge, no experimental measurement has ever been made to determine the bending rigidity coefficients needed in morphological thermodynamics method for any fluid-solid interface.

A large literature exists on the study of confined fluids by theoretical and simulation methods. Models with simple pore geometry (e.g., slit or cylinder) are widely studied. In such models, the pore-size distribution and connectivity among pores are neglected. Fluid adsorption and diffusion in ordered porous material, e.g. zeolites, have been studied by simulations. To account for the quenched disorder, models for random porous media have been proposed also, e.g., Madden-Glandt model and various variants.^{40,85,108,136} Despite these considerable efforts, it is unfortunate to note that no unifying picture of various confined fluids has emerged. Today, we do not have yet a

precise idea about the respective roles played by pore-connectivity, pore-size distribution, pore morphology, or quenched disorder. In a bulk fluid, a molecule is surrounded by other fluid molecules while in a fluid adsorbed in a porous solid, a large number of fluid molecules are located near a fluid-solid interface. These molecules feel the interaction with both fluid and solid molecules. The nature of fluid-solid interaction can vary significantly, from repulsive to attractive ones. This additional interaction can make the confined fluid behave very differently from the bulk one. Although a confined fluid appears complicated due to the complex confining environment of adsorbent, one can wonder if there is any connection between confined and bulk fluids. Currently, we know quite a few about this. Acquiring such knowledge does not only advance our understanding of these complex systems but also can have important applications. In this chapter, we report several relations which allow for connecting some properties of a confined fluid to those of a bulk one. By rescaling the density of a confined fluid, the adsorption isotherms (also free energy or grand potential per particle) of fluids in a large variety of confining environments can collapse to the corresponding bulk ones.

2.2 Model and method

We investigated the thermodynamic properties (chemical potential, Helmholtz free energy, and grand potential) of confined fluids by considering a large variety of models (hard-sphere or Lenard-Jones fluids in slit-pores, ordered or disordered porous matrices). Simulations were carried out with the help of Monte-Carlo methods (in grand-canonical or canonical ensembles).

A. Model

A-1. HS fluid confined in various porous environments

In the present work, we consider only one-component fluid (denoted as species 1). The fluid-fluid interaction between hard spheres of radius, R_1 , is given by

$$u_{11}(|\mathbf{r}_i - \mathbf{r}_j|) = \begin{cases} \infty & |\mathbf{r}_i - \mathbf{r}_j| < 2R_1 \\ 0 & |\mathbf{r}_i - \mathbf{r}_j| \geq 2R_1 \end{cases}. \quad (2.1)$$

where \mathbf{r}_i and \mathbf{r}_j are the position vectors of the i th and j th fluid particle respectively.

Various confining environments are considered. For Madden-Glandt model of random porous matrices (denoted as species 0), the following fluid-matrix interaction is given by

$$u_{10}(|\mathbf{r} - \mathbf{q}_j|) = \begin{cases} \infty & |\mathbf{r} - \mathbf{q}_j| < R_0 + R_1 \\ \varepsilon_0 & R_0 + R_1 \leq |\mathbf{r} - \mathbf{q}_j| < R_0 + R_1 + d, \\ 0 & R_0 + R_1 + d \leq |\mathbf{r} - \mathbf{q}_j| \end{cases}, \quad (2.2)$$

where R_0 is matrix particle radius, \mathbf{q}_j the position vector of the j th matrix particle, ε_0 and d are respectively the potential-well depth and width. In the case of $\varepsilon_0 = 0$ and $d = 0$, we have a hard sphere (HS) matrix. The configurations of an HS matrix are generated from an equilibrium system with the following interaction,

$$u_{00}(|\mathbf{q}_i - \mathbf{q}_j|) = \begin{cases} \infty & |\mathbf{q}_i - \mathbf{q}_j| < 2R_0 \\ 0 & |\mathbf{q}_i - \mathbf{q}_j| \geq 2R_0 \end{cases}. \quad (2.3)$$

For an overlapping hard sphere (OHS) matrix, matrix particles are placed totally randomly, i.e., $u_{00}(|\mathbf{q}_i - \mathbf{q}_j|) = 0$. We considered also a slit pore with the width of L and the interaction between fluid and the pore wall is given by

$$w(z_i) = \begin{cases} \infty & |z_i| \geq (L - \sigma_1)/2 \\ \varepsilon_0 & L/2 - d \leq |z_i| < (L - \sigma_1)/2, \\ 0 & |z_i| < L/2 - d \end{cases}, \quad (2.4)$$

where $\sigma_1 = 2R_1$ and z_i is the coordinate along the coordinate axis perpendicular to the slit walls (note that the origin of the coordinate system is placed at the middle of the slit pore). In the case of $\varepsilon_0 = 0$ and $d = 0$, we have the simple case of a slit pore with two hard walls. For slit pores, we calculate the fluid density by using the physical volume, i.e., $V = AL$ (A : surface area) but not the volume accessible to the centers

of fluid particles.

A-2. LJ fluid confined in various porous environments

To demonstrate the validity of the scaling relation when an attractive fluid-fluid interaction is also present, a Lenard-Jones fluid with the following interaction is considered as well,

$$u_{11}(|\mathbf{r}_i - \mathbf{r}_j|) = \begin{cases} u_{\text{LJ}}(|\mathbf{r}_i - \mathbf{r}_j|) - u_{\text{LJ}}(r_{11}^c) & |\mathbf{r}_i - \mathbf{r}_j| \leq r_{11}^c \\ 0 & |\mathbf{r}_i - \mathbf{r}_j| > r_{11}^c \end{cases}, \quad (2.5)$$

$$u_{\text{LJ}}(r) = 4\varepsilon_1 \left[(\sigma_1/r)^{12} - (\sigma_1/r)^6 \right], \quad (2.6)$$

where $r_{11}^c = 10R_1$, $\sigma_1 = 2R_1$ and ε_1 is the potential well depth. When this LJ fluid is confined in an LJ matrix, the fluid-matrix is given by

$$u_{10}(|\mathbf{r}_i - \mathbf{q}_j|) = \begin{cases} u_{\text{LJ}}(|\mathbf{r}_i - \mathbf{q}_j|) - u_{\text{LJ}}(r_{10}^c) & |\mathbf{r}_i - \mathbf{q}_j| \leq r_{10}^c \\ 0 & |\mathbf{r}_i - \mathbf{q}_j| > r_{10}^c \end{cases}, \quad (2.7)$$

$$u_{\text{LJ}}(r) = 4\varepsilon_{10} \left[(\sigma_{10}/r)^{12} - (\sigma_{10}/r)^6 \right], \quad (2.8)$$

Where $r_{10}^c = 5(R_1 + R_0)$, and cross parameters $(\sigma_{10}, \varepsilon_{10})$ can be calculated with the Lorentz-Berthelot (LB) mixing ruler

$$\varepsilon_{10} = \sqrt{\varepsilon_0 \varepsilon_1}, \quad (2.9)$$

$$\sigma_{10} = \frac{\sigma_1 + \sigma_0}{2}. \quad (2.10)$$

where $\sigma_0 = 2R_0$, ε_0 is the potential-well depth for matrix-matrix interaction. In LJ matrix systems, we have chosen ε_0 is from $0.7\varepsilon_1$ to $5.25\varepsilon_1$. And the matrix-matrix interaction is

B. Method

Canonical-ensemble Monte Carlo (CEMC) simulations are carried out for generating matrix configurations and those of a fluid confined in a particular matrix configuration. A cubic simulation box of volume, V , is used with periodic boundary

condition in three space directions when a fluid confined in a matrix is considered. For slit pores, the simulation box is made with two square walls separated by a distance equal to L and the periodic boundary condition is applied only in the two space directions parallel to the walls. For each simulation, about $2 \times 10^5 - 1 \times 10^6$ trial moves for each fluid particle are performed. Since finite-size matrices are used, any observable quantity fluctuates with matrix realizations and an average made typically with about 10 matrix realizations leads to converged results. The excess chemical potential of the fluid, μ_1^{ex} , is calculated for different density, ρ_1 ($\rho_1 = N_1 / V$, N_1 : the number of fluid particles), by using Widom's test particle method.²²⁶ Then, Helmholtz free energy is determined by a thermodynamic integration, i.e.,

$$\frac{\beta F}{N_1} = \ln(\rho_1 \Lambda_1^3) - 1 + \frac{1}{\rho_1} \int_0^{\rho_1} \beta \mu^{ex}(\rho) d\rho, \quad (2.11)$$

where Λ_1 is the thermal wavelength of fluid particles and in this work, we set $\Lambda_1 = \sigma_1$. Finally, we obtain readily compressibility factor from the following thermodynamic relation,

$$\frac{\beta \Omega}{N_1} = -\beta \mu + \frac{\beta F}{N_1}. \quad (2.12)$$

C. Conditions of considered systems

The computational conditions of all the considered systems are summarized in **Table 2.1**. The confining environments considered in this work can be classified into two big categories: i) porous matrices and ii) slit pores. According to their different morphologies of pore space, we can divide porous matrices into four different types. Disordered porous matrices are generated by quenching an equilibrium system according to the procedure proposed by Madden and Glandt⁴⁰ and denoted, in **Table 2.1**, as HSM_d if matrix-matrix interaction is HS one or LJM_d when the matrix-matrix interaction is LJ one. In contrast, ordered porous matrices can be generated by arranging matrix particle into an ordered structure. In this work, we studied only the case that

matrix particles are placed on a simple cubic lattice and the acronyms used for such matrices are HSM_o (HS for fluid-matrix interaction) and LJM_o (LJ for fluid-matrix interaction). The third type of matrices we considered, is templated matrix. Following the procedure proposed by Van Tassel et al,^{108,136} a templated quenching an equilibrium binary system and removing its one component after quenching. We considered only templated HS matrix, denoted by THSM in **Table 2.1**, with the same number of template and matrix particles and moreover they have the same size. The fourth type of matrices is the hard sponge one,^{79,171} denoted as HSG in **Table 2.1**.

The meaning of the title labels in **Table 2.1** is the following,

f-s: fluid-solid interaction (here the word “solid” is used to denote either hard wall or matrix particles);

f-f: fluid-fluid interaction;

τ : fluid matrix particle size ratio, σ_1 / σ_0 ;

T^* : temperature, $T^* = k_B T / \varepsilon_{ref}$ (ε_{ref} : reference energy unit, all the well-depth parameters for square-well or LJ potentials, e.g., ε_0 , ε_1 , are defined with respect to this reference unit);

Symbol: symbols used for curves plotted in different figures of the paper.

The definitions of all the other reduced parameters given in **Table 2.1** are given below as well.

Slit width: $L^* = L / \sigma_1$;

SW(d^* , ε_0^*): square-well potential with width, $d^* = d / \sigma_1$, and depth, $\varepsilon_0^* = \varepsilon_0 / \varepsilon_{ref}$;

LJ(ε_1^*): LJ potential with depth, $\varepsilon_1^* = \varepsilon_1 / \varepsilon_{ref}$;

ρ_0^* : matrix density, $\rho_0^* = \rho_0 \sigma_0^3$ ($\rho_0 = N_0 / V$, N_0 : number of matrix particles).

Table 2.1. Computation parameters for canonical or grand-canonical ensemble Monte-Carlo simulations

Pore	f-s	f-f	τ	T^*	Symbol
Slit (width: 5)	HW	HS	-	-	
Slit (width: 5)	SW(1,-1)	HS	-	1	
Slit (width: 5)	SW(1,1)	HS	-	1	
Slit (width: 3.5)	HW	HS	-	-	
Slit (width: 7)	HW	HS	-	-	
HSM_d ($\rho_0^*=0.2$)	HS	HS	0.5	-	
HSM_d ($\rho_0^*=0.55$)	HS	HS	0.2	-	
HSM_d ($\rho_0^*=0.25$)	SW(1,-1)	HS	0.2	1	
HSM_d ($\rho_0^*=0.25$)	SW(1,1)	HS	0.2	1	
HSM_d ($\rho_0^*=0.5$)	SW(1,-1)	HS	0.1	1	
HSM_d ($\rho_0^*=0.5$)	SW(1,1)	HS	0.1	1	
HSM_o ($\rho_0^*=0.578$)	SW(1,-2)	HS	0.1	1	
HSM_o ($\rho_0^*=0.578$)	SW(1,2)	HS	0.1	1	
HSM_o ($\rho_0^*=0.125$)	HS	HS	0.2	-	
HSM_o ($\rho_0^*=0.75$)	HS	HS	0.1	-	
THSM ($\rho_0^*=0.2$)	HS	HS	0.5	-	
THSM ($\rho_0^*=0.15$)	HS	HS	0.2	-	
THSM ($\rho_0^*=0.5$)	HS	HS	0.1	-	
HSG ($\rho_0^*=1.172$)	HSG	HS	0.1	-	

Slit (width: 5)	HW	LJ (1)	-	3.5	
LJM_d ($\rho_0^*=0.25$)	LJ (1)	LJ (1)	0.2	3.5	
LJM_d ($\rho_0^*=0.5$)	LJ (1)	LJ (1)	0.1	3.5	
LJM_o ($\rho_0^*=0.5$)	LJ (1)	LJ (1)	0.2	3.5	
LJM_d ($\rho_0^*=0.5$)	LJ (1.75)	LJ (1)	0.2	3.5	
LJM_d ($\rho_0^*=0.5$)	LJ (0.7)	LJ (1)	0.2	3.5	
LJM_d ($\rho_0^*=0.5$)	LJ (3.5)	LJ (1)	0.2	3.5	
LJM_d ($\rho_0^*=0.5$)	LJ (7)	LJ (1)	0.2	3.5	
LJM_d ($\rho_0^*=0.5$)	LJ (5.25)	LJ (1)	0.2	3.5	

2.3 Results and discussion

Inspired by the exact and analytical results for some models (ideal gas in a variety of confining environments) and scrutinizing our simulation results for many more complex confined fluids with interactions, we found the following scaling relation:

$$\beta\mu(\chi\rho, T) = \beta\mu^{bulk}(\rho, T), \quad (2.13)$$

$$\beta f(\chi\rho, T) = \beta f^{bulk}(\rho, T), \quad (2.14)$$

$$-\beta\omega(\chi\rho, T) = Z^{bulk}(\rho, T), \quad (2.15)$$

where $\beta = 1/(k_B T)$ (k_B : Boltzmann constant, T : temperature), μ and μ^{bulk} are respectively chemical potential of confined and bulk fluid, ρ the number density of the bulk fluid in equilibrium with the confined one ($\rho = N/V$, V : volume), f and f^{bulk} are respectively free-energy per particle of confined and bulk fluid, i.e., $f = F/N^{conf}$, $f^{bulk} = F^{bulk}/N$ (N^{conf} : particle number of confined fluid), ω grand-potential per particle of a confined fluid, Z^{bulk} is the compressibility factor in the bulk, i.e., $Z^{bulk} = \beta P^{bulk}/\rho$, (P^{bulk} : bulk fluid pressure, note that the compressibility factor is simply the negative of grand-potential per particle). The scaling factor is given by:

$$\chi = \phi_0 + \Gamma A / (\beta P^{bulk} V), \quad (2.16)$$

where ϕ_0 is geometric porosity of the porous adsorbent under consideration (see ⁷⁹ for definition), Γ adsorption per unit surface area, and A area of the fluid-solid interface of the confined fluid. ΓA can be calculated simply from:

$$\Gamma A = (\rho^{conf} - \phi_0 \rho) V, \quad (2.17)$$

where $\rho^{conf} = N^{conf}/V$. It is to note that only ΓA is needed but not Γ and A separately and ΓA can be measured experimentally. When the second term on the right

hand side of eq. (2.16) is dropped out, we have immediately:

$$\beta\mu(\phi_0, \rho, T) = \beta\mu^{bulk}(\rho, T); \quad (2.18)$$

$$\beta f(\phi_0, \rho, T) = \beta f^{bulk}(\rho, T); \quad (2.19)$$

$$-\beta\omega(\phi_0, \rho, T) = Z^{bulk}(\rho, T). \quad (2.20)$$

We name this as pure-confinement scaling which holds rigorously for an ideal gas in hard matrices, e.g., a hard-sphere (HS), an overlapping HS (OHS) or a hard-sponge matrix. From scaled particle theory,^{61,66,79,84,193,195} we can show that the pure-confinement scaling holds also for HS fluids confined in HS and OHS matrices when the size ratio of matrix to fluid particle is large.¹⁹³

The simulation results presented below demonstrate the validity of the scaling relation given in eq.(2.13)–(2.16), named as confinement-adsorption scaling, for a large variety of confined fluids under broad conditions. To show the general and robust character of this scaling relation, we considered virtually all types of confined fluids, i.e., in various porous environments like isolated slit pores, connected ordered or random porous matrices including sponge-like ones and different types of fluid-fluid and fluid-solid interactions. **Fig. 2.1(a)** shows the collapse of adsorption isotherms of an HS fluid confined in 19 different environments to the bulk $\mu \sim \rho$ isotherm after scaling according to eq. (2.18) while in **Fig. 2.1(b)**, the results before scaling are presented. The robustness of the scaling relation is demonstrated by the large diversity of the considered confining environments, from isolated slit pores to random porous matrices with pure repulsive or repulsive plus attractive fluid-solid interactions. To establish the general validity of the scaling relation, we carried out also simulations with a Lennard-Jones (LJ) fluid (see results in **Fig. 2.2**). These results show the general character of the scaling relation which holds also for fluids with attractive interaction.

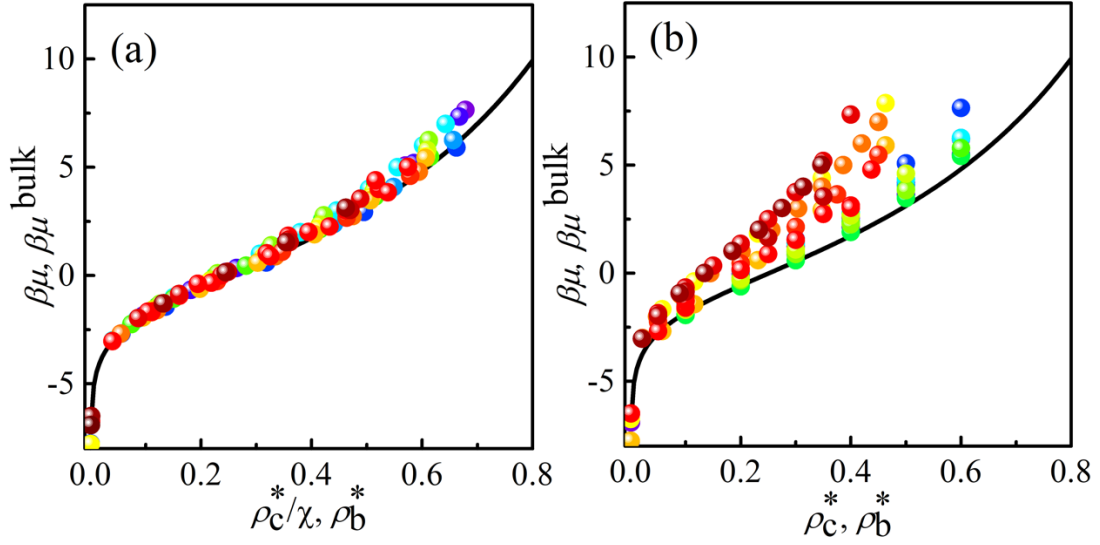


Figure 2.1. Monte-Carlo simulation results for an HS fluid confined in 19 different confining environments: a) Chemical potential, $\beta\mu$, as a function of scaled density ρ_c^* / χ ($\rho_c^* = \rho^{conf} \sigma^3$, σ : HS diameter); b) Chemical potential, $\beta\mu$, as a function of non scaled density ρ_c^* . The full line is the bulk $\beta\mu^{bulk} \sim \rho_b^*$ isotherm from Carnahan-Starling equation of state. Subscripts, b and c , denote respectively bulk and confined fluids.

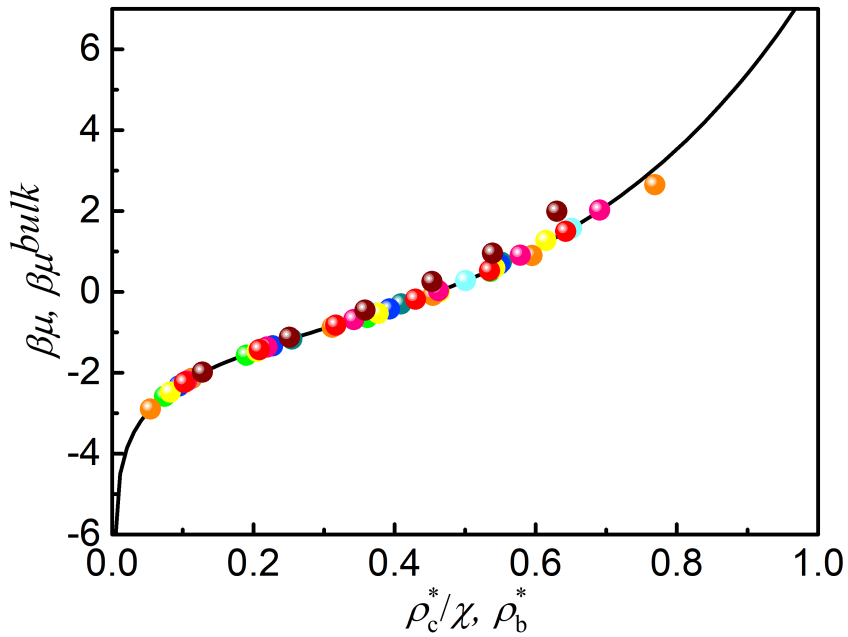


Figure 2.2. Monte-Carlo simulation results for an LJ fluid confined at $T^* = 3.5$ in 4 different confining environments: Chemical potential, $\beta\mu$ as function of scaled density, ρ_c^* / χ ($\rho_c^* = \rho^{conf} \sigma^3$, σ : LJ size parameter). The full line is the bulk $\beta\mu^{bulk} \sim \rho_b^*$ isotherm from the equation of state given in [235](#).

The scaling relation holds not only for the adsorption isotherms but also for some other thermodynamic quantities, *e.g.*, free-energy per particle and grand-potential per particle. **Fig. 2.3** shows the collapse of βf and $-\beta\omega$ for different confined HS fluids to the corresponding bulk curves. The same scaling relation holding for chemical potential, free-energy per particle and grand-potential per particle implies immediately that βf and $-\beta\omega$ collapse to the corresponding bulk curves if they are expressed as a function of chemical potential, *i.e.*:

$$\beta f(\mu, T) = \beta f^{bulk}(\mu, T); \quad (2.21)$$

$$-\beta\omega(\mu, T) = Z^{bulk}(\mu, T). \quad (2.22)$$

This invariance is remarkably illustrated in **Fig. 2.4**. One obvious importance of such invariance relations is that they allow for determining some thermodynamic functions of a confined fluid from the corresponding bulk ones. It is well known that the experimental measurement of thermodynamic properties of confined fluids is much more difficult or impossible currently. To our best knowledge, no direct experimental determination of pressure and free energy has ever been made for fluids confined in nanoporous materials.

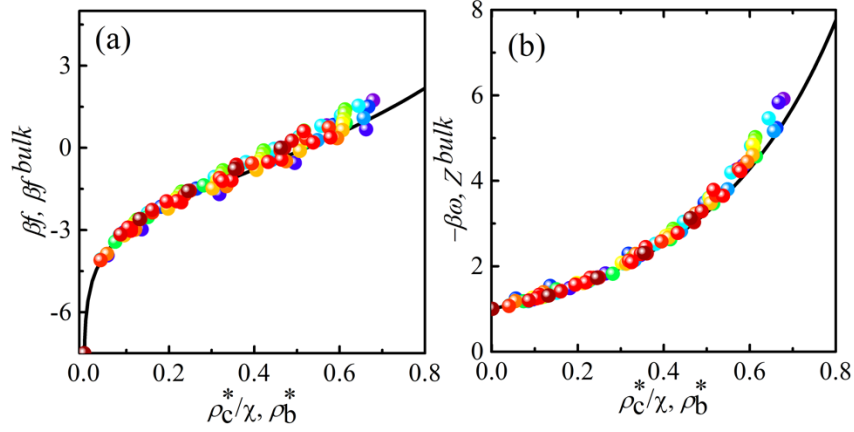


Figure 2.3. Monte-Carlo simulation results for an HS fluid confined in 19 different confining environments: a) Free energy per particle, βf , as function of scaled density ρ_c^* / χ ($\rho_c^* = \rho^{conf} \sigma^3$, σ : HS diameter); b) Minus grand-potential per particle, $-\beta\omega$, as a function of non scaled density ρ_b^* . Full lines are respectively corresponding bulk $\beta f^{bulk} \sim \rho_b^*$ and $Z^{bulk} \sim \rho_b^*$ curves from Carnahan-Starling equation of state.

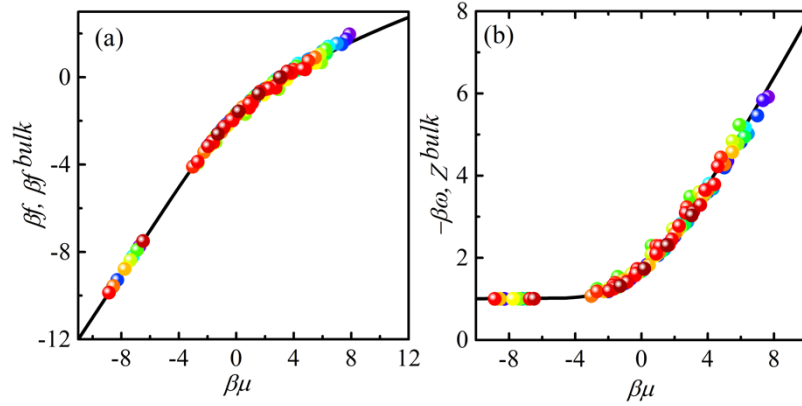


Figure 2.4. Monte-Carlo simulation results for an HS fluid confined in 19 different confining environments: a) Free-energy per particle, βf , as function of chemical potential, $\beta\mu$; b) Minus grand-potential per particle, $-\beta\omega$, as function of chemical potential, $\beta\mu$. Full lines are respectively corresponding bulk $\beta f^{bulk} \sim \beta\mu$ and $Z^{bulk} \sim \beta\mu$ curves from Carnahan-Starling equation of state.

Although the simulation results presented above establish the validity of the

confinement-adsorption scaling and the invariance described by eqs. (2.21) and (2.22), a derivation of these relations from first-principles is currently lacking. Nevertheless, the confinement-adsorption scaling has some intimate connection with Gibbs theory for interfacial systems^{236,237} and the morphological thermodynamics advocated by Mecke et al.^{209,210,217,220,238} In fact, Gibbs theory can be derived from the scaling relation given in eq. (2.13). We start from the following equivalent form of eq. (2.13),

$$\beta\mu(\rho^{conf}, T) = \beta\mu^{bulk}\left(\frac{\rho^{conf}}{\chi}, T\right). \quad (2.23)$$

Expanding the RHS of this equation to the first order around ρ / ϕ_0 , we obtain,

$$\begin{aligned} \beta\mu(\rho^{conf}, T) &= \beta\mu^{bulk}\left(\frac{\rho^{conf}}{\phi_0}, T\right) + \left(\frac{\rho^{conf}}{\chi} - \frac{\rho^{conf}}{\phi_0}\right) \frac{\partial[\beta\mu^{bulk}(\rho^{conf}/\phi_0, T)]}{\partial(\rho^{conf}/\phi_0)} \\ &= \beta\mu^{bulk}\left(\frac{\rho^{conf}}{\phi_0}, T\right) + \left(\rho - \frac{\rho^{conf}}{\phi_0}\right) \frac{\partial[\beta\mu^{bulk}(\rho^{conf}/\phi_0, T)]}{\partial(\rho^{conf}/\phi_0)} \\ &= \beta\mu^{bulk}\left(\frac{\rho^{conf}}{\phi_0}, T\right) - \frac{\Gamma A}{\phi_0 V} \frac{\partial[\beta\mu^{bulk}(\rho^{conf}/\phi_0, T)]}{\partial(\rho^{conf}/\phi_0)} \end{aligned} \quad (2.24)$$

Eq. (2.17) was used when going to the last equality of eq.(2.24). Integrating both sides of the above equation with respect to ρ^{conf} leads to,

$$\begin{aligned} \frac{\beta F(N^{conf}, V, T)}{V} &= \int \beta\mu(\rho^{conf}, T) d\rho^{conf} \\ &= \phi_0 \frac{\beta F^{bulk}(N^{conf}, V\phi_0, T)}{V\phi_0} - \int \frac{\Gamma A}{V} \frac{\partial[\beta\mu^{bulk}(\rho^{conf}/\phi_0, T)]}{\partial(\rho^{conf}/\phi_0)} d(\rho^{conf}/\phi_0) \\ &= \phi_0 \frac{\beta F^{bulk}(N^{conf}, V\phi_0, T)}{V\phi_0} + \frac{\beta\gamma A}{V} \end{aligned} \quad (2.25)$$

where γ is the surface tension at fluid-solid interface and A the surface area of the pore space boundary used for calculation the porosity, ϕ_0 . Gibbs adsorption equation was used when going to the last equality in the above equation. Eq. (2.25) is nothing else but the free energy of the inhomogeneous system expressed as the bulk contribution plus the surface term following Gibbs theory, i.e.,

$$F(N^{conf}, V, T) = F^{bulk}(N^{conf}, V\phi_0, T) + \gamma A \quad (2.26)$$

Subtracting μN^{conf} from both sides of the above equation, we obtain also:

$$\Omega(\mu, V, T) = \Omega^{bulk}(\mu, V, \phi_0, T) + \gamma A \quad (2.27)$$

where Ω , Ω^{conf} denote respectively the grand potential of confined or bulk fluid. According to morphological thermodynamics, the grand potential of an inhomogeneous fluid is written as the sum of a bulk term and a surface term with the surface tension including three contributions (flat surface term plus two curvature terms).²⁸⁻³² Although not appearing explicitly in our scaling relation, the surface tension is embodied in it. The above demonstration reveals this unambiguously and thus evidences an intimate connection between our scaling relation and the general theoretical frameworks like Gibbs theory and morphological thermodynamics. At first sight, it may appear surprising that rescaling alone fluid density can account for various fluid-solid interaction. In fact, this interaction is taken into account through the adsorption term, i.e., ΓA [see eq.(2.16)]. The discussion just given above shows further and explicitly that the interface contribution to the free energy is indeed included in our scaling relation.

Scaling relations have been found previously for some dynamic properties, e.g., entropy scaling for the diffusion coefficient of an HS fluid confined in slit pores^{168,239,240} or an LJ fluid in a zeolite,²⁴¹ or for the relaxation time of a glass-making liquid in slit pores.²⁴² Mittal, Errington, and Truskett found that the $D \sim s^{ex}$ (D : diffusion coefficient; s^{ex} : excess entropy per particle) curves of an HS fluid confined in various slit pores collapse to the bulk curve when the fluid density is calculated with the total volume instead of that accessible to the particle centers.¹⁶⁸ This way to obtain curve-collapse is, in fact, a particular case of the general scaling reported in the present work. First, the situation considered by these authors corresponds to what we called pure-confinement regime, i.e., without the second term of the scaling factor given in eq. (2.16). Our investigations show that the general scaling relation holds under wider conditions. Second, applying eq.(2.16) to the particular case of slit pores under the pure-

confinement regime consists simply in calculating the fluid density by using the total volume as did Mittal, Errington, and Truskett.¹⁶⁸ In a later study, Mittal showed that data collapse to the bulk curve can be obtained also if the diffusion coefficient is plotted as a function of compressibility factor.²⁴² Our finding reported here provides the thermodynamics foundation for this. It is to note that in the case of an HS fluid, the reduced free energy per particle, βf , is equal to the reduced entropy per particle, s/k_B . So, our results are perfectly consistent with those of Mittal et al.^{168,239,240} Moreover, in light of our finding, we can make an immediate prediction that $D \sim \mu$ curves for confined fluids collapse also to the corresponding bulk one.

2.4 Conclusion

Our simulation results establish the validity of a scaling relation for several thermodynamic functions which connects confined and bulk fluids. The invariance with respect to confining environments is discovered for Helmholtz free energy and grand-potential per particle if they are expressed as a function of chemical potential. This confers a particular significance to the use of chemical potential as an independent variable in the study of confined fluids or inhomogeneous fluids. The invariance described by eqs. (2.21) and (2.22) holds rigorously for an ideal gas confined in various pores under all the allowed thermodynamics conditions. It is really surprising that such invariance holds also when fluid-fluid interaction is present. **Fig. 2.4b** shows pretty good data-collapse in the density region where the compressibility factor deviates largely from its value for an ideal gas. It is very intriguing that confined fluids can bear perfectly a hallmark of an ideal gas far beyond the low-density region. Although a derivation of the scaling relation from first-principles is currently unavailable, we have revealed its intimate connection with general theoretical frameworks like Gibbs theory or morphological thermodynamics for inhomogeneous fluids. We believe this is why the scaling relation works so well under wide conditions and for a large variety of confining environments. The most significant message conveyed by our results is that

the apparently disconnected behaviors of confined fluids are not so disparate but can be nicely organized via scaling. The scaling relation shows clearly that the porosity (space accessibility) and fluid-solid interaction (through the adsorption term) is of primary importance for determining the thermodynamics of confined fluids. The other characteristics, like pore-connectivity, pore-shape, pore-size distribution, etc., play a less significant role. As an immediate and interesting application, our finding allows for circumventing some experimental difficulty for direct determination of some thermodynamic properties of confined fluids. A challenge in perspective is to see if the scaling relation holds also for the fluid adsorption in flexible porous materials, e.g., metal-organic frameworks (MOFs) or to find the modifications needed if necessary.

3. Development of augmented scaled particle theory

3.1 Introduction

Worked out by H. Reiss, H. L. Frisch and J. L. Lebowitz in 1959,^{204,243} scaled particle theory (SPT) has become one of the most successful theories in liquid physics with widespread applications. Since then, there have been continuous efforts to extend and improve it (see, e.g. ^{66,77,79,84,195,243–254}, which is by no means an exhaustive list of the very large number of papers on SPT in the literature). The original motivation for SPT is to derive a simple equation of state (EOS) for a bulk hard sphere (HS) fluid. Then, it was recognized that SPT provides not only the thermodynamic properties of an HS fluid in bulk but also the surface tension of an HS fluid near a spherical hard wall. Within the framework of SPT, this surface tension contains three terms, i.e., the surface tension at a flat hard wall and two contributions due to surface curvatures (mean and Gaussian curvatures). Investigations of more and more complex inhomogeneous systems, e.g., fluids adsorbed in various porous materials, arouse increasing interests in interfacial properties. Although early investigations go back to Tolman,²³³ it might appear surprising that our knowledge about curved interfaces is still quite limited.

However, the accuracy of its predictions is not as high as other recent equation of state like Carnahan-Starling (CS).²⁵⁵ To obtain an equation of state from SPT, a form of the reversible work of inserting a large hard sphere potential or a form of the central function G must be presumed. Normally, the reversible work is presented by a Laurent series,

$$\beta W(R_s) = \beta P \frac{4}{3} \pi R_s^3 + \sum_{i=0}^N \omega_i R_s^{2-i}, \quad (3.1)$$

where P is the pressure of the hard sphere fluid, ω_i is the coefficient and R_s is the radius of the inserted particle. In original work, $N = 2$ in Laurent series and three exact conditions of the reversible work was used to solve those three coefficients, the pressure

is solved by using the Gibbs-Duhem equation. In 1975, Mandell and Reiss²⁴⁹ made $N = 5$ and used five exact conditions to obtain an improved equation of state. However, the accuracy of this version is still limited, particularly at high densities. Recently, Corti and his co-workers²⁵⁶ made $N = 7$ and used five exact conditions and two approximate conditions to modified SPT. However, since an integral equation contained in those conditions, this improved SPT does not have an analytical expression. They found that increasing the number of conditions does not lead to improvement of the predictive accuracy of the fluid properties by itself.

Mecke and co-workers have made efforts to develop a general framework, named as morphological thermodynamics, to account for more complex surface morphology.^{208–210,224,257} According to Hadwiger theorem^{211,212} in integral geometry, the morphological thermodynamics postulates that the thermodynamic potential of an inhomogeneous system is determined only by four terms, i.e., one bulk contribution proportional to system's volume and three surface contributions proportional respectively to surface area, mean and Gaussian curvatures of the interface. It is to be pointed out that in SPT, the chemical potential for creating a spherical cavity inside a fluid is assumed to have this form. The foundation of morphological thermodynamics has been questioned recently.^{220–224} From molecular dynamics simulations, B.B. Laird et al found that contributions from the terms beyond the four Hadwiger's terms are not negligible.²²³ By examining the diagrammatic expansion of surface tension, I. Urrutia²²⁴ and H. Hansen-Goos²²¹ revealed also non vanishing contribution from a non Hadwiger term, and this expression implied that the non-Hadwiger coefficient only occurs when $R_s > R_l(2/\sqrt{3}-1)$, where R_l is the radius of the fluid particle. This work implies that the form of the reversible work should be presented by using multiple Laurent series in different range of R_s . It should be noted that this idea proves the basis of previous work^{249,250,256,258} about improved SPT, however, the result of non Hadwiger term from theoretical work does not have a good agreement with simulation result. In Corti's work²⁵⁶, they used a set of Laurent series to describe the reversible work. The result

improved the predictive accuracy of both thermodynamical properties and surface properties, however, this improved SPT cannot offer an analytical equation of state, since an integral equation is contained.

From these recent advances, it is clear now that the thermodynamic expression for chemical potential in the original SPT does not account for the contribution from non Hadwiger terms. One can raise naturally the following questions. Is it possible to include some non Hadwiger terms in SPT? How this can be carried out in a simple way, e.g., obtaining still analytic and improved results? We address these issues in the present work.

3.2 Original SPT

A brief recall of SPT is given first to introduce some notations and formulas needed in the following section. For the chemical potential to insert a hard scaled particle with a radius, R_s (a variable one), into a fluid of hard spheres of radius, R , the following exact but formal result is well known,²⁰⁴

$$\beta\mu_s(R_s) = \ln\left(\Lambda^3 \frac{N\Delta(R_s, R) + 1}{V}\right) - \ln p_0(R_s) \quad (3.2)$$

where Λ is the thermal wavelength, $\beta = 1/kT$ (k : Boltzmann constant, T : temperature), V is the system volume, and N is the number of hard spheres. We consider here the case that the scaled particle has the same mass as the HS particles already in the system and so they have the same thermal wavelength. The scaled particle becomes indistinguishable from the other fluid particles only when $R_s = R$. In eq. (3.2), we account for this indistinguishability by

$$\Delta(R_s, R) = \begin{cases} 1 & R_s = R \\ 0 & R_s \neq R \end{cases}, \quad (3.3)$$

In eq.(3.2), $p_0(R_s)$ is the insertion probability and the following exact expression holds,

$$p_0(R_s) = 1 + \sum_{n=1}^{\infty} F_n(R_s) \quad (3.4)$$

with

$$F_n(R_s) = \frac{1}{n!V} \int d\mathbf{r}_s \int d\mathbf{r}_1 \int d\mathbf{r}_2 \dots \int d\mathbf{r}_n \rho^{(n)}(\mathbf{r}_1, \mathbf{r}_2, \dots, \mathbf{r}_n) \prod_{i=1}^n f(|\mathbf{r}_s - \mathbf{r}_i|) \quad (3.5)$$

where $\rho^{(n)}(\mathbf{r}_1, \mathbf{r}_2, \dots, \mathbf{r}_n)$ is the distribution function of n particles located respectively at $\mathbf{r}_1, \mathbf{r}_2, \dots, \mathbf{r}_n$ and

$$f(|\mathbf{r}_s - \mathbf{r}_i|) = e^{-\beta u_s(|\mathbf{r}_s - \mathbf{r}_i|)} - 1, \quad (3.6)$$

and

$$u_s(|\mathbf{r}_s - \mathbf{r}_i|) = \begin{cases} \infty & |\mathbf{r}_s - \mathbf{r}_i| < R_s + R \\ 0 & |\mathbf{r}_s - \mathbf{r}_i| \geq R_s + R \end{cases} \quad (3.7)$$

A property of key importance of eq.(3.4) is that the higher order terms appear only successively when the radius of the scaled particle increases. For example, we have

$$F_1(R_s) = -\eta \left(1 + \frac{R_s}{R}\right)^3 \quad R_s > -R, \quad (3.8)$$

$$F_2(R_s) = \begin{cases} 0 & -R < R_s < 0 \\ 2\pi \int_{2R}^{2R+2R_s} dr r^2 \rho^{(2)}(r) \Omega_2(r, R_s) & R_s \geq 0 \end{cases}, \quad (3.9)$$

$$F_n(R_s) = 0 \quad n \geq 3 \quad -R < R_s \leq R(2 - \sqrt{3})/\sqrt{3}, \quad (3.10)$$

where $\eta = 4\pi\rho R^3/3$ is the packing fraction of hard spheres ($\rho = N/V$: density) and $\Omega(|\mathbf{r}_1 - \mathbf{r}_2|)$ is the volume of the overlapping region of two spheres having a radius of $R_s + R$ and separated by a distance of $|\mathbf{r}_1 - \mathbf{r}_2|$, which is given by

$$\Omega_2(|\mathbf{r}_1 - \mathbf{r}_2|) = \frac{2\pi}{3} \left(R_s + R - \frac{|\mathbf{r}_1 - \mathbf{r}_2|}{2} \right)^2 \left[2(R_s + R) + \frac{|\mathbf{r}_1 - \mathbf{r}_2|}{2} \right], \quad 0 < |\mathbf{r}_1 - \mathbf{r}_2| \leq 2(R_s + R). \quad (3.11)$$

Although eqs.(3.2) and (3.3) indicate a possible road for obtaining chemical potential, one encounters quickly several major obstacles on this road. First, eq. (3.4) is an

infinite series and we do not know how it converges for an arbitrary value of R_s . Moreover, only $F_1(R_s)$ has an analytical expression and it is more and more difficult to determine the other higher order terms. For $F_2(R_s)$, we only know its first three derivatives are continuous at $R_s = R(2 - \sqrt{3})/\sqrt{3}$.

The strategy used for deriving the original SPT is to use the above exact result in a limited range of R_s , i.e.,

$$\beta\mu_s(R_s) = \ln\left(\frac{\Lambda^3}{V}\right) - \ln\left[1 - \eta\left(1 + \frac{R_s}{R}\right)^3\right] \quad -R < R_s \leq 0. \quad (3.12)$$

For larger values of R_s , the following thermodynamic expression is proposed,

$$\beta W(R_s) = \ln\left(\Lambda^3 \frac{N\Delta(R_s, R) + 1}{V}\right) + w_0 + w_1 R_s + \frac{1}{2} w_2 R_s^2 + \frac{4\pi R_s^3 \beta P}{3} \quad R_s > 0, \quad (3.13)$$

Where P is the pressure of the HS fluid and the terms involving lower powers of R_s account for the surface tension around the scaled particle with w_2 being related to the flat surface contribution and w_1 , w_0 to the respective contributions from the mean and Gaussian curvatures. In eq. (3.13), there is not non Hadwiger terms, i.e., terms proportional to $(1/R_s)^n$ ($n = 1, 2, 3, \dots$). Matching eqs. (3.12) and (3.13) at $R_s = 0$, i.e., requiring the continuity of the function and the two first derivatives, one obtains,

$$w_0 = -\ln(1 - \eta), \quad (3.14)$$

$$w_1 = \frac{3\eta}{1 - \eta} \frac{1}{R}, \quad (3.15)$$

$$w_2 = \frac{3\eta}{1 - \eta} \left(2 + \frac{3\eta}{1 - \eta}\right) \frac{1}{R^2}. \quad (3.16)$$

The chemical potential, μ , and the pressure, P , can be obtained from,

$$\beta\mu = \beta W(R_s = R), \quad (3.17)$$

and Gibbs-Duhem equation, i.e.,

$$\frac{\partial(\beta P)}{\partial \rho} = \rho \frac{\partial(\beta \mu)}{\partial \rho}. \quad (3.18)$$

Finally, one obtains,

$$\frac{\beta P^{SPT}}{\rho} = \frac{1 + \eta + \eta^2}{(1 - \eta)^3}, \quad (3.19)$$

$$\beta \mu^{SPT} = \ln(\Lambda^3 \rho) - \ln(1 - \eta) + \frac{6\eta}{1 - \eta} + \frac{9}{2} \left(\frac{\eta}{1 - \eta} \right)^2 + \eta \frac{\beta P^{SPT}}{\rho}, \quad (3.20)$$

for the pressure and chemical potential of a bulk HS fluid. Moreover, one obtains also the following dimensionless result for the surface tension of an HS fluid on a spherical hard wall of radius, R_s ,

$$\tilde{\gamma}^{SPT}(R_s) = 4\pi R^2 \beta \gamma^{SPT}(R_s) = \tilde{\gamma}_0^{SPT} + \tilde{\gamma}_{-1}^{SPT} \frac{R}{R_s} + \tilde{\gamma}_{-2}^{SPT} \left(\frac{R}{R_s} \right)^2, \quad (3.21)$$

where γ_0^{SPT} is the SPT result for the surface tension of an HS fluid on a flat hard wall,

$$\tilde{\gamma}_0^{SPT} = \frac{w_2 R^2}{2} = \frac{3\eta}{2(1 - \eta)} \left(2 + \frac{3\eta}{1 - \eta} \right), \quad (3.22)$$

and γ_{-1} , γ_{-2} account for respectively the contributions to the surface tension from mean and Gaussian curvatures which have the following expressions within the framework of SPT,

$$\tilde{\gamma}_{-1}^{SPT} = w_1 R = \frac{3\eta}{1 - \eta}, \quad (3.23)$$

$$\tilde{\gamma}_{-2}^{SPT} = w_0 = -\ln(1 - \eta). \quad (3.24)$$

3.3 Augmented SPT

A. Single-point matching formulation

A conceptually simple strategy for including the leading non Hadwiger term in an

SPT type theory is to add a term proportional to $1/R_s$ into eq.(3.13). However, the immediate difficulty one meets here is that the divergence of this term at $R_s = 0$ makes the usual matching procedure impossible at this point. One possible way to circumvent this difficulty is to replace $1/R_s$ by $(1 - e^{-R_s/\delta})^3/R_s$ with δ being a positive constant to be determined later, and n can be considered from one to four. This additional term will change the formulation of other terms, ω_i ($i = 0, 1, 2$) and P . And the influence will be decreased with the increasing of n . If n is equal to one, all results of ω_i ($i = 0, 1, 2$) and P will be modified. If n is equal to four, only results of P will be changed. Here, only the version of $n = 3$, which has the best prediction of non-Hadwiger term, will be introduced here, the detail results of other versions will be presented in [Appendix A](#). The convergence factor removes the singularity at $R_s = 0$ and keeps the correct asymptotic form of the non Hadwiger term for large values of R_s . So, we propose the following expression for the chemical potential to insert a scaled particle with a radius of R_s ($R_s > 0$),

$$\beta\Phi(R_s) = \ln\left(\Lambda^3 \frac{N\Delta(R_s, R) + 1}{V}\right) + \phi_{-1} \frac{(1 - e^{-R_s/\delta})^3}{R_s} + \phi_0 + \phi_1 R_s + \frac{1}{2} \phi_2 R_s^2 + \frac{4\pi R_s^3 \beta P}{3}. \quad (3.25)$$

To determine the parameters, ϕ_n ($n = -1, 0, 1, 2$), we following a procedure similar to that used in SPT, i.e., matching eq.(3.24) with eq.(3.1) at $R_s = 0^+$ as follows,

$$\beta\mu_s(R_s = 0^+) = \beta\Phi(R_s = 0^+), \quad (3.26)$$

$$\beta\mu'_s(R_s = 0^+) = \beta\Phi'(R_s = 0^+), \quad (3.27)$$

$$\beta\mu''_s(R_s = 0^+) = \beta\Phi''(R_s = 0^+), \quad (3.28)$$

$$\beta\mu'''_s(R_s = 0^+) = \beta\Phi'''(R_s = 0^+), \quad (3.29)$$

where

$$\beta\mu_s(R_s = 0^+) = -\ln(1-\eta), \quad (3.30)$$

$$\beta\mu'_s(R_s = 0^+) = \frac{1}{R} \frac{3\eta}{1-\eta}, \quad (3.31)$$

$$\beta\mu''_s(R_s = 0^+) = \frac{1}{R^2} \frac{3\eta(2+\eta)}{(1-\eta)^2}, \quad (3.32)$$

and the third derivatives is equal to,

$$\beta\mu'''_s(R_s = 0^+) = \frac{6\eta(1+7\eta+\eta^2)}{R^3(1-\eta)^3} - \frac{9\eta(Z-1)}{R^3(1-\eta)} \quad (3.33)$$

where $Z = \beta P/\rho$ is the compressibility. From this matching, we obtain,

$$\phi_0 = w_0 = -\ln(1-\eta), \quad (3.34)$$

$$\phi_1 = w_1 = \frac{1}{R} \frac{3\eta}{1-\eta}, \quad (3.35)$$

$$\phi_2 = w_2 - \frac{2\phi_{-1}}{R} \left(\frac{R}{\delta}\right)^3 \frac{1}{R^2} = \frac{1}{R^2} \left[\frac{3\eta}{1-\eta} \left(2 + \frac{3\eta}{1-\eta}\right) - \frac{2\phi_{-1}}{R} \left(\frac{R}{\delta}\right)^3 \right], \quad (3.36)$$

$$\frac{\phi_{-1}}{R} = \left(\frac{\delta}{R}\right)^4 \left[\frac{\eta(5-2\eta)}{3(1-\eta)} \frac{\beta P}{\rho} - \frac{\eta(5\eta+8\eta^2+5\eta^3)}{3(1-\eta)^3} \right]. \quad (3.37)$$

From eqs. (3.25), (3.34)-(3.37), we obtain the following expression for the chemical potential,

$$\begin{aligned} \beta\mu = \beta\Phi(R_s = R) = & \ln(\Lambda^3\rho) - \ln(1-\eta) + \frac{6\eta}{1-\eta} + \frac{9}{2} \left(\frac{\eta}{1-\eta}\right)^2 + \eta \frac{\beta P}{\rho} \\ & + \frac{\phi_{-1}}{R} \left[\left(1 - e^{-R/\delta}\right) - \left(\frac{R}{\delta}\right)^3 \right]. \end{aligned} \quad (3.38)$$

Substituting eq.(3.37) into eq.(3.38) leads to an equation involving chemical potential, μ , and pressure, P . With the help of Gibbs-Duhem equation, one can eliminate either μ or P and obtain a first order differential equation for P or μ . Because this is a differential equation with non-constant coefficients, it is not possible to solve it analytically. Nevertheless, this difficulty can be circumvented by an iterative procedure to obtain successively analytic results for chemical potential and pressure. One can start

the iteration by substituting the SPT result for the pressure into the right-hand side (RHS) of eqs.(3.37) and (3.38), which leads to the following results after the first iteration and we name it as ASPT1,

$$\frac{\phi_{-1}}{R} = \left(\frac{\delta}{R}\right)^4 \left(\frac{\eta}{1-\eta}\right)^3 \left(2 + \frac{3\eta}{1-\eta}\right), \quad (3.39)$$

$$\beta\mu^{ASPT1} = \beta\mu^{SPT} - a(\delta) \left(\frac{\eta}{1-\eta}\right)^3 \left(2 + \frac{3\eta}{1-\eta}\right), \quad (3.40)$$

where

$$a(\delta) = \left(\frac{\delta}{R}\right) \left[1 - (1 - e^{-R/\delta})^3 \left(\frac{\delta}{R}\right)^3\right], \quad (3.41)$$

Substituting then the result for chemical potential given in eq.(3.40) into Gibbs-Duhem equation and integrating the latter, we obtain the following ASPT1 result for pressure,

$$\frac{\beta P^{ASPT1}}{\rho} = \frac{\beta P^{SPT}}{\rho} - 6a(\delta) \left\{ \frac{1}{2} \frac{\eta}{1-\eta} \left[\left(\frac{\eta}{1-\eta}\right)^3 + \frac{1}{3} \left(\frac{\eta}{1-\eta}\right)^2 + \frac{1}{3} \frac{\eta}{1-\eta} - 1 \right] - 1 - \frac{1}{\eta} \ln(1-\eta) \right\}, \quad (3.42)$$

The surface tension near a spherical hard wall is given by

$$\begin{aligned} \tilde{\gamma}^{ASPT1}(R_s) = 4\pi R^2 \beta\gamma^{ASPT1}(R_s) = & \tilde{\gamma}_0^{ASPT1} + \tilde{\gamma}_{-1}^{ASPT1} \frac{R}{R_s} + \tilde{\gamma}_{-2}^{ASPT1} \left(\frac{R}{R_s}\right)^2 \\ & + \tilde{\gamma}_{-3}^{ASPT1} \left(\frac{R}{R_s}\right)^3 (1 - e^{-R_s/\delta})^3, \end{aligned} \quad (3.43)$$

where

$$\tilde{\gamma}_0^{ASPT1} = \frac{\phi_2 R^2}{2} = \tilde{\gamma}_0^{SPT} - \tilde{\gamma}_{-3}^{ASPT1} \left(\frac{R}{\delta}\right)^3, \quad (3.44)$$

$$\tilde{\gamma}_{-1}^{ASPT1} = \phi_1 R = \tilde{\gamma}_{-1}^{SPT}, \quad (3.45)$$

$$\tilde{\gamma}_{-2}^{ASPT1} = \phi_0 = \tilde{\gamma}_{-2}^{SPT}, \quad (3.46)$$

$$\tilde{\gamma}_{-3}^{ASPT1} = \frac{\phi_{-1}}{R} = \left(\frac{\eta}{1-\eta}\right)^3 \left(2 + \frac{3\eta}{1-\eta}\right) \left(\frac{\delta}{R}\right)^4, \quad (3.47)$$

In the results given above, there remains a parameter, i.e., δ , to be determined. We will propose, in Section 3.3, a pragmatic recipe for this and discuss in more details the accuracy of ASPT1.

The same idea can be used to treat the multi-components system. As presented in previous work,¹⁹³ the excess chemical potential for inserting a scaled particle with a radius, R_s , into a n -component system is

$$\mu_s^{ex}(R_s) = -\ln[p_0(R_s)], \quad (3.48)$$

where $p_0(R_s)$ is the probability of finding a spherical cavity with radius equal to $R_s + \min\{R_1, \dots, R_n\}$, and the exact result for this insertion probability of a small scaled particle is

$$p_0(R_s) = 1 - \sum_{\lambda=1}^n \eta_\lambda (1 + R_s/R_\lambda)^3, \quad -\min\{R_1, \dots, R_n\} \leq R_s \leq 0, \quad (3.49)$$

where η_λ is the packing fraction of species λ . Then the chemical potential and its first three derivatives when $R_s = 0^+$ can be derived as following,

$$\beta\mu_s^{ex}(R_s = 0^+) = -\ln(1 - \xi_3), \quad (3.50)$$

$$\beta\mu_s'(R_s = 0^+) = \frac{6\xi_2}{1 - \xi_3}, \quad (3.51)$$

$$\beta\mu_s''(R_s = 0^+) = 24 \frac{\xi_1}{1 - \xi_3} + 36 \frac{\xi_2^2}{(1 - \xi_3)^2}, \quad (3.52)$$

$$\beta\mu_s'''(R_s = 0^+) = 48 \frac{\xi_0}{1 - \xi_3} + 9 \frac{\xi_1 \xi_2}{(1 - \xi_3)^2} - 9 \frac{\xi_2^3}{(1 - \xi_3)^2} - 72 \frac{(Z-1)\xi_0}{1 - \xi_3}. \quad (3.53)$$

where $Z = \beta P / \sum_{i=1}^n \rho_i$ is the compressibility, and $\xi_i = \frac{\pi}{6} \sum_{j=1}^n \rho_j (2R_j)^i$. Then the

expression of the chemical potential to insert a scaled particle with a radius R_s ($R_s > 0$) is same with the one for one-component system, i.e., eq.(3.25). To determine the

parameters, ϕ_n , the following four conditions are used,

$$\beta\mu_s(R_s = 0^+) = \beta\Phi(R_s = 0^+), \quad (3.54)$$

$$\beta\mu'_s(R_s = 0^+) = \beta\Phi'(R_s = 0^+), \quad (3.55)$$

$$\beta\mu''_s(R_s = 0^+) = \beta\Phi''(R_s = 0^+), \quad (3.56)$$

$$\beta\mu'''_s(R_s = 0^+) = \beta\Phi'''(R_s = 0^+). \quad (3.57)$$

Then the four unknown parameters, ϕ_n ($n = -1, 0, 1, 2$), are obtained as following,

$$\phi_{-1} = -\delta^4 \left[\frac{40}{3} \frac{\xi_0}{1-\xi_3} + 48 \frac{\xi_2^3}{(1-\xi_3)^3} + 48 \frac{\xi_1 \xi_2}{(1-\xi_3)^2} \right] - \delta^4 Z \xi_0 \left(\frac{40}{3} + 8 \frac{\xi_3}{1-\xi_3} \right), \quad (3.58)$$

$$\phi_2 = 12 \left[2 \frac{\xi_1}{1-\xi_3} + 3 \frac{\xi_2^2}{(1-\xi_3)^2} \right] - \frac{2\phi_{-1}}{\delta^3}, \quad (3.59)$$

$$\phi_1 = 6 \frac{\xi_2}{1-\xi_3}, \quad (3.60)$$

$$\phi_0 = -\ln(1-\xi_3). \quad (3.61)$$

By using the same iterative procedure, the chemical potential of i -component equals to

$$\beta\mu_i^{ex} = -\ln(1-\xi_3) + \phi_1 R_i + \frac{\phi_2}{2} R_i^2 + 8\xi_0 Z^{SPT} R_i^3 + \phi_{-1} \frac{(1-e^{-R_i/\delta})^3}{R_i}, \quad (3.62)$$

where Z^{SPT} is the compressibility of original SPT, then by using Gibbs-Duhem equation, the compressibility of ASPT1 for multi-component system can be expressed as

$$Z = \xi_0 \left[\frac{\xi_0}{1-\xi_3} + 3 \frac{\xi_1 \xi_2}{(1-\xi_3)^2} + 3 \frac{\xi_2^3}{1-\xi_3} \right]. \quad (3.63)$$

Here, I would like to mention that if the number of components is equal to one, all above results will be reduced to the corresponding ones of a one-component system, automatically.

B. Double-point matching formulation

ASPT1 presented above is not an entirely self-contained theory in the sense that it

contains an adjustable parameter, i.e., δ . In the followings, we will show it is also possible to develop an augmented scaled particle theory without any adjustable parameter. To circumvent the difficulty due to the divergence of the leading non Hadwiger term, $1/R_s$, at $R_s = 0$, we propose to extrapolate the exact result for a small scaled particle, i.e., eq.(3.12), to a thermodynamics expression for a large scaled particle in two steps instead of one used for SPT or ASPT1. The first extrapolation is carried out for a scaled particle with a radius in the region of $0 \leq R_s \leq d = (2/\sqrt{3}-1)R$ (note that $R + d$ is the radius of a sphere which can contain at most three hard spheres of radius, R). We propose the following expression for the chemical potential of the scaled particle with a radius in this region,

$$\beta U(R_s) = \ln\left(\frac{\Lambda^3}{V}\right) + u_0 + u_1 R_s + \frac{1}{2} u_2 R_s^2 + \frac{4\pi R_s^3 \beta P_1}{3} \quad 0 \leq R_s \leq d \quad (3.64)$$

Since the non Hadwiger term, $1/R_s$, is not included here, there is no singularity at $R_s = 0$, we can make the matching of eqs. (3.2) and (3.64) without any problem, i.e.,

$$\beta \mu_s(R_s = 0^+) = \beta U(R_s = 0^+), \quad (3.65)$$

$$\beta \mu'_s(R_s = 0^+) = \beta U'(R_s = 0^+), \quad (3.66)$$

$$\beta \mu''_s(R_s = 0^+) = \beta U''(R_s = 0^+), \quad (3.67)$$

$$\beta \mu'''_s(R_s = 0^+) = \beta U'''(R_s = 0^+). \quad (3.68)$$

From this matching, we obtain,

$$u_0 = w_0 = -\ln(1-\eta) \frac{1}{2}, \quad (3.69)$$

$$u_1 = w_1 = \frac{3\eta}{1-\eta} \frac{1}{R}, \quad (3.70)$$

$$u_2 = w_2 = \frac{3\eta}{1-\eta} \left(2 + \frac{3\eta}{1-\eta}\right) \frac{1}{R^2}, \quad (3.71)$$

$$\begin{aligned}
8\pi\beta P_1 &= \frac{6\eta}{1-\eta} \left[1 + \frac{9\eta}{1-\eta} + 9 \left(\frac{\eta}{1-\eta} \right)^2 - \frac{R^3 F_2''(R_s = 0^+)}{6(1-\eta)} \right] \frac{1}{R^3}, \\
&= \frac{6\eta}{1-\eta} \left[1 + \frac{9\eta}{1-\eta} + 9 \left(\frac{\eta}{1-\eta} \right)^2 - \frac{3}{2} \left(\frac{\beta P_1}{\rho} - 1 \right) \right] \frac{1}{R^3},
\end{aligned} \tag{3.72}$$

where

$$F_2''(R_s = 0^+) = 16\pi^2 \rho^2 (2R)^3 g(2R^+) = \frac{18\eta}{R^3} \left(\frac{\beta P_1}{\rho} - 1 \right), \tag{3.73}$$

and $g(2R^+)$ is the contact radial distribution function and the Virial equation for the pressure of an HS fluid was used when going to the last equality in eq.(3.72). It is to note that eq.(3.72) yields immediately an expression for the pressure, i.e.,

$$\frac{\beta P_1}{\rho} = \frac{1}{1-2\eta/5} \left[1 + \frac{18}{5} \frac{\eta}{1-\eta} \left(1 + \frac{\eta}{1-\eta} \right) \right]. \tag{3.74}$$

At this stage, the above equation of state can be considered as the result of a new variant of scaled particle theory. As we will show in Section 3 that eq.(3.74) underestimates the pressure and gives less accurate results than the original SPT. It is emphasized that we will use eq.(3.64) and the coefficients given in eqs.(3.69)-(3.71) and (3.74) as the results of a first extrapolation of the chemical potential to insert a larger scaled particle with a radius in the region of $0 \leq R_s \leq d = (2/\sqrt{3}-1)R$.

For a scaled particle with a radius larger than d , we use the following expression for its chemical potential including the leading non Hadwiger term,

$$\begin{aligned}
\beta W(R_s) &= \ln \left(\Lambda^3 \frac{N\Delta(R_s, R) + 1}{V} \right) + w_{-1} \frac{1}{R_s} + w_0 + w_1 (R_s - d) \\
&\quad + \frac{1}{2} w_2 (R_s - d)^2 + \frac{4\pi (R_s - d)^3 \beta P}{3}
\end{aligned} \tag{3.75}$$

$R_s \geq d,$

The coefficients in eq.(3.75) ($w_n, n = -1, 0, 1, 2,$) are determined by matching eqs.

(3.64) and (3.75) at $R_s = d$, i.e.,

$$\beta W(R_s = d) = \beta U(R_s = d), \tag{3.76}$$

$$\beta W'(R_s = d) = \beta U'(R_s = d), \quad (3.77)$$

$$\beta W''(R_s = d) = \beta U''(R_s = d), \quad (3.78)$$

$$\beta W'''(R_s = d) = \beta U'''(R_s = d). \quad (3.79)$$

We obtain then,

$$w_0 = u_0 + Ru_1 \frac{d}{R} + \frac{R^2 u_2}{2} \left(\frac{d}{R}\right)^2 + \eta \frac{\beta P_1}{\rho} \left(\frac{d}{R}\right)^3 - \frac{w_{-1}}{R} \frac{R}{d}, \quad (3.80)$$

$$Rw_1 = Ru_1 + R^2 u_2 \frac{d}{R} + 3\eta \frac{\beta P_1}{\rho} \left(\frac{d}{R}\right)^2 + \frac{w_{-1}}{R} \left(\frac{R}{d}\right)^2, \quad (3.81)$$

$$R^2 w_2 = R^2 u_2 + 6\eta \frac{\beta P_1}{\rho} \frac{d}{R} - \frac{2w_{-1}}{R} \left(\frac{R}{d}\right)^3, \quad (3.82)$$

$$\frac{w_{-1}}{R} = \left(\frac{d}{R}\right)^4 \eta \frac{\beta(P - P_1)}{\rho}. \quad (3.83)$$

Now, we find readily the following result for chemical potential,

$$\begin{aligned} \beta\mu &= \beta W(R_s = R) \\ &= \ln(\Lambda^3 \rho) + \eta \frac{\beta P}{\rho} - \ln(1 - \eta) + \frac{6\eta}{1 - \eta} + \frac{9}{2} \left(\frac{\eta}{1 - \eta}\right)^2 \\ &\quad - \left[1 - \left(1 - \frac{d}{R}\right)^4\right] \eta \frac{\beta(P - P_1)}{\rho} \end{aligned} \quad (3.84)$$

Taking derivative with respect to density on both sides of eq.(3.84) and using Gibbs-Duhem equation, i.e., eq.(3.18), allow for obtaining a first order differential equation either for the chemical potential or for the pressure. Again, the resulting differential equation does not have constant coefficients and this prevents us from solving it analytically. By adopting the same iterative procedure as for ASPT1 [i.e., using the SPT value for pressure on the RHS of eq.(3.84), we obtain the following results (named as ASPT2) for chemical potential and pressure after the first iteration,

$$\beta\mu^{ASPT2} = \beta\mu^{SPT} - A \left[5 \frac{\eta}{1 - \eta} - \frac{25}{2} \frac{2\eta/5}{1 - 2\eta/5} - 3 \left(\frac{\eta}{1 - \eta}\right)^2 + 3 \left(\frac{\eta}{1 - \eta}\right)^3 \right], \quad (3.85)$$

$$\frac{\beta P^{ASPT2}}{\rho} = \frac{\beta P^{SPT}}{\rho} - A \left\{ 20 \left[1 + \frac{1}{\eta} \ln(1-\eta) \right] - \frac{9}{2} \left(\frac{\eta}{1-\eta} \right)^2 + 3 \left(\frac{\eta}{1-\eta} \right)^3 - \frac{25}{2} \left[1 + \frac{5}{2\eta} \ln(1-2\eta/5) + \frac{2\eta/5}{1-2\eta/5} - \frac{\eta}{1-\eta} \right] \right\}, \quad (3.86)$$

where

$$A = \frac{256\sqrt{3} - 439}{9}. \quad (3.87)$$

From eq.(3.75), we obtain the following ASPT2 result for the surface tension (dimensionless one) of an HS fluid against a spherical hard wall,

$$\begin{aligned} \tilde{\gamma}^{ASPT2}(R_s) &= 4\pi R^2 \beta \gamma^{ASPT2}(R_s) \\ &= \tilde{\gamma}_0^{ASPT2} + \tilde{\gamma}_{-1}^{ASPT2} \frac{R}{R_s} + \tilde{\gamma}_{-2}^{ASPT2} \left(\frac{R}{R_s} \right)^2 + \tilde{\gamma}_{-3}^{ASPT2} \left(\frac{R}{R_s} \right)^3, \end{aligned} \quad (3.88)$$

where

$$\tilde{\gamma}_0^{ASPT2} = \tilde{\gamma}_0^{SPT} - 4\tilde{\gamma}_{-3}^{ASPT2} \left(\frac{3}{2\sqrt{3}-3} \right)^3, \quad (3.89)$$

$$\tilde{\gamma}_{-1}^{ASPT2} = \tilde{\gamma}_{-1}^{SPT} + 6\tilde{\gamma}_{-3}^{ASPT2} \left(\frac{3}{2\sqrt{3}-3} \right)^2, \quad (3.90)$$

$$\tilde{\gamma}_{-2}^{ASPT2} = \tilde{\gamma}_{-2}^{SPT} - 4\tilde{\gamma}_{-3}^{ASPT2} \frac{3}{2\sqrt{3}-3}, \quad (3.91)$$

$$\tilde{\gamma}_{-3}^{ASPT2} = \left\{ \frac{\eta}{1-\eta} \left[5 - \frac{3\eta}{1-\eta} + 3 \left(\frac{\eta}{1-\eta} \right)^2 \right] - \frac{25}{2} \frac{2\eta/5}{1-2\eta/5} \right\} \left(\frac{2\sqrt{3}-3}{3} \right)^4. \quad (3.92)$$

The same idea can be used to treat the multi-component system. The expression of chemical potential for a multi-component system can be expressed as following,

$$\beta\mu_s^{ex}(R_s) = \begin{cases} \ln \left[1 - \sum_{\lambda=1}^n \eta_{\lambda} (1 + R_s/R_{\lambda})^3 \right], & -R_i \leq R_s < 0 \\ u_0 + u_1 R_s + \frac{1}{2} u_2 R_s^2 + \frac{4\pi R_s^3 \beta P_1}{3}, & 0 \leq R_s \leq d, \quad (3.93) \\ w_{-1} \frac{1}{R_s} + w_0 + w_1 (R_s - d) + \frac{1}{2} w_2 (R_s - d)^2 \\ \quad + \frac{4\pi (R_s - d)^3 \beta P}{3}, & R_s \geq d \end{cases}$$

where $d = (2/\sqrt{3} - 1)R_i$ represents the radius of i -component fluid particle. One should be noted that R_i should present, in principle, the radius of the smallest fluid particle. However, this restriction is not used in this paper. Eqs. (3.65)-(3.68) and (3.76)-(3.79) are used to solve the parameters, w_n . Then w_n is obtained as following,

$$w_{-1} = 8BR_i^4 Z^{SPT} \xi_0 - BR_i^4 \left[\frac{8\xi_0}{1-2\xi_3/5} + \frac{144\xi_1\xi_2/5}{(1-2\xi_3/5)(1-\xi_3)} + \frac{144\xi_2^3/5}{(1-2\xi_3/5)(1-\xi_3)^2} \right], \quad (3.94)$$

$$w_0 = -\ln(1-\xi_3) - 4(3+2\sqrt{3})\frac{w_{-1}}{R_i}, \quad (3.95)$$

$$w_1 = \frac{6\xi_2}{1-\xi_3} + 18(7+4\sqrt{3})\frac{w_{-1}}{R_i^2}, \quad (3.96)$$

$$w_2 = 12 \left[\frac{2\xi_1}{1-\xi_3} + \frac{3\xi_2^2}{(1-\xi_3)^2} \right] - 24(45+26\sqrt{3})\frac{w_{-1}}{R_i^3}, \quad (3.97)$$

where $B = (97 - 56\sqrt{3})/9$. Then, the excess chemical potential equals to

$$\beta\mu_i^{ex} = -\ln(1-\xi_3) + w_1 R_i + \frac{w_2}{2} R_i^2 + 8\xi_0 Z^{SPT} R_i^3 + \frac{w_{-1}}{R_i}. \quad (3.98)$$

Same with the APST1 for multi-component system, the above results also can be reduced to the corresponding ones of a one-component system. Also, same with the original SPT, the above results can be obtained by considering a simple mixing rule from the one-component system.¹⁹³

3.4 Results and discussion

In this section, we are going to assess the accuracy of our two ASPT. Our new results will be compared with molecular simulation and previous works, i.e. SPT_{7M} ²⁵⁶, original SPT^{204,243}, CS-SPT²⁵⁸, CS-SPT_M²⁴⁶, and MFMT²⁵⁹. One should note SPT_{7M} does not have an analytical expression, we only compare with SPT_{7M} in chemical potential and surface tension. MFMT, CS-SPT, and CS-SPT_M are obtained by using Carnahan-Starling equation of state as an input which means the expressions of pressure and chemical potential from those two versions are same with Carnahan-Starling equation of state.

A. Determination of the adjustable parameter in ASPT1

Before ASPT1 can be used in practice, we still need to determine parameter, δ . An appealing recipe for this is to adjust δ in such a way that the pressure given by eq.(3.41) is as close as that of Carnahan-Starling equation, which has the following expression,

$$\frac{\beta P^{CS}}{\rho} = \frac{\beta P^{SPT}}{\rho} - \left(\frac{\eta}{1-\eta} \right)^3. \quad (3.99)$$

Since P^{SPT} is different from P^{CS} only at high fluid densities, requiring $P^{ASPT1} = P^{CS}$ at a high fluid density (with $\eta = 0.5$ being chosen here) should allow for obtaining accurate values of pressure from ASPT1. This leads to the following equation for determining δ ,

$$\frac{\delta}{R} \left[1 - \left(\frac{\delta}{R} \right)^3 (1 - e^{-R/\delta})^3 \right] = \frac{1}{4(3 \ln 2 - 1)}. \quad (3.100)$$

From eqs.(3.40) and (3.41), we see that any positive root of eq.(3.100) smaller than $R/3$ can decrease the pressure given by SPT so that P^{ASPT1} becomes possibly close to P^{CS} . Solving eq.(3.100), we find only one positive root in the considered region, $\delta/R = 0.234499$. Alternatively, if we require $P^{ASPT1} = P^{ASPT2}$ at $\eta = 0.5$, we obtain the

following equation for δ ,

$$\frac{\delta}{R} \left[1 - \left(\frac{\delta}{R} \right)^3 \left(1 - e^{-R/\delta} \right)^3 \right] = \frac{256\sqrt{3} - 439}{576(3\ln 2 - 1)} \left(\frac{123}{8} + \frac{125}{2} \ln 5 - 165 \ln 2 \right) \quad (3.101)$$

From this equation, we find $\delta/R = 0.181952$. The two values for δ give essentially the same results for pressure (see [Fig. 3.1](#)) and in the following discussions, we will use $\delta/R = 0.234499$ for ASPT1.

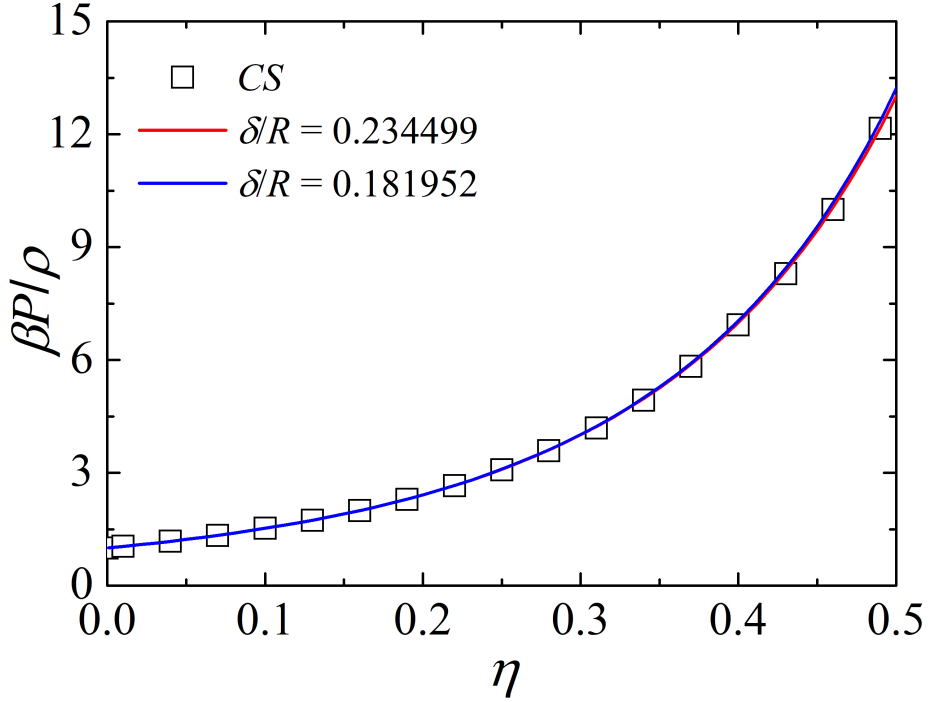


Figure 3.1. Comparison of pressure of a hard sphere fluid. The CS results are presented by black squares, the red line is ASPT1 with $\delta/R = 0.234499$, and the blue line is ASPT1 with $\delta/R = 0.181952$.

B. Pressure

[Fig. 3.2](#) shows the comparison of the pressure, $\beta P / \rho$, obtained by ASPT1 and ASPT2 with the results of molecular simulation and previous work, i.e. SPT_{7M}, CS, and SPT3. Our results are much closer to simulation values than original SPT. In fact, ASPT1 and ASPT2 are nearly indistinguishable from the simulation and Carnahan-Starling equation of state on the scale of the plot. Unquestionably, the additional term,

$1/R_s$, significantly improve the accuracy of pressure. This can be considered as evidence of morphological thermodynamic is only a good approximation. **Fig. 3.2** also shows ASPT2 slightly overestimated the pressure at high packing fraction.

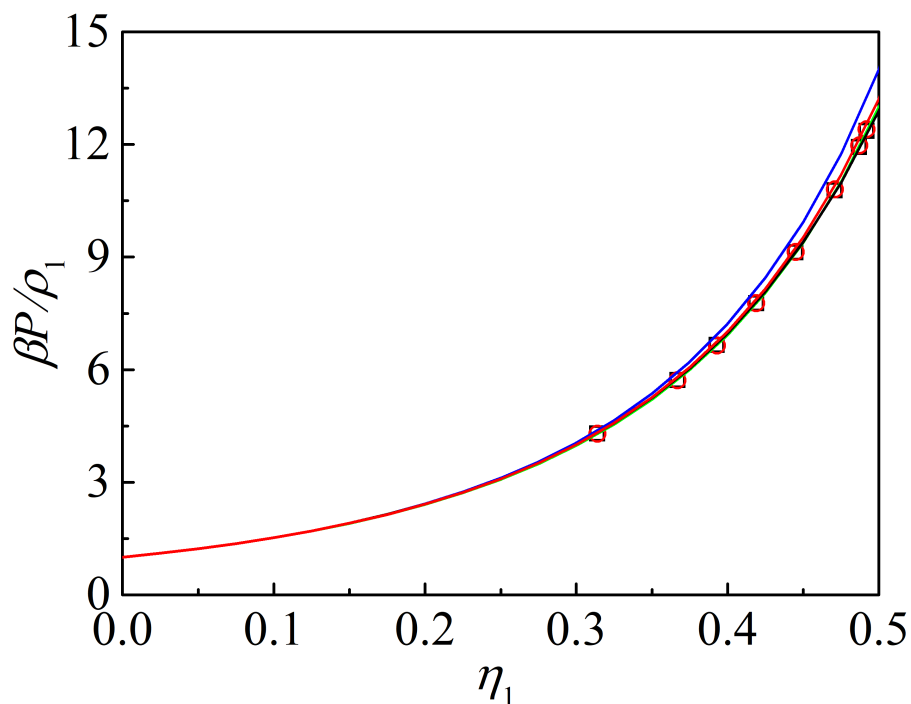


Figure 3.2. Comparison of pressure of a hard sphere fluid. The simulation results are presented by black squares, the red circle is SPT_{7M} , the green line CS, the blue line SPT_3 , the black line ASPT1, the red line ASPT2.

In **Table 3.1** we compare the first 10 Virial coefficients obtained from ASPT1 and ASPT2 with the prediction from original SPT, Carnahan-Starling equation of state, and the exact values. One unanticipated finding is that the prediction of Virial coefficients from ASPT2 is more accurate than all other versions, while ASPT2 was found to slightly overestimate the pressure in **Fig. 3.1**. From **Table 3.1**, it shows that all equations of state can offer exact first three Virial coefficients, all equations of state overestimate the Virial coefficients but the ASPT1 underestimate it. The choice of the parameter, δ , is the reason, and if we decrease δ , the prediction will be closer to the exact ones,

however, the prediction of pressure and surface tension becomes worse. Carnahan-Starling equation of state still has the best accuracy among those equations of state. The prediction from ASPT and ASPT2 are better than original SPT, especially ASPT2 almost has the same accuracy with Carnahan-Starling equation of state. One should note that all SPT results always overestimate or underestimate the Virial coefficients, but the prediction of Carnahan-Starling equation of state underestimates the fourth and fifth Virial coefficients and overestimates the others.

Table 3.1. Virial coefficients for hard sphere fluid

n	Exact	SPT	CS	ASPT1	ASPT2
2	4	4	4	4	4
3	10	10	10	10	10
4	18.3647	19	18	18.6526	18.5595
5	28.2245(10)	31	28	29.3325	29.1675
6	39.81545(15)	46	40	41.368	41.5656
7	53.3418(15)	64	54	54.0742	55.631
8	68.534(88)	85	70	66.7614	71.3043
9	85.805(58)	109	88	78.7375	88.5556
10	105.8(4)	136	108	89.3093	107.369

C. Surface tension

Now, we proceed to assess the accuracy of ASPT1 and ASPT2. SPT does not only provide the expression of some thermodynamic properties but also provides the expressions of some surface properties, such as surface tension and Tolman length. [Fig. 3.2](#) plots the planar surface tension of hard sphere fluid obtained from CS-SPT, CS-SPTM, original SPT, MFMT, molecular simulation, and two new ASPT. From [Fig. 3.2](#), it shows all versions of SPT have the same trend with molecular simulation but the CS-

SPT. CS-SPT appears a different trend with molecular simulation results in the high packing fraction. The original SPT overestimates the surface tension. Except CS-SPT and original SPT, all equations of state are nearly indistinguishable from the simulation results on the scale of the plot.

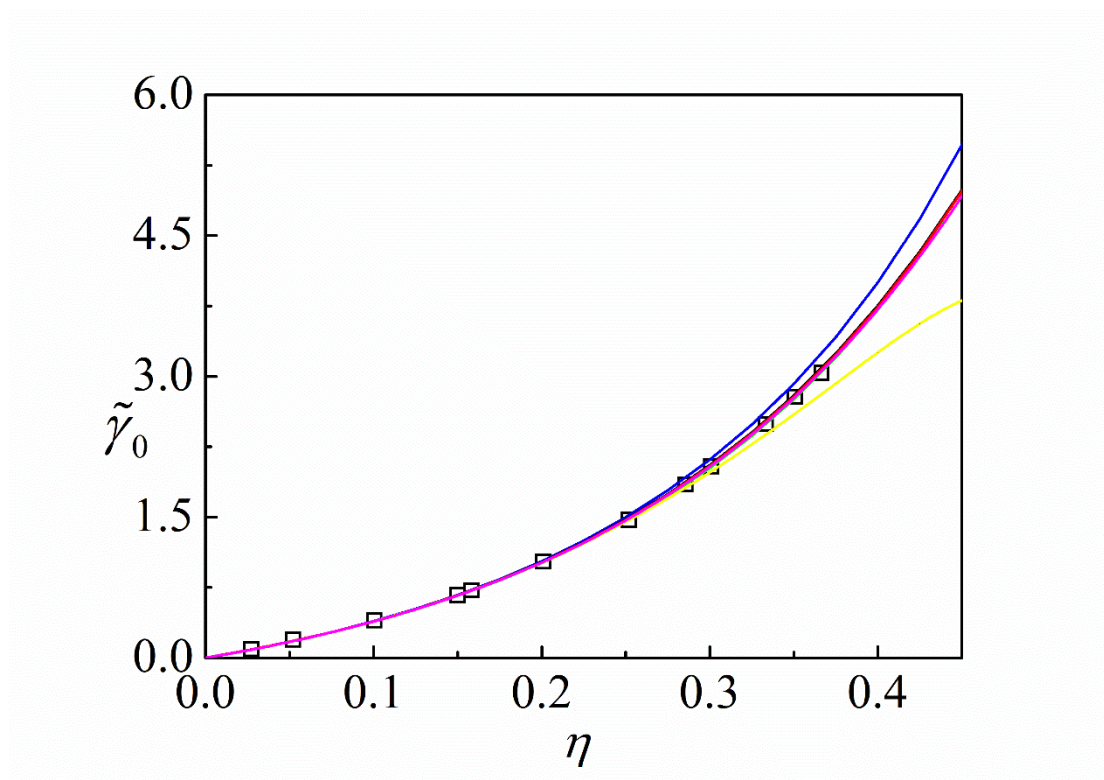


Fig. 3.2. Comparison of surface tension of a hard sphere fluid. The simulation results are presented by black squares, the green line MFMT, the blue line SPT, the black line SPT5, the red line ASPT2, the yellow line CS-SPT, the magenta line CS-SPTM

In most recent work, Urrutia²²⁴ reported the first four exact Virial coefficients of planar surface tension as following,

$$\tilde{\gamma}_0 = 3\eta + \frac{15}{2}\eta^2 + \frac{759}{70}\eta^3 + O(\eta^4) \quad (3.102)$$

Table 3.2 shows the comparison of the Virial coefficients obtained from MFMT, CS-SPT, CS-SPT_M, original SPT, ASPT1, and ASPT2 with exact values. **Table 3.2** shows that all equations of state can offer the exact first two Virial coefficients of planar surface. For fourth Virial coefficient, the result from CS-SPT_M is slightly better than

any other equations of state result. ASPT1 and ASPT2 improve the prediction of fourth Virial coefficient compare with original SPT. Although CS-SPT does not have the same trend with molecular simulation result in high packing fraction, the first four virial coefficients are more accurate than original SPT, which means in the high packing fraction, the planar surface tension is dominant under the higher Virial coefficients.

Table 3.2: Virial coefficients of planar surface tension

n	Exact	CS-SPT	CS-SPT _M	SPT	MFMT	ASPT1	ASPT2
2	3	3	3	3	3	3	3
3	7.5	7.5	7.5	7.5	7.5	7.5	7.5
4	10.842	11.667	10.854	12	10.333	11.531	11.257

When a hard sphere fluid in contact with a curved surface, the surface tension should be written as following,

$$\tilde{\gamma} = \tilde{\gamma}_0 + \tilde{\gamma}_{-1} \frac{R}{R_s} + \tilde{\gamma}_{-2} \left(\frac{R}{R_s} \right)^2, \quad (3.103)$$

where R_s is the radius of a spherical wall, $\tilde{\gamma}_{-1} = \delta_T R \tilde{\gamma}_0$, $\tilde{\gamma}_{-2} = \delta_T R \tilde{\gamma}_0$ is the Tolman length and $\tilde{\gamma}_{-2}/4\pi$ is the bending rigidity. Since the prediction of $\tilde{\gamma}_{-1}$ and $\tilde{\gamma}_{-2}$ from ASPT1 are identical with original SPT, in the following discussion, we will only consider original SPT. **Fig. 3.3** plots the prediction of $\tilde{\gamma}_{-1}$ from MFMT, original SPT, CS-SPT, CS-SPT_M, ASPT2, and molecular simulation results. **Fig. 3.3** shows that all equations of state have a good agreement with simulation results but the CS-SPT. Compare CS-SPT and CS-SPT_M, one can find that using two Laurent series to describe the reversible work will significantly improve the predictive accuracy of surface properties. Compare with original SPT, MFMT, and ASPT2 slightly improve the prediction of $\tilde{\gamma}_{-1}$. One should be noted that CS-SPT_M has a different trend with the other equation of state. In moderate packing fraction, the prediction of CS-SPT_M is

lower than simulation results. In high packing fraction, the prediction of CS-SPT_M is higher than the results from other equation of state. Because lack of simulation result, we do not know which result is correct in high packing fraction, it means that the future study is needed.

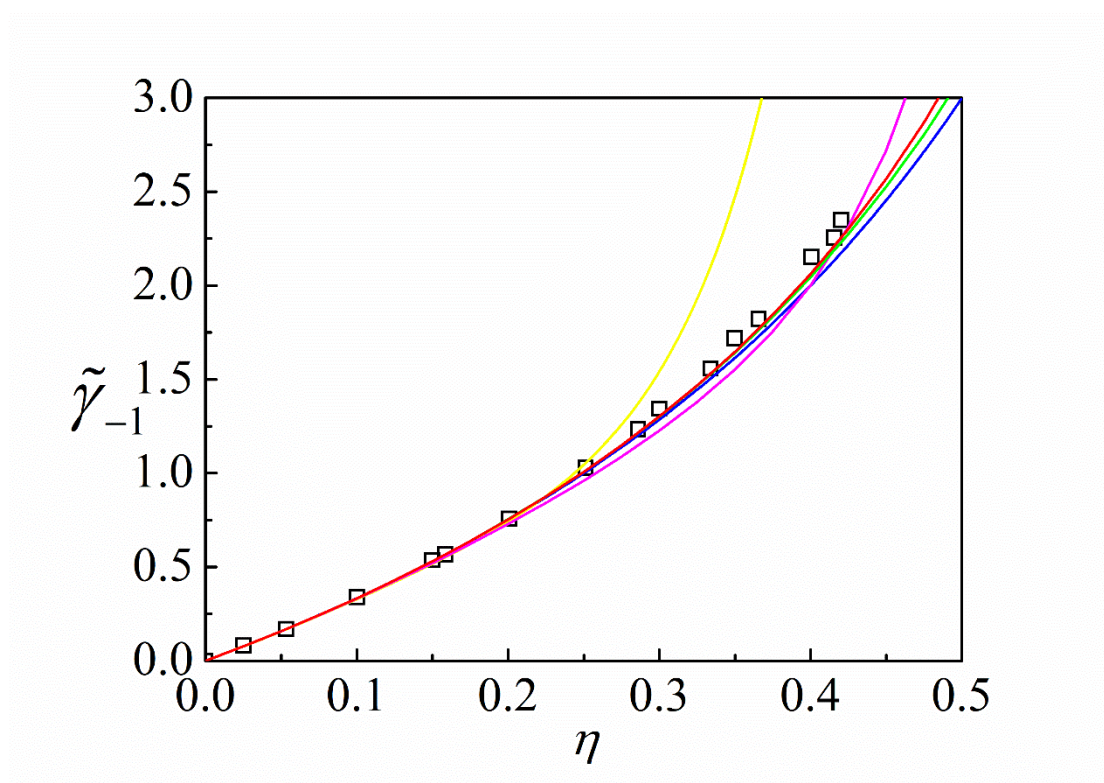


Figure 3.3. Comparison of $\tilde{\gamma}_{-1}$ of a hard sphere fluid. The simulation results are presented by black squares, the green line MFMT, the blue line SPT, the red line ASPT2, the yellow line CS-SPT, the magenta line CS-SPT_M

The first four Virial coefficients of $\tilde{\gamma}_{-1}$ was provided by Urrutia²²⁴, the expression is given as following,

$$\tilde{\gamma}_{-1} = 3\eta \left[1 + \eta + \left(\frac{8}{35} + \frac{27\sqrt{3}}{16\pi} \right) \eta^2 \right] + O(\eta^4). \quad (3.104)$$

Table 3.3 shows that all equation of state can provide exact first three Virial coefficients of $\tilde{\gamma}_{-1}$. The prediction of the fourth Virial coefficient from CS-SPT has a different sign

with the exact result, this can explain why the prediction of $\tilde{\gamma}_{-1}$ from CS-SPT is bad. The prediction from CS-SPTM is also away from the exact one, but much better than CS-SPT. The prediction from ASPT2 is closer to the exact value than original SPT. One unanticipated finding was that the prediction from MFMT is more accurate, while the prediction of $\tilde{\gamma}_{-1}$ is not good.

Table 3.3: Virial coefficients of $\tilde{\gamma}_{-1}$

n	Exact	CS-SPT	CS-SPT _M	SPT	MFMT	ASPT2
2	3	3	3	3	3	3
3	3	3	3	3	3	3
4	3.477	-3.333	0.903	3	3.333	3.172

In the final part of this section, $\tilde{\gamma}_{-2}$ are considered. Since the prediction of $\tilde{\gamma}_{-2}$ from CS-SPT and CS-SPT_{5M} are terrible, we will not compare them here. **Fig. 3.4** plots the prediction of $\tilde{\gamma}_{-2}$ from MFMT, ASPT2, and molecular simulation. As shown in **Fig. 3.4**, except for ASPT2, all equation of state has the same accuracy in $\tilde{\gamma}_{-2}$. The prediction from ASPT2 slightly improves the original SPT's result. As previous part, here, the Virial coefficients of $\tilde{\gamma}_{-2}$ will be considered. Urrutia²²⁴ also reported the first four Virial coefficients as following,

$$\tilde{\gamma}_{-2} = \eta \left[1 + \frac{1}{2}\eta + \left(\frac{81\sqrt{3}}{16\pi} - \frac{289}{105} \right) \eta^2 \right] + O(\eta^4). \quad (3.105)$$

Numerical results of Virial coefficients are shown in **Table 3.4**. It shows that all equations of state can provide exact first three Virial coefficients, and all equations of state overestimate the fourth virial coefficients. Hence, the future study in $\tilde{\gamma}_{-2}$ is necessary.

Table 3.4: Virial coefficients of $\tilde{\gamma}_{-2}$

n	Exact	SPT	MFMT	ASPT2
2	1	1	1	1
3	0.5	0.5	0.5	0.5
4	0.03872	0.3333	0.3333	0.31556

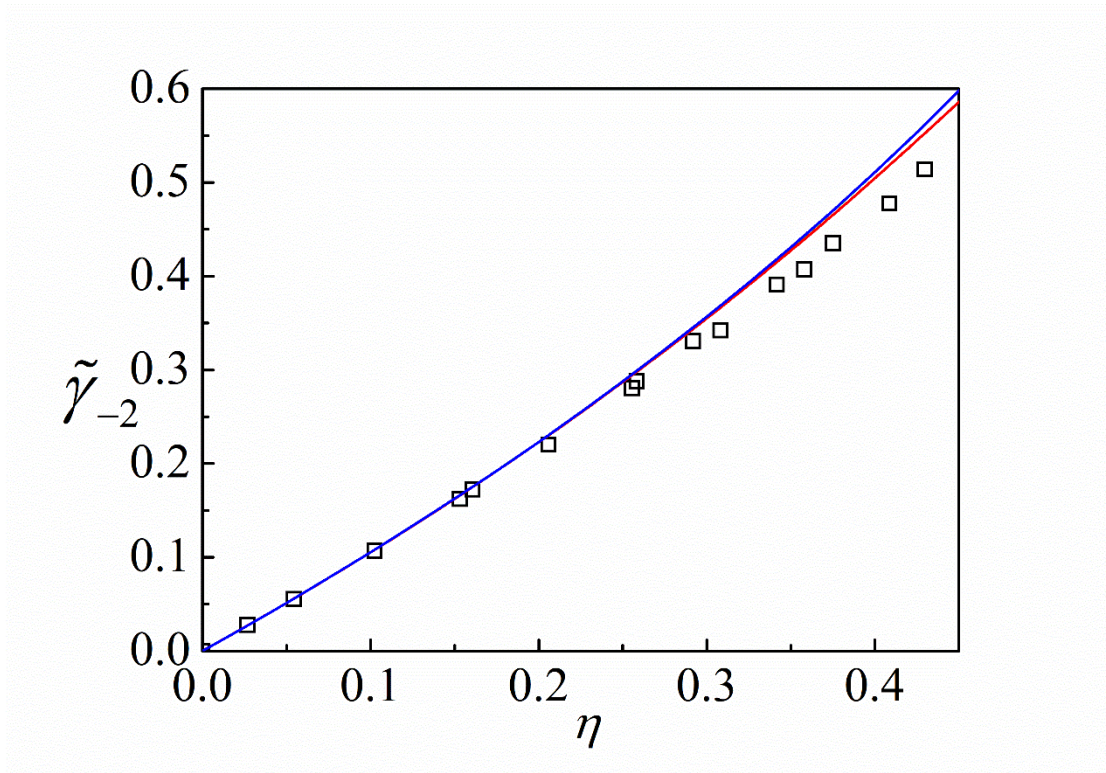


Figure 3.4. Comparison of $\tilde{\gamma}_{-2}$ of a hard sphere fluid. The simulation results are presented by black squares, the green line MFMT, the blue line original SPT, the red line ASPT2.

Above discussion show that we cannot say an equation of state has a good accuracy just because the prediction of Virial coefficients has a great agreement with the exact value. When an equation of state has good accuracy, it means the prediction of Virial coefficients also has good accuracy. However, if the equation of state can accurately provide the first a few of virial coefficients, it does not mean this equation of state has

good accuracy.

D. Non-Hadwiger coefficient

As said at the beginning of this paper, we want to build a simple analytical equation of state that can provide an acceptable prediction of Non-Hadwiger coefficient. In this part, the non-Hadwiger obtained from different equation of state are considered.

Hansen-Goos²²¹ has reported a very accurate expression of Non-Hadwiger coefficient, however, his theory, SFMT, need planar surface tension and Tolman length as input. **Fig. 3.5** shows the prediction of non-Hadwiger coefficient from CS-SPT, CS-SPT_M, ASPT1, ASPT2, SFMT, and molecular simulation. As it shows, the prediction from SFMT has the best accuracy. Except for SFMT, only ASPT1's prediction has the same magnitude with simulation result. ASPT2 significantly underestimates the Non-Hadwiger coefficient. Although the prediction from ASPT1 and ASPT2 have the same shape with simulation, the value of non-Hadwiger coefficient is larger than simulation results at least two orders of magnitude.

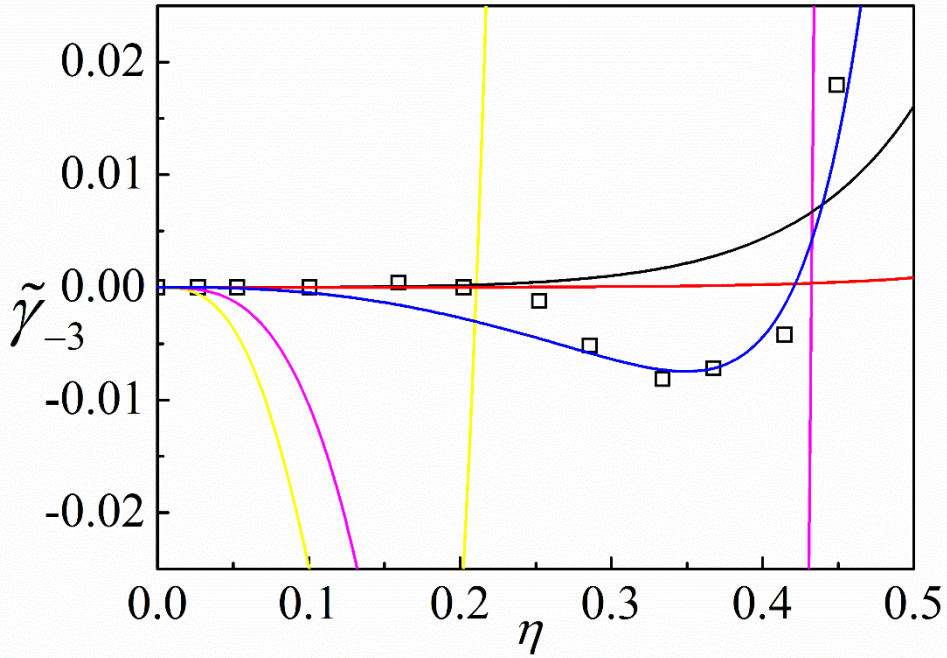


Figure 3.5. Comparison of non-Hadwiger coefficient of a hard sphere fluid. The simulation results are presented by black squares, the blue line SFMT, the red line ASPT2, the black line ASPT1, the yellow line CS-SPT, the magenta line CS-SPT_M

E. Multi-component system

Now, the accuracy of the two ASPT for the multi-component system is considered. The comparison of the prediction of excess chemical potential from our two new ASPT, original SPT, and BMCSL equation of state²⁶⁰ are shown in **Fig. 3.6**. It shows that ASPT1 and ASPT2 strongly improve the prediction from original SPT for both big particle component and small particle component, and the results are nearly indistinguishable from the BMCSL equation of state on the scale of the plot. In original SPT, if the number of components is reduced to one, all results will reduce to the corresponding ones of a one-component system. It can be readily checked that ASPT1 and ASPT2 also have this property. Also, ASPT1 and ASPT2 can be obtained by using some simple mixing rules, just like showed in ¹⁹³. All results above show our two new

methods are reasonable and consistent.

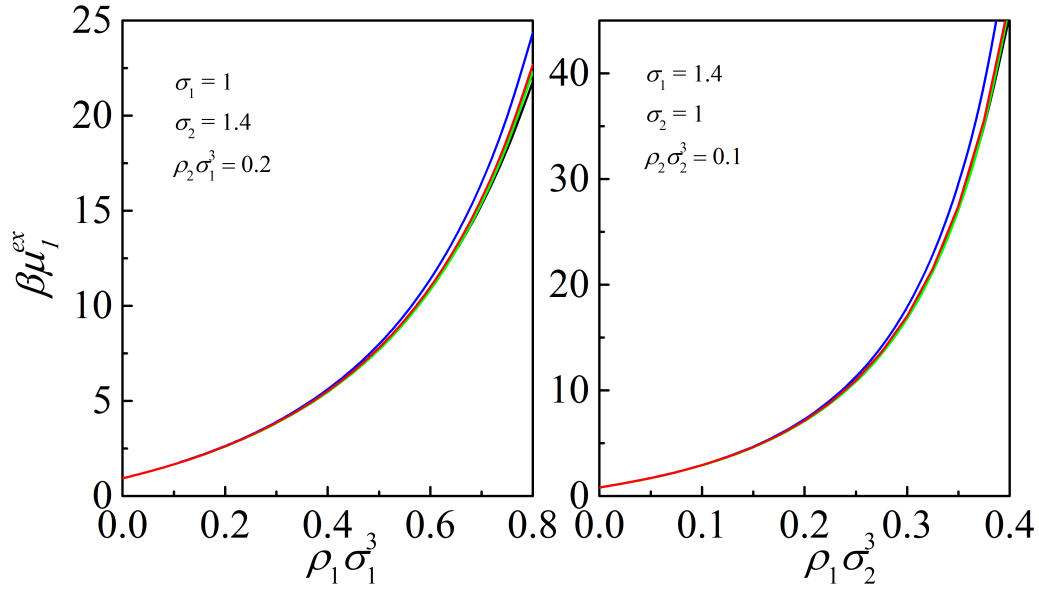


Figure 3.6. Comparison of the excess chemical potential of a binary mixture system. The BMSL results are presented by the green line, the black line is ASPT1, the red line ASPT2, and the blue line original SPT.

3.5 Concluding remarks

In the present work, we found the original expression of the chemical potential is not completed. Based on previous works on SPT and morphological thermodynamic, we reported two new ways to present the chemical potential. The first one contains an arbitrary parameter. The second one uses two Laurent series to describe the chemical potential. Both of them do not only significantly improve the accuracy of thermodynamic properties, i.e. pressure and chemical potential, but also improve the accuracy of surface properties, i.e. surface tension and Tolman length. Also, the same idea can be used to treat the multi-components hard sphere fluids system, and the improvement is significant.

The success of ASPT1 and ASPT2 indicates that the morphological thermodynamic is not an exact theory, it is only a very good approximation. However, ASPT1 can only provide an acceptable result of Non-Hadwiger coefficient, which

means we still need future study in this term. Since the original expression of the reversible work is not completed and when we add an additional term, $1/R$, the accuracy has significantly improved. It is natural to ask a question if the more terms, $1/R^2$ and $1/R^3$, are added, the higher accuracy of SPT will be obtained?

Unfortunately, since lack of the understanding of reversible work of inserting a scaled particle, eq.(3.4), we do not have enough conditions to build a new SPT that contains more term.

4. A general equation of state for confined fluid: morphological thermodynamics

4.1 Introduction

In theoretical studies, for describing the porous material, many models are introduced, i.e., hard sphere matrix model, overlapping hard sphere matrix, hard sponge matrix, and Slit pore, as shown in [Fig. 4.1](#). The models of disordered porous medium are always built with the help of some fixed particles. Although all three models for random porous medium introduced above has analytical equation of state obtained from SPT, the derivation of all those equations of state is very complex and depends on the model of porous medium. So, it still remains a great challenge to build a general framework to understand the behavior of fluid confined in different porous medium. Although all three models for random porous medium introduced above has analytical equation of state obtained from SPT, the derivation of all those equations of state is very complex and depends on the model of porous medium. So, it still remains a great challenge to build a general framework to understand the behavior of fluid confined in different porous medium.

In recent, Mecke and his co-workers proposed a general framework, named as morphological thermodynamics.^{207,209,210,234} This framework gives us some hope to build a general theory for different confined fluid. This method is from a beautiful mathematics theorem, Hadwiger's volume theorem.^{211,212} It is not only a beautiful mathematics theorem but also offers a very powerful way to study confined fluid.

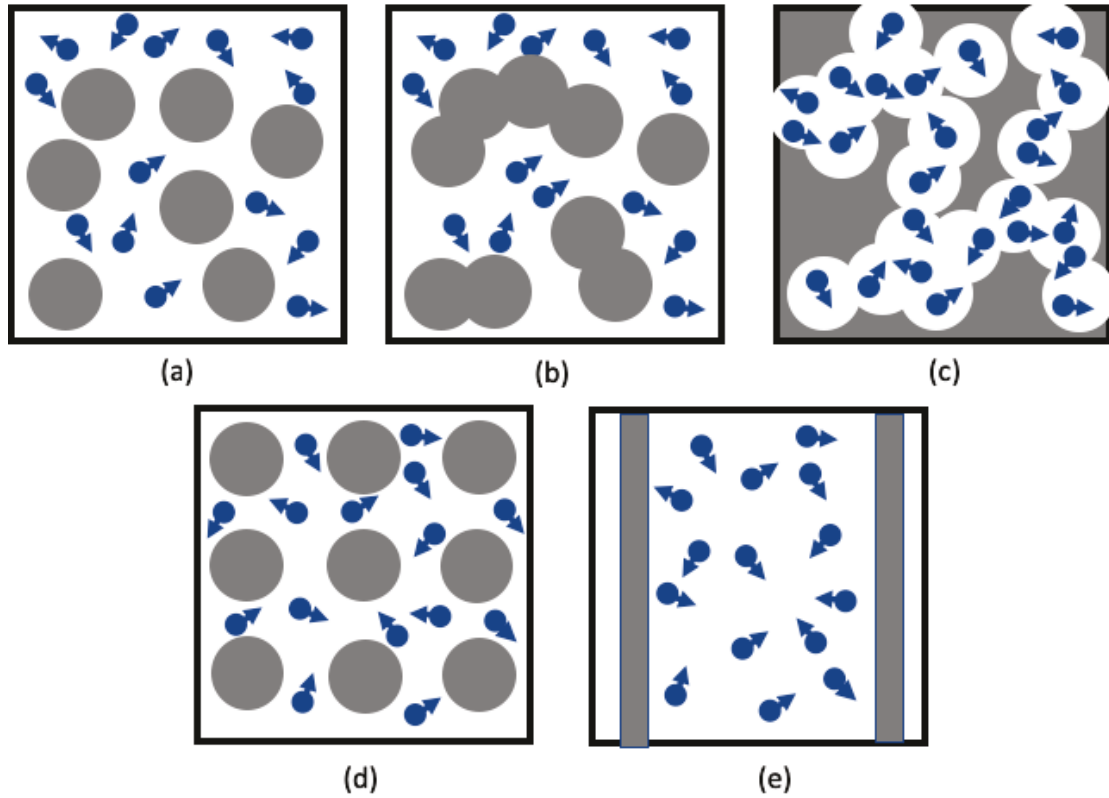


Figure 4.1. Schematic presentation of the different models of porous medium: (a) HS matrix, (b) OHS matrix, (c) sponge matrix, (d) ordered matrix, (e) slit pore. Matrix particles are presented as large gray circles and fluid particles as blue small circles with an arrow.

Recently, some studies^{220–222,224,261} showed that the morphological thermodynamics is an approximate method but an exact one. Laird²²³ used molecular dynamics simulation (MD) to calculate the interfacial tension, γ , between spherical or cylindrical particle and hard sphere fluid. They fitted the MD result to determine a polynomial of $1/R$. Hansen-Goos²²¹ used Virial expansion to determine an exact surface tension expression, and this expression implied the existence of non-Hadwiger coefficient. To quantify the first non-Hadwiger coefficient, some simulations were carried out, the numerous results showed that the first non-Hadwiger coefficient is smaller than the smallest morphological thermodynamics coefficient in one order of magnitude. In those articles, they did not prove that the non-Hadwiger term coefficients with higher order are always in the same sign. In this case, the sum of non-Hadwiger

terms may be equal to zero. In fact, their studies considered a fluid near spherical or cylindrical particle, it means that the interface between fluid and the obstacle particle is concave from fluid view, while the Hadwiger's volume theorem is only valid in convex interface.

The remaining Chapter is organized as follows. A brief introduction of morphological thermodynamics and a general equation of state for different confined fluid will be presented in the next section. Then the accuracy of the general equation of state in different confinement systems will be assessed in Section 4.3.

4.2 Theory

A. A brief introduction of Morphological thermodynamics

Hadwiger's volume theorem is one of the most important and beautiful theorems in geometric convexity.^{211,212} It says if there exists a mapping ($\mu: k^d \rightarrow \mathbf{R}$) from a convex set (k^d) onto a real number (\mathbf{R}), and this mapping satisfies three restrictions: (I) Continuity. (II) Motion invariance. (III) Additivity. Then the mapping function can be rewritten as following:

$$\mu(\mathbf{K}) = \sum_{i=0}^d c_i V_i(\mathbf{K}), \quad (4.1)$$

c_i is constant. For three dimensional system V_3 is volume, V_2 is the surface area, V_1 is the integrated mean curvature, and V_0 is the Euler characteristic. Imitate this theorem, a similar expression of the grand potential of a confined fluid, Ω , can be obtained,

$$\Omega = -pV\phi_0 + \sigma A + \kappa_1 C + \kappa_2 X, \quad (4.2)$$

where V is the system volume, ϕ_0 is the geometric porosity⁷⁹, A is the surface area of the matrix, C and X are the integrated mean curvature and the Euler characteristic of the matrix component, respectively. p , σ , κ_1 and κ_2 are the

coefficients only about the fluid property. It means that the grand potential of confined fluid can be expressed as a linear combination of four geometric properties of matrix, and the four coefficients can be obtained from bulk system. However, for now, we do not know how to obtain those four coefficients from bulk fluid. Here, a simple confined system of ideal gas fluid will be introduced to explain this expression of grand potential of confined fluid, the model as introduced in **Fig. 4.2**. Some clues of how to obtain those four coefficients from bulk system can be also obtained from this toy model.

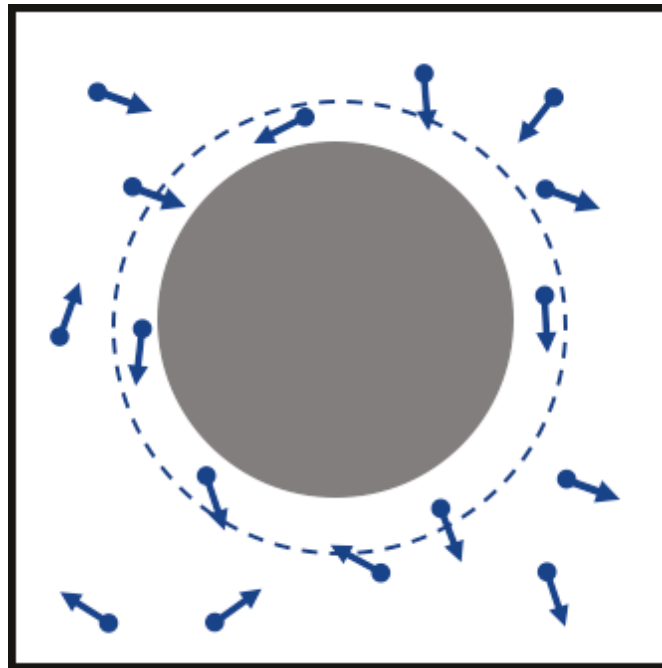


Figure 4.2. Schematic presentation of an ideal gas fluid around a spherical matrix particle with a square well potential.

Consider an ideal gas fluid around a spherical matrix particle, and the interaction between fluid and matrix particle is square well potential,

$$u_{10}(|\mathbf{r}_i|) = \begin{cases} \infty, & |\mathbf{r}_i| < R_0 \\ \varepsilon, & R_0 \leq |\mathbf{r}_i| < R_0 + d, \\ 0, & |\mathbf{r}_i| \geq R_0 + d \end{cases} \quad (4.3)$$

where \mathbf{r} is the position of fluid particle i , assume the matrix particle is in the original

of the coordinate. R_0 is the radius of the matrix particle. In this work, 0 is used to denote matrix component, ε is the well depth and d is the width of the well. Then the grand partition function is

$$\Xi = \sum_{N=0}^{\infty} \frac{z^N}{N!} \left\{ \int \exp[-\beta u_{10}(\mathbf{r})] d\mathbf{r} \right\}^N = \exp[z \int \exp(-\beta u_{01}) d\mathbf{r}], \quad (4.4)$$

where $z = \exp(\beta\mu)$ is the activity, μ is the chemical potential. The grand potential is equal to

$$\beta\Omega = -\ln \Xi = -z \int \exp[-\beta u_{10}(\mathbf{r})] d\mathbf{r} \quad (4.5)$$

The integration in the equation above, $I = \int \exp[-\beta u_{10}(\mathbf{r})] d\mathbf{r}$, can be derived as

$$I = \left(V - \frac{4}{3} \pi R_0^3 \right) + (e^{-\beta\varepsilon} - 1) \left(4\pi R_0^2 d + 4\pi R_0 d^2 + \frac{4}{3} \pi d^3 \right) \quad (4.6)$$

The four geometric properties of this matrix particle are

$$\phi_0 = 1 - \frac{4}{3V} \pi R_0^3, \quad (4.7)$$

$$A = 4\pi R_0^2, \quad (4.8)$$

$$C = 4\pi R_0, \quad (4.9)$$

$$X = 4\pi. \quad (4.10)$$

Then the grand potential can be rearranged as following,

$$\beta\Omega = -zV\phi_0 + \sigma A + \kappa_1 C + \kappa_2 X, \quad (4.11)$$

where

$$\sigma = -z(e^{-\beta\varepsilon} - 1)d, \quad (4.12)$$

$$\kappa_1 = -z(e^{-\beta\varepsilon} - 1)d^2, \quad (4.13)$$

$$\kappa_2 = -\frac{z}{3}(e^{-\beta\varepsilon} - 1)d^3. \quad (4.14)$$

Hence, we find the expression of grand potential for an ideal gas fluid around a spherical matrix particle satisfies morphological thermodynamics expression, and the four coefficients are obtained. In different situations, such as ideal gas fluid confined in a

spherical container, ideal gas fluid around or confined in a cylinder, the same results can be also obtained. Since the details of the calculation are similar to this example, we will not show them here. We also found in some cases this expression is not established, such as, when fluid around two big spheres and there is a region that fluid suffered interaction from both two big spheres. (see [Appendix B](#)). It should be mentioned that, z is equal to the pressure of the equilibrated bulk system. Maybe those four coefficients can be obtained from the equilibrated bulk system, instead of the bulk system has the same fluid density as in [Chapter 2](#). One should note that, normally, the surface area of the matrix particle has two different definitions²²⁰, the first is equal to $4\pi R_0^2$ which called solid surface area, the second is $4\pi(R_0 + R_1)^2$ which called reference surface area, where R_1 is the radius of fluid particle. When the fluid is ideal gas fluid, those two definitions are equivalent. In the following work, we will use the first definition. Hadwiger's volume theorem is about a mapping from a convex set to a number, however, in above example, the interface between fluid and matrix particle is concave from the fluid's view, and in Hansen-Goos' work²²¹, he also considered a fluid around a spherical particle. This situation does not satisfy the Hadwiger's volume theorem, so we also calculated the fluid confined in a spherical container, we found the non-Hadwiger term still exists. We have to say the morphological thermodynamic is only a very accurate approximation.

B. A new general equation of state

In this section, a new general equation of state for a hard sphere fluid confined in different porous medium will be introduced. In morphological thermodynamics expression, the grand potential of a confined fluid is equal to

$$\beta\Omega = -p(\mu, T)V\phi_0 + \sigma(\mu, T)A + \kappa_1(\mu, T)C + \kappa_2(\mu, T)X, \quad (4.15)$$

here, the independent variables are chemical potential, μ , and temperature, T , which means we assume those four coefficients can be obtained from the equilibrated bulk system. Compare the grand potential, we are more interested in adsorption amount, with

the help of thermodynamic relation,

$$N = -\frac{\partial \beta \Omega}{\partial \beta \mu}, \quad (4.16)$$

the relation between chemical potential and confined fluid density, ρ_c , is

$$\rho_c = \frac{\partial p(\mu, T)}{\partial \mu} \phi_0 - \frac{\partial \sigma(\mu, T)}{\partial \mu} \frac{A}{V} - \frac{\partial \kappa_1(\mu, T)}{\partial \mu} \frac{C}{V} - \frac{\partial \kappa_2(\mu, T)}{\partial \mu} \frac{X}{V}. \quad (4.17)$$

Since the relation between the chemical potential and fluid density for bulk system is already known. With the help of chain rule, the equation above can be rearranged as

$$\begin{aligned} \rho_c = & \frac{\partial p(\rho_b, T)}{\partial \rho_b} \frac{\partial \rho_b}{\partial \mu} \phi_0 - \frac{\partial \sigma(\rho_b, T)}{\partial \rho_b} \frac{\partial \rho_b}{\partial \mu} \frac{A}{V} \\ & - \frac{\partial \kappa_1(\rho_b, T)}{\partial \rho_b} \frac{\partial \rho_b}{\partial \mu} \frac{C}{V} - \frac{\partial \kappa_2(\rho_b, T)}{\partial \rho_b} \frac{\partial \rho_b}{\partial \mu} \frac{X}{V} \end{aligned} \quad (4.18)$$

The well-known Gibbs-Duhem relation is

$$\left(\frac{\partial p}{\partial \rho_b} \right)_T = \rho_b \left(\frac{\partial \mu}{\partial \rho_b} \right)_T. \quad (4.19)$$

The relation between confined fluid density and bulk fluid density is equal to

$$\rho_c = \rho_b \phi_0 - \frac{\partial \sigma(\rho_b, T)}{\partial \rho_b} \frac{\partial \rho_b}{\partial \mu} \frac{A}{V} - \frac{\partial \kappa_1(\rho_b, T)}{\partial \rho_b} \frac{\partial \rho_b}{\partial \mu} \frac{C}{V} - \frac{\partial \kappa_2(\rho_b, T)}{\partial \rho_b} \frac{\partial \rho_b}{\partial \mu} \frac{X}{V}. \quad (4.20)$$

The relation between those three coefficients and bulk fluid density can be obtained from scaled particle theory¹⁹³.

$$\beta \sigma = \frac{1}{4\pi R_1^2} \frac{3\eta_b(2+\eta_b)}{2(1-\eta_b)^2}, \quad (4.21)$$

$$\beta \kappa_1 = \frac{1}{4\pi R_1} \frac{3\eta_b}{1-\eta_b}, \quad (4.22)$$

$$\beta \kappa_2 = -\frac{1}{4\pi} \ln(1-\eta_b), \quad (4.23)$$

$$\beta \mu = \ln(\rho_b \Lambda^3) - \ln(1-\eta_b) + \frac{14\eta_b - 13\eta_b^2 + 5\eta_b^3}{2(1-\eta_b)^3} \quad (4.24)$$

where $\eta_b = 4\pi\rho_b R_1^3 / 3$ is the packing fraction of bulk fluid, and Λ is the fluid

thermal wavelength.

Now, we obtained a general relation between confined fluid density and equilibrated bulk fluid density. Combine eq. (4.20) to eq. (4.24), the relation between confined fluid density, ρ_c , and chemical potential, μ , can be obtained. This derivation is irrelevant with the model of porous medium, so we can use this model to study different confined fluid. It should be mentioned that scaled particle theory can also offer an accurate equation of state for different kinds of confined fluid like showed in previous works⁷⁹. The derivation of our new general equation of state is easier to scaled particle theory, while the final expression is more complex than scaled particle theory.

4.3 Results and discussion

In this section, we are going to assess the accuracy of our new general equation of state in the different porous medium, i.e., Madden-Glandt model, sponge-like models, slit pore model. Our new results will be compared with molecular simulation and scaled particle theory⁷⁹. We will start from the disordered porous medium.

A. Madden Glandt disorder porous medium

Here, we consider two kinds of Madden-Glandt models, the hard sphere one (HS) which the interaction between matrix particles are hard sphere potential and overlapping hard sphere one (OHS) which has no interaction between matrix particles. For the HS matrix, the expressions for four geometric properties are

$$\phi_0 = 1 - \frac{4}{3V} \pi \rho_0 R_0^3, \quad (4.25)$$

$$A = 4\pi \rho_0 R_0^2 V, \quad (4.26)$$

$$C = 4\pi \rho_0 R_0 V, \quad (4.27)$$

$$X = 4\pi \rho_0 V, \quad (4.28)$$

where ρ_0 is the density of matrix component. For the overlapping HS matrix, the

expression of four geometric properties are

$$\phi_0 = e^{-\eta_0}, \quad (4.29)$$

$$A/V = 4\pi\rho_0 e^{-\eta_0} R_0^2, \quad (4.30)$$

$$C/V = 4\pi\rho_0(1 - 3\eta_0/2)e^{-\eta_0} R_0, \quad (4.31)$$

$$X/V = 4\pi\rho_0(1 - 9\eta_0 + 9\eta_0^2/2)e^{-\eta_0} \quad (4.32)$$

Fig. 4.3 (a)-(c) plots the prediction of chemical potential for an HS matrix from our new equation of state, SPT2b1, and molecular simulation results in different matrix properties. Both our equation of state and SPT2b1 have a good agreement with simulation results in different matrix radius and different matrix density. **Fig. 4.3** (d)-(e) shows the results of our new equation of state, SPT2b1, and molecular simulation results for an OHS matrix. Same with the results for HS matrix, our new equation of state and SPT2b1 are nearly indistinguishable from the simulation results on the scale of the plot. Unquestionable, the morphological thermodynamic is a very accurate approximation.

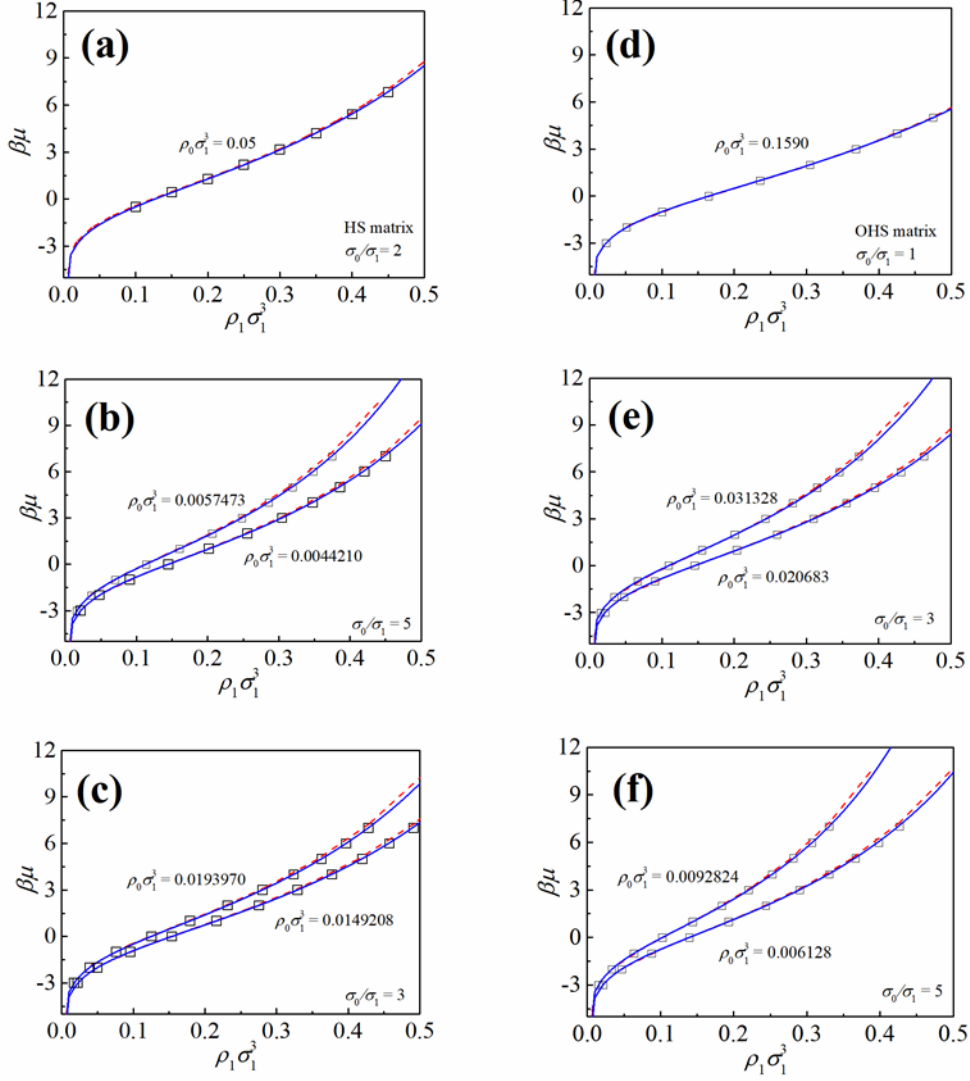


Figure 4.3. Comparison of the new general equation of state with SPT2b1 and simulation, the simulation results are presented by black square, the red dash lines are new general EOS, the blue solid lines are SPT2b1: (1) HS fluid in HS matrices (left panel); (2) HS fluid in OHS matrices (right panel).

B. Hard sponge disordered porous medium

In this section, our new equation of state will be applied to describe hard sphere fluid confined in a hard sponge matrix. This model can be considered as an opposite system of the OHS matrix. Not like OHS matrix, in this model, the material particles are considered as cavity. It should be noted that the interface between the matrix and

fluid is a convex surface in this model, while in OHS matrix, it is a concave surface.

The four geometric properties of hard sponge model are

$$\phi_0 = 1 - e^{-\eta_0}, \quad (4.33)$$

$$A/V = 4\pi\rho_0 e^{-\eta_0} R_0^2, \quad (4.34)$$

$$C/V = 4\pi\rho_0(1 - 3\eta_0/2)e^{-\eta_0} R_0, \quad (4.35)$$

$$X/V = 4\pi\rho_0(1 - 9\eta_0 + 9\eta_0^2/2)e^{-\eta_0}. \quad (4.36)$$

Fig. 4.4 shows the prediction of chemical potential for a hard sponge matrix in different porosity. As in the previous section, both our new equation of state and SPT2b1 have a great agreement with simulation results. It should be noted that when porosity is small, our new equation of state slightly underestimated the chemical potential in the high fluid density region. Compare **Fig. 4.3** and **Fig. 4.4**, one can find that the pore shape is not important.

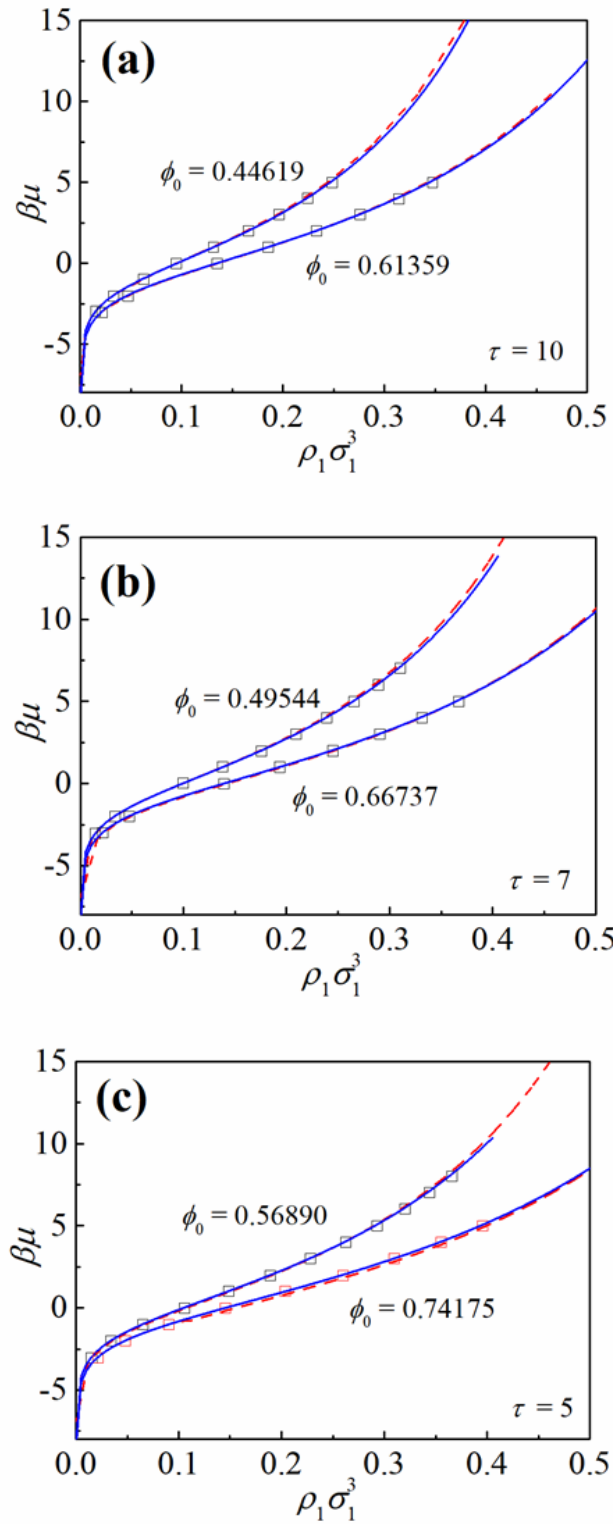


Figure 4.4. Comparison of the new general equation of state with SPT2b1 and simulation of HS fluid in hard sponge matrices, the simulation results are presented by black squares, red dash lines are new general EOS, and blue solid lines are SPT2b1.

C. Ordered porous medium

In the previous section, we considered our new equation of state for different kinds of disordered porous medium. In this section, the ordered porous medium will be considered. Here, we use a cubic lattice model to describe the ordered porous medium, the matrix particles placed in the lattice points. The four geometric properties are same with HS matrix. **Fig. 4.5** shows the comparison of the chemical potential, μ , obtained by our new equation of state with the results of molecular simulation. Our results are very close to the simulation values even in a high matrix density. The accuracy of our new equation of state will decrease while the increasing matrix density and the decreasing radius of the matrix particle. In high fluid density, our new equation of state is overestimating the chemical potential. Compare this result with the HS matrix one, we found when matrix particle is larger than the fluid particle, the disorder effect is not important.

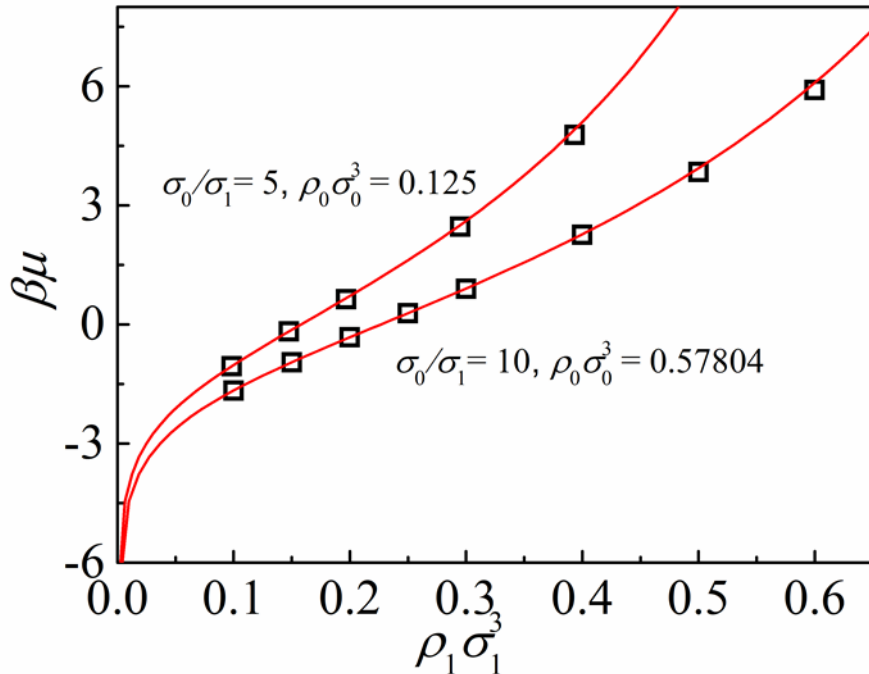


Figure 4.5. Comparison of the new general equation of state with simulation of HS fluid in the ordered porous medium, the simulation results are presented by black squares, the red dash lines are new general EOS.

D. Slit pore system

All models we considered in the previous section have a curved surface, a simple porous medium model, slit pore, which has a planar interface between fluid and porous medium, will be considered this section. In this model, the porosity, ϕ_0 , is equal to one, and the surface area per unit volume equals

$$A/V = 2 / H, \quad (4.37)$$

where H is the distance between two solid surfaces. Two curvatures, C and X , are equal to zero. Since this model is simpler than previous models, we consider if we can use a simpler equation to describe this system. Here, the fluid density and temperature are considered as independent variables. Then from morphological thermodynamics, the free energy, βF_s , of a hard sphere fluid confined in a slit pore can be given by:

$$\beta F_s = \beta F_b + \beta \gamma 2A, \quad (4.38)$$

where βF_b is the free energy of bulk system which has the same fluid density with confined system, and $\beta \gamma$ is the surface tension of a hard sphere fluid near a planar wall, since there are two planar walls in this system, the surface area of solid-fluid interface is $2A$. βF_b and $\beta \gamma A$ can be offered by SPT:

$$\beta \gamma = \frac{1}{8\pi R^2} \left[6 \frac{\eta}{1-\eta} + \left(3 \frac{\eta}{1-\eta} \right)^2 \right], \quad (4.39)$$

$$\frac{\beta F_b}{V} = \rho \ln(\rho \Lambda^3 - 1) + \rho \left[-\ln(1-\eta) + 3 \left(\frac{\eta}{1-\eta} \right) + \frac{3}{2} \left(\frac{\eta}{1-\eta} \right)^2 \right], \quad (4.40)$$

where η is the packing fraction, and R is the radius of fluid particle. Then the chemical potential of fluid confined in slit pore can be obtained as following,

$$\beta \mu_s = \frac{\partial \beta F_b / V}{\partial \rho} + \frac{\partial 2\beta \gamma A / V}{\partial \rho} = \beta \mu_b + \frac{2}{L} \frac{\partial \beta \gamma}{\partial \rho}, \quad (4.41)$$

where L is the distance between two planar walls.

$$\frac{\partial \beta \gamma}{\partial \rho} = \frac{\partial \beta \gamma}{\partial \eta} \frac{\partial \eta}{\partial \rho} = \frac{1}{8\pi R^2} \frac{6(1+2\eta)}{(1-\eta)^3} \frac{4}{3} \pi R^3 = R \frac{1+2\eta}{(1-\eta)^3}, \quad (4.42)$$

$$\beta \mu_s = \ln(\rho \Lambda^3) - \ln(1-\eta) + \frac{14\eta - 13\eta^2 + 5\eta^3}{2(1-\eta)^3} + \frac{\sigma}{L} \frac{1+2\eta}{(1-\eta)^3}, \quad (4.43)$$

where σ is the diameter of fluid particle. Here, we obtain an equation of state for a hard sphere fluid confined in a hard wall system. However, in this system, we are more interested in a fluid confined in a square well wall system. To determine this equation of state, we use first order perturbation theory to calculate the equation of state for this system. The interaction between fluid and wall, u_{10} , is

$$u_{10}(h) = \begin{cases} \infty, & |h| > L/2 \\ \varepsilon, & L/2 - d \leq |h| < L/2, \\ 0, & |h| < L/2 - d \end{cases} \quad (4.44)$$

where d is the width of fluid-wall potential, ε is the depth of fluid-wall potential. Here, the reference system is the system that $\varepsilon = 0$ which is the hard wall system. Hence, the interaction between fluid and wall can be divided into two parts, the reference part, and the perturbation part,

$$u_{10}(h, \lambda) = u_{10}^{ref}(h) + \lambda u_{10}^{per}(h), \quad (4.45)$$

where

$$u_{10}^{per}(h) = \begin{cases} 0, & |h| > L/2 \\ \varepsilon, & L/2 - d \leq |h| < L/2, \\ 0, & |h| < L/2 - d \end{cases} \quad (4.46)$$

Then the free energy is

$$\beta F_{sw} = \beta F_s + \beta \langle w_{01} \rangle_0, \quad (4.47)$$

where F_s is the free energy of a hard sphere fluid confined in a hard wall system,

$w_{01} = \sum_{i=1}^N u_{01}^{per}(h_i)$, and $\langle \dots \rangle_0$ is the ensemble average of reference system, which

means the perturbation part will not change the fluid density profile. The ensemble average can be rewritten as

$$\langle w_{01} \rangle_0 = A \int \rho^{ref}(h) u_{01}^{per}(h) dh. \quad (4.48)$$

Now, once we know the density profile of the reference system, the free energy can be obtained. We assume the excess adsorption is adsorbed in the region where the interaction between solid surface and fluid is equation to ε , and in the remaining region, the fluid density is equal to the fluid density of the equilibrated bulk system, ρ_b . The density distribution is

$$\rho^{ref}(h) = \begin{cases} 0, & |h| > L/2 \\ \rho_b, & L/2 - d \leq |h| < L/2 \\ \rho_c, & |h| < L/2 - d \end{cases} \quad (4.49)$$

For the reference system, the bulk density can be solved from the Gibbs adsorption equation,

$$\left(\frac{\partial \beta \gamma}{\partial \beta \mu} \right)_T = \Gamma_N, \quad (4.50)$$

where Γ_N is the excess adsorption amount per unit area at the interface. It can be obtained as

$$\Gamma_N = \frac{A}{2A} \int \rho(h) - \rho_b dh = \frac{1}{2} (\rho_c \times 2d - \rho_b \times 2d) = d(\rho_c - \rho_b), \quad (4.51)$$

$$\rho_b = \rho - \frac{2\Gamma_N}{L}, \quad (4.52)$$

$$\rho_c = \rho + \left(\frac{1}{d} - \frac{2}{L} \right) \Gamma_N, \quad (4.53)$$

where ρ is the average density. Then the ensemble average of w_{01} is equal to

$$\langle w_{01} \rangle_0 = A \rho_c \beta \varepsilon 2d = 2dA\beta\varepsilon \left[\rho + \left(\frac{1}{d} - \frac{2}{L} \right) \Gamma_N \right]. \quad (4.54)$$

Since,

$$\Gamma_N = \left(\frac{\partial \beta \gamma}{\partial \beta \mu} \right)_T = \left(\frac{\partial \beta \gamma}{\partial \eta} \right)_T \left(\frac{\partial \eta}{\partial \beta \mu} \right)_T. \quad (4.55)$$

As we known,

$$\frac{\partial \eta}{\partial \beta \mu} = \frac{\eta(1-\eta)^4}{(1+2\eta)^2 + \sigma\eta(5+4\eta)/L}, \quad (4.56)$$

$$\frac{\partial \beta \gamma}{\partial \eta} = \frac{3}{4\pi R^3} \frac{1+2\eta}{(1-\eta)^3}. \quad (4.57)$$

Hence, the excess adsorption amount is

$$\Gamma_N = \frac{3}{4\pi R^3} \frac{(1+2\eta)(1-\eta)\eta}{(1+2\eta)^2 + \sigma\eta(5+4\eta)/L}. \quad (4.58)$$

The dimensionless excess adsorption amount is

$$\Gamma_N^* = \frac{4\pi R^3}{3} \Gamma_N. \quad (4.59)$$

Then the free energy of this system can be obtained,

$$\frac{\beta F_{sw}}{V} = \frac{\beta F_s}{V} + \frac{1}{V} \langle w_{01} \rangle_0 = \frac{\beta F_s}{V} + \frac{2d\beta\epsilon}{L} \left[\rho + \left(\frac{1}{d} - \frac{2}{L} \right) \Gamma_N \right], \quad (4.60)$$

and the chemical potential is

$$\beta \mu_{sw} = \frac{\partial \beta F_{sw}/V}{\partial \rho} = \beta \mu_b + \frac{\sigma}{L} \frac{1+2\eta}{(1-\eta)^3} + \frac{2d\beta\epsilon}{L} \left[1 + 2 \left(\frac{1}{d} - \frac{2}{L} \right) R \frac{\partial \Gamma_N^*}{\partial \eta} \right]. \quad (4.61)$$

From the equation above, one can find that the first term is the bulk chemical potential, the second term denotes the interaction between a hard sphere fluid and a hard wall, and the last term denotes the interaction between a hard sphere fluid and the square well interaction. To verify this eq. (4.61), the molecular simulation for a hard sphere fluid confined in slit pore were performed. In **Fig. 4.6**, one can find eq. (4.61) has great accuracy in different conditions, even in a high fluid density. To our best knowledge, for this moment the results presented in our study provide the most accurate theoretical description of the thermodynamic properties of a hard sphere fluid confined in a slit pore.

Fig. 4.6 shows the comparison of the chemical potential, μ , obtained by our new equation of state with the results of molecular simulation. **Fig. 4.6 a)** shows the results of a hard sphere fluid confined in a hard wall system, it shows the results are nearly

indistinguishable from the molecular simulation results on the scale of the plot in different pore width. **Fig. 6** b) and c) shows the results of a hard sphere confined in a square well pore with different width of potential and different depth of potential. Those results indicate our new equation of state works well for fluid confined in slit pore system with different parameters. Compare these results and the results for previous models, one should find that the pore size distribution and pore connectivity are not very important.

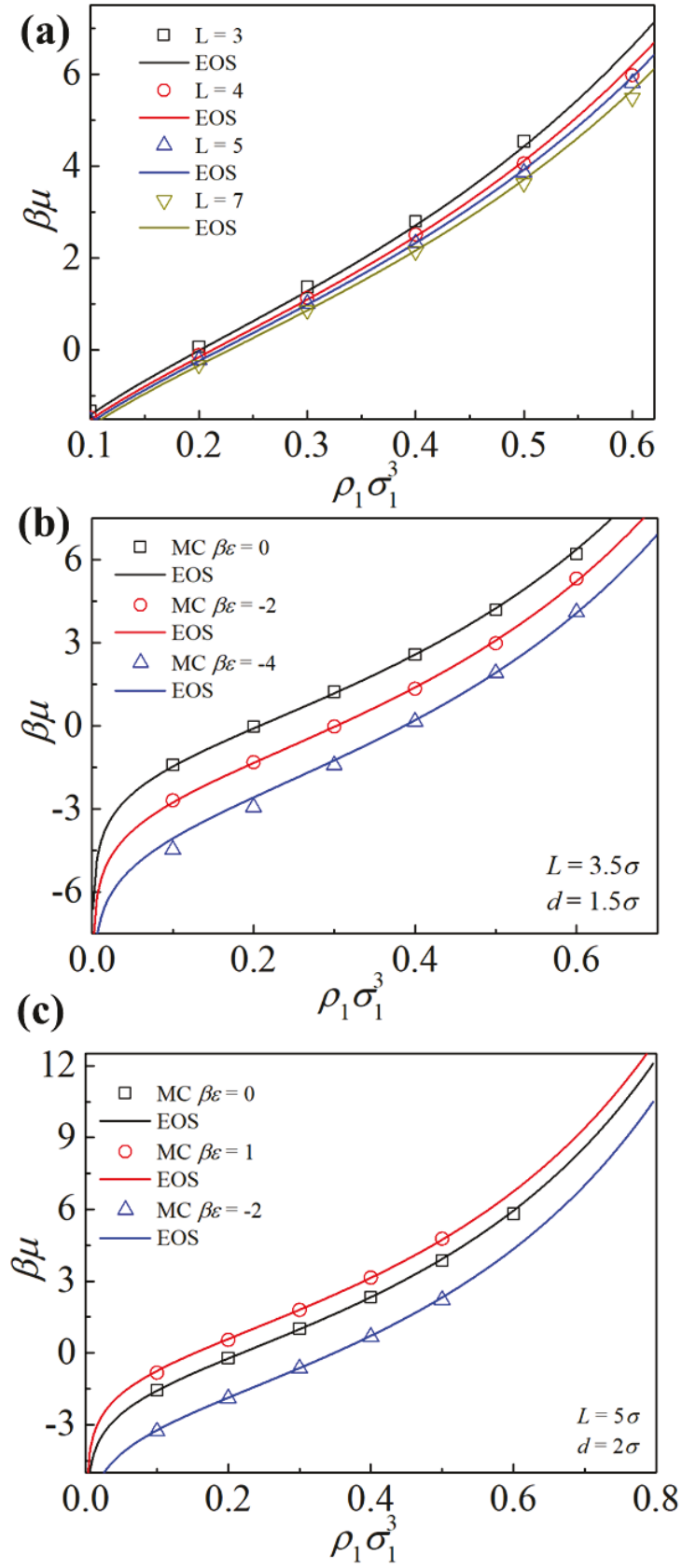


Figure 4.6. Comparison of the new general equation of state with the simulation of HS fluid in slit pore.

4.4 Concluding remarks

In the present section, we introduced the morphological thermodynamic with the help of ideal gas fluid, we present even for an ideal gas fluid, in some cases, the morphological thermodynamic still does not hold. A new general equation of state is obtained from morphological thermodynamic. To our best knowledge, for now, this is the first equation of state for confined fluid that is irrelevant with the model of porous medium. In a large range, our new equation of state works well.

Since this new equation of state provides an accurate theoretical description of the thermodynamic properties of a hard sphere fluid confined in the different porous medium. Our new equation of state indicates that porosity and other geometric properties play primary roles for the thermodynamic of confined fluid. All the other parameters, i.e., pore shape, pore connectivity, pore size distribution, disorder effect, are much less important.

5. Quench effect on the chemical potential

5.1 Introduction

In 1988, Madden and Glandt proposed an interesting model for random porous material and developed a statistical-mechanics for investigating the structure and thermodynamics of fluids confined in random porous media.⁴⁰ In this model, the disordered porous material is mimicked by a random matrix that can be generated from quenching a fluid system at its equilibrium state. Thus, the quenched “fluid” particles constitute the matrix (thereafter called matrix particles), and the voids among them are pores. This simple model successfully characterizes the main features of disordered porous materials, e.g., pore connectivity, pore size distribution, etc., and thus have been widely applied in both molecular simulations and theoretical studies of fluid confined in random porous media. Since the fluid species are mobile within the matrix configuration, this model is also called as quench-annealed mixture with quenched species referring to the matrix and annealed species referring to the confined fluid. It is to point out also that the way for constructing such a porous matrix mimics the spinodal-decomposition procedure for fabricating some porous materials experimentally.

Although many investigations have been devoted to study fluids confined in random porous media since Madden-Glandt model was proposed, no precise measure has ever been proposed to describe quantitatively the quench effect for the adsorption of a fluid in a random porous material. We propose to measure such an effect by the difference of free energy to insert a fluid particle into a quench-annealed system or into the corresponding equilibrium binary mixture. It can appear perplexing that there are still quite some fundamental questions related to quench effect that we cannot answer straightforwardly. Without attempting to be exhaustive, we can list the following ones:

- 1) What is the consequence of quenching?
- 2) Does a quench-annealed system or its corresponding equilibrium binary

mixture appear more crowded? Crowdedness means here more difficult to insert another fluid particle, i.e., with high chemical potential.

- 3) When the quench effect becomes significant?
- 4) In the case of a large quench effect, which are the dominant factors contributing to the considerable increase of chemical potential?

In this chapter, we will address these issues by studying some simple model systems. In the next section, we present first the considered model and the methods we used for carrying out our investigation. In Section 5.3, the obtained results are presented, analyzed and discussed. The insights gained from this study are summarized in the last section and we point out also the implications useful for designing new functionalized porous materials, e.g., for high-capacity gas adsorbents, etc.

5.2 Model and methods

A. Model

In the present work, we consider a hard sphere (HS) fluid (denoted as species 1) of N_1 particles confined in a quenched HS matrix (denoted as species 0) of N_0 particles. The interactions between the particles of the different species are described by,

$$u_{11}(|\mathbf{r}_i - \mathbf{r}_j|) = \begin{cases} \infty & |\mathbf{r}_i - \mathbf{r}_j| < 2R_1 \\ 0 & |\mathbf{r}_i - \mathbf{r}_j| \geq 2R_1 \end{cases}, \quad (5.1)$$

$$u_{10}(|\mathbf{r}_i - \mathbf{q}_j|) = \begin{cases} \infty & |\mathbf{r}_i - \mathbf{q}_j| < R_1 + R_0 \\ 0 & |\mathbf{r}_i - \mathbf{q}_j| \geq R_1 + R_0 \end{cases}, \quad (5.2)$$

$$u_{00}(|\mathbf{q}_i - \mathbf{q}_j|) = \begin{cases} \infty & |\mathbf{q}_i - \mathbf{q}_j| < 2R_0 \\ 0 & |\mathbf{q}_i - \mathbf{q}_j| \geq 2R_0 \end{cases}, \quad (5.3)$$

where R_1 and R_0 are respectively the radius of fluid and matrix particles, \mathbf{r}_i and \mathbf{r}_j are respectively the position vectors of the i th and the j th fluid particles while \mathbf{q}_i and \mathbf{q}_j are those of matrix particles.

B. Theory

The fact that the matrix particles in a quench-annealed system are immobile has some consequences on both structural and thermodynamic properties. In the present work, we focus on the quench effect on thermodynamics only and examine in particular such effect on the chemical potential in order to learn how quenching affects the insertion of a fluid particle. The difference between the chemical potential for inserting a fluid particle into a quench-annealed system and that for inserting the same particle into the corresponding equilibrium binary mixture appears to be a natural measure for quantifying the quench effect, i.e.,

$$\beta\Delta\mu_1 = \beta\mu_1^{QA} - \beta\mu_1^{Equil}. \quad (5.4)$$

where $\beta = 1/(k_B T)$ (k_B : Boltzmann constant; T : temperature). In the followings, we call $\beta\Delta\mu_1$ quench chemical potential. Now, we point out first that the measure defined in eq.(5.4) has an exact diagrammatic expansion. Following the work of Madden and Glandt⁴⁰ and that of Morita and Hiroike^{262–264}, one obtains readily the following expansions,

$$\beta\mu_1^{Equil} = \ln(\Lambda_1^3 \rho_1) - \{ \text{sum of all topologically distinct, simple, connected graphs which are composed of one white fluid point, some or no black fluid points, weighted by } \rho_1, \text{ black matrix points, weighted by } \rho_0, \text{ some or no } f_{11} \text{ bonds between pairs of fluid points, some } f_{10} \text{ or no } f_{00} \text{ bonds between pairs of matrix points, some or no } f_{01} \text{ bonds between pairs of matrix and fluid points, and which have no articulation points} \} \quad (5.5)$$

and

$\beta\mu_1^{QA} = \ln(\Lambda_1^3 \rho_1) - \{\text{sum of all topologically distinct, simple, connected graphs which are composed of one white fluid point, some or no black fluid points, weighted by } \rho_1, \text{ black matrix points, weighted by } \rho_0, \text{ some or no } f_{11} \text{ bonds between pairs of fluid points, some } f_{00} \text{ bonds between pairs of matrix points, some or no } f_{01} \text{ bonds between pairs of matrix and fluid points, and which have no articulation points, no shielding set}\}$ (5.6)

where ρ_1 and ρ_0 are the density of species 1 and 0 respectively, Λ_1 is the thermal wave-length of fluid particles and the various Mayer functions are defined as,

$$f_{00}(|\mathbf{q}_i - \mathbf{q}_j|) = e^{-\beta u_{00}(|\mathbf{q}_i - \mathbf{q}_j|)} - 1, \quad (5.7)$$

$$f_{01}(|\mathbf{q}_i - \mathbf{r}_j|) = e^{-\beta u_{01}(|\mathbf{q}_i - \mathbf{r}_j|)} - 1, \quad (5.8)$$

$$f_{11}(|\mathbf{r}_i - \mathbf{r}_j|) = e^{-\beta u_{11}(|\mathbf{r}_i - \mathbf{r}_j|)} - 1. \quad (5.9)$$

Eqs.(5.5) and (5.6) yield straightforwardly,

$$\beta\Delta\mu_1 = \{\text{sum of all the graphs in eq.(5.5) with shielding set}\}, \quad (5.10)$$



where circles denote fluid points and squares denote matrix points. Due to its diagrammatic characteristics described in eq.(5.10), we call sometimes $\beta\Delta\mu_1$ shielding chemical potential as well (an interchangeable name with quench chemical potential). We will discuss in the next section how some interesting information about quench effect can be deduced from the formal results presented here.

C. Application of scaled particle theory

It is also well-known that even for simple models like HS, it is not possible to calculate exactly and analytically the sum of graphs like that in eq.(5.10). Nevertheless, various approaches, some being even analytic, exist for calculating chemical potential in both an equilibrium binary system and a quench-annealed system. In particular, scaled particle theory (SPT) is a well-known and successful approach which allows for

calculating analytically the thermodynamic properties of various bulk HS systems and has been extended recently to quench-annealed systems as well. In this Chapter, we will apply SPT to determine the chemical potential of an HS fluid in an HS matrix and that of the corresponding binary HS mixture in order to assess quench effect. Previous investigations have shown that the variant called SPT2b1 gives very accurate results for the chemical potential of an HS fluid in an HS matrix.⁷⁹ This is why for our study here we use SPT2b1 and its expression for the chemical potential of an HS fluid in an HS matrix is given by,

$$\begin{aligned} \beta\mu_1^{ex(QA)} = & \beta\mu_{1f}^{ex} - \ln(1 - \eta_1 / \phi_0) + \left[7 + 3\tau(4 + \tau) \frac{\eta_0}{1 - \eta_0} + 9\tau^2 \left(\frac{\eta_0}{1 - \eta_0} \right)^2 + \frac{\phi_0 - \phi}{\phi} \right] \times \\ & \frac{\eta_1 / \phi_0}{1 - \eta_1 / \phi_0} + \frac{1}{2} \left[15 + 3\tau(10 + \tau) \frac{\eta_0}{1 - \eta_0} + 18\tau^2 \left(\frac{\eta_0}{1 - \eta_0} \right)^2 \right] \left(\frac{\eta_1 / \phi_0}{1 - \eta_1 / \phi_0} \right)^2 \\ & + 3 \left(1 + \frac{\tau\eta_0}{1 - \eta_0} \right)^2 \left(\frac{\eta_1 / \phi_0}{1 - \eta_1 / \phi_0} \right)^3 \end{aligned} \quad (5.11)$$

where $\beta\mu_1^{ex-QA} = \beta\mu_1^{QA} - \ln(\Lambda_1^3 \rho_1)$, $\eta_i = 4\pi R_i^3 \rho_i / 3$ ($i = 0, 1$) is the packing fraction, $\tau = R_1 / R_0$ is the ratio of the radius of fluid particle to matrix particle, $\phi_0 = 1 - \eta_0$ is the geometric porosity, and $\beta\mu_{1f}^{ex}$ is the chemical potential to insert one fluid particle into an empty matrix which is given by

$$\beta\mu_{1f}^{ex} = -\ln(1 - \eta_0) + \tau(3 + 3\tau + \tau^2) \frac{\eta_0}{1 - \eta_0} + \frac{3\tau(3 + 2\tau)}{2} \left(\frac{\eta_0}{1 - \eta_0} \right)^2 + 3\tau^3 \left(\frac{\eta_0}{1 - \eta_0} \right)^3 \quad (5.12)$$

and ϕ in eq. (5.11) is the matrix porosity measured with a fluid particle as the probe (note that ϕ_0 is the porosity measured with a point particle),

$$\phi = e^{-\beta\mu_{1f}^{ex}}. \quad (5.13)$$

In order to facilitate comparison, we cast the expression of chemical potential of the corresponding binary mixture in a form similar to that given in eq.(5.11), i.e.,

$$\begin{aligned}
\beta\mu_1^{ex(Equil)} = & \beta\mu_{1l}^{ex} - \ln(1 - \eta_1 / \phi_0) + \left[7 + \tau(15 + 6\tau + \tau^2) \frac{\eta_0}{1 - \eta_0} + 6\tau^2(3 + \tau) \left(\frac{\eta_0}{1 - \eta_0} \right)^2 \right. \\
& + 9\tau^3 \left(\frac{\eta_0}{1 - \eta_0} \right)^3 \left. \right] \frac{\eta_1 / \phi_0}{1 - \eta_1 / \phi_0} + \frac{1}{2} \left[15 + 3\tau(7 + \tau) \frac{\eta_0}{1 - \eta_0} + 3\tau^2(15 + 2\tau) \times \right. \\
& \left. \left(\frac{\eta_0}{1 - \eta_0} \right)^2 + 18\tau^3 \left(\frac{\eta_0}{1 - \eta_0} \right)^3 \right] \left(\frac{\eta_1 / \phi_0}{1 - \eta_1 / \phi_0} \right)^2 + 3 \left(1 + \frac{\tau\eta_0}{1 - \eta_0} \right)^3 \left(\frac{\eta_1 / \phi_0}{1 - \eta_1 / \phi_0} \right)^3
\end{aligned}
\tag{5.14}$$

The two first terms on the right-hand side of both eqs.(5.11) and (5.14) are identical. The rest of the RHS of eqs. (5.11) and (5.14) is a third order polynomial of $\frac{\eta_1 / \phi_0}{1 - \eta_1 / \phi_0}$ but with different coefficients for $\beta\mu_1^{ex-QA}$ or $\beta\mu_1^{ex-Equil}$. So, the quench effect shows up through these coefficients.

D. Simulation

In order to check the validity of the prediction about the quench effect given by SPT, we carried out a series of Monte Carlo (MC) simulations^{226,265} of an HS fluid in an HS matrix. A cubic simulation box was used with periodic boundary conditions. Each simulation run is performed with a particular matrix realization and the fluid particles can move in the volume which is not occupied by matrix particles. The matrix configurations are generated by using canonical ensemble Monte-Carlo simulations (CEMC). Since matrices of finite size are used in the simulation, any observable quantity fluctuates with matrix realizations and hence an average over matrix realizations should be taken also. In the present work, we generated matrix realizations of sizes ranging from 200 to a few thousands matrix particles. The average over matrix configurations is calculated with typically 20 realizations. For each matrix realization, a GCEMC simulation about 10000 trial moves per particle is performed during which the average fluid density is calculated. For all the numerical results presented below, we use the diameter of fluid particle, i.e., $\sigma_1 = 2R_1$, as the unit of length. Matrices with different particle radii ($R_0 = 0.5 - 2.5\sigma_1$) as well as of different porosities were

considered.

To determine the quench effect, it is necessary to calculate the chemical potential of an equilibrium HS binary mixture corresponding to the quench-annealed system. To facilitate the comparison between the two systems, we performed CEMC simulations for the equilibrium HS binary mixture so that the densities of the two components can be prescribed. The chemical potential is calculated by using Widom's test particle method²²⁸.

5.3 Results and discussion

In this section, we will show successively in which cases there is no quench effect at all, when it starts to manifest itself and the situations in which the quench effect becomes strong.

A. Strictly vanishing quench effect

Although the results given in eqs. (5.6) and (5.10) are quite formal ones, they can provide already some interesting information about the quench effect. Eq. (5.10) shows immediately that there is no quench effect at the order of ρ_0 since all the diagrams in the sum given in eq.(5.10) are of an order equal or higher than ρ_0^2 . Moreover, if all the diagrams in the sum given in eq.(5.6) have only one fluid point (it is necessarily the white one), none of these diagrams contains any shielding set. Hence, the quench effect vanishes in this case as well. This corresponds to the situation that there is only one particle of species 1. So, insertion of a fluid particle into an empty matrix (no fluid particle inside the matrix) or into a bulk fluid of species 0 (not quenched but mobile particles) costs exactly the same amount of energy. The above discussion shows that the quench effect appears only when some fluid-fluid and matrix-matrix interactions exist at the same time, i.e., beyond the case of a single fluid particle and beyond the linear order of matrix density.

In the case of a single particle of species 1, it is possible to calculate the excess

chemical potential exactly and analytically under some conditions, e.g., a point particle in an HS matrix (see [Fig. 5.1](#) for a sketch). In this case, the interaction potentials become,

$$u_{10}(|\mathbf{r}_i - \mathbf{q}_j|) = \begin{cases} \infty & |\mathbf{r}_i - \mathbf{q}_j| < R_0 \\ 0 & |\mathbf{r}_i - \mathbf{q}_j| \geq R_0 \end{cases}, \quad (5.15)$$

$$u_{00}(|\mathbf{q}_i - \mathbf{q}_j|) = \begin{cases} \infty & |\mathbf{q}_i - \mathbf{q}_j| < 2R_0 \\ 0 & |\mathbf{q}_i - \mathbf{q}_j| \geq 2R_0 \end{cases}. \quad (5.16)$$

For this case, we obtain straightforwardly the following exact and analytical result,

$$\beta\mu_1^{ex(QA)} = \beta\mu_1^{ex(Equil)} = -\ln\left(1 - \frac{4\pi R_0^3 \rho_0}{3}\right). \quad (5.17)$$

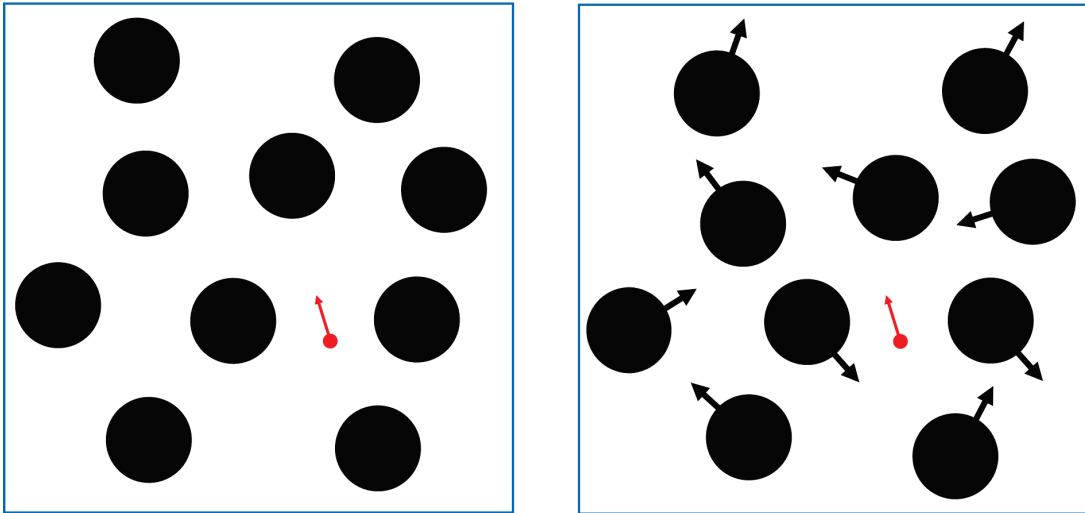


Figure 5.1. Sketch of a single point fluid particle (red point) in a hard sphere matrix (black spheres) and the corresponding equilibrium binary mixture with both species being mobile: the particles with an arrow are mobile while those without arrow are quenched in position.

The explicit result given in eq.(5.17) confirms the general conclusion that no quench effect in the case of one fluid particle in an empty matrix. It is to be pointed out that if the point particles have a finite density (i.e., an ideal gas with density ρ_1 in an HS

matrix with density ρ_0), the results given in eq.(5.17) hold as well. It is worth to note also that in the limit of $R_1 \rightarrow 0$, the SPT results given in eqs.(5.11) and (5.14) reduce both to that of eq.(5.17).

In the case of one HS of radius, R_1 , in a matrix of point particles (see [Fig. 5.2](#) for a sketch), i.e., the interaction potential being,

$$u_{10}(|\mathbf{r}_i - \mathbf{q}_j|) = \begin{cases} \infty & |\mathbf{r}_i - \mathbf{q}_j| < R_1 \\ 0 & |\mathbf{r}_i - \mathbf{q}_j| \geq R_1 \end{cases}, \quad (5.18)$$

the excess chemical potential can be also calculated exactly and analytically and we obtain,

$$\beta\mu_1^{ex(QA)} = \beta\mu_1^{ex(Equil)} = \frac{4\pi R_1^3 \rho_0}{3}. \quad (5.19)$$

Once again, this explicit calculation confirms the conclusion obtained from the diagrammatic expansion, i.e., no quench effect at the level of a single fluid particle. Moreover, eq.(5.19) shows that the excess chemical potential is of the linear order of ρ_0 and this result confirms also another conclusion from the diagrammatic expansion, i.e., the quench effect manifesting itself at the order equal or higher than ρ_0^2 . In this case, SPT results, i.e., eqs.(5.11) and (5.14) reduce again to the exact one of eq.(5.19).

Here, one can raise naturally the question whether the SPT results given in eqs.(5.11) and (5.14) are consistent with the exact result that the quench chemical potential vanishes at the linear order of matrix density. From eqs.(5.11) and (5.14), we obtain the following expression for the quench chemical potential,

$$\begin{aligned}
\beta\Delta\mu_1 &= \beta\mu_1^{\text{ex}(QA)} - \beta\mu_1^{\text{ex}(Equil)} \\
&= \left[\frac{\phi_0 - \phi}{\phi} - \tau(3 + 3\tau + \tau^2) \frac{\eta_0}{1 - \eta_0} - \tau^2(9 + 6\tau) \left(\frac{\eta_0}{1 - \eta_0} \right)^2 - 9\tau^3 \left(\frac{\eta_0}{1 - \eta_0} \right)^3 \right] \frac{\eta_1 / \phi_0}{1 - \eta_1 / \phi_0} \\
&\quad - \frac{1}{2} \left[3\tau(4 + 2\tau) \frac{\eta_0}{1 - \eta_0} + 3\tau^2(9 + 2\tau) \left(\frac{\eta_0}{1 - \eta_0} \right)^2 + 18\tau^3 \left(\frac{\eta_0}{1 - \eta_0} \right)^3 \right] \left(\frac{\eta_1 / \phi_0}{1 - \eta_1 / \phi_0} \right)^2 \\
&\quad - 3 \left[\frac{\tau\eta_0}{1 - \eta_0} + 2\tau^2 \left(\frac{\eta_0}{1 - \eta_0} \right)^2 + \tau^3 \left(\frac{\eta_0}{1 - \eta_0} \right)^3 \right] \left(\frac{\eta_1 / \phi_0}{1 - \eta_1 / \phi_0} \right)^3 \quad (5.20)
\end{aligned}$$

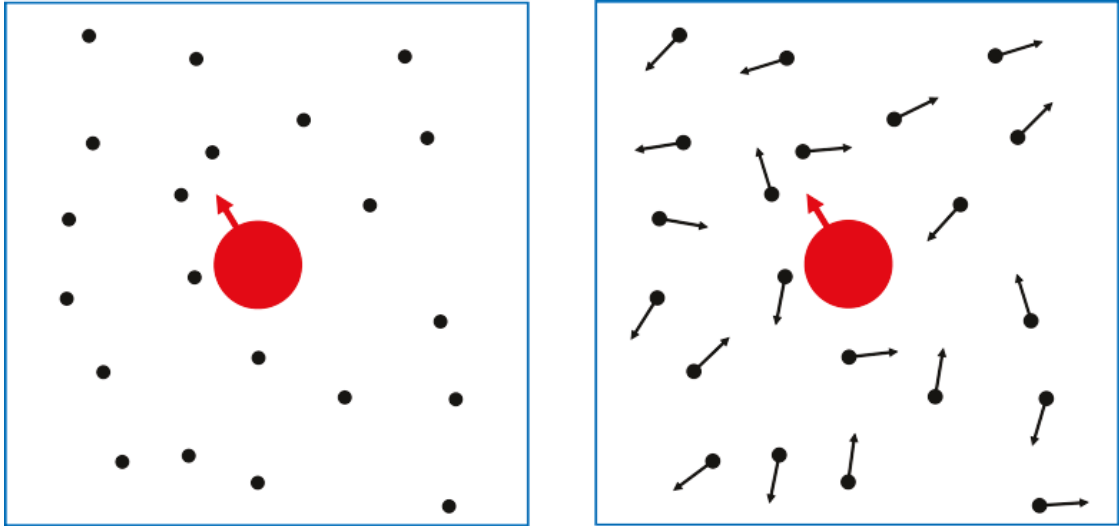


Figure 5.2. Sketch of a single hard sphere (red sphere) in a matrix of point particles (black points) and the corresponding equilibrium binary mixture with both species being mobile: the particles with an arrow are mobile ones while those without arrow are quenched in position.

Calculating the contribution to $\beta\Delta\mu_1$ from the linear term in η_0 yields,

$$\lim_{\eta_0 \rightarrow 0} \frac{\beta\Delta\mu_1}{\eta_0} = \left[\lim_{\eta_0 \rightarrow 0} \frac{\phi_0 - \phi}{\phi\eta_0} - \tau(3 + 3\tau + \tau^2) \right] \frac{\eta_1}{1 - \eta_1} - \frac{3\tau(4 + 2\tau)}{2} \left(\frac{\eta_1}{1 - \eta_1} \right)^2 - 3\tau \left(\frac{\eta_1}{1 - \eta_1} \right)^3 \quad (5.21)$$

From eqs.(5.12) and(5.13), we obtain,

$$\lim_{\eta_0 \rightarrow 0} \frac{\phi_0 - \phi}{\phi\eta_0} = \tau(3 + 3\tau + \tau^2). \quad (5.22)$$

Substituting eq.(5.22) into eq.(5.21), we see that the first term on the right-hand side of eq.(5.21) vanishes. So, at the order of $\rho_0\rho_1$, the quench chemical potential is strictly zero. It is known that SPT for a bulk binary mixture is exact to this order while, to our best knowledge, no calculation of any Virial coefficient has been calculated for a confined fluid. The vanishing quench chemical potential at the order of $\rho_0\rho_1$ implies that our SPT for confined fluid is also exact to this order. The non-vanishing part in eq.(5.21) comes only from the contributions of the higher order terms for which SPT does not give exact results. So, to the orders for which SPT is exact, the result for quench chemical potential from SPT is consistent with the exact result, i.e., vanishing quench effect at the linear order of matrix density. It is quite reassuring to see, from the above discussions, that SPT either reproduces the exact results in some particular cases or is consistent with the general conclusion for vanishing quench effect.

In a more general situation, i.e., finite fluid and matrix densities, SPT results in eqs.(5.11) and (5.14) show that quench effect vanishes also in the limit to $\tau \rightarrow 0$, i.e.,

$$\beta\mu_1^{ex(QA)} = \beta\mu_1^{ex(Equil)} = -\ln(\phi_0 - \eta_1) + \frac{7\eta_1 / \phi_0}{1 - \eta_1 / \phi_0} + \frac{15}{2} \left(\frac{\eta_1 / \phi_0}{1 - \eta_1 / \phi_0} \right)^2 + 3 \left(\frac{\eta_1 / \phi_0}{1 - \eta_1 / \phi_0} \right)^3 \quad (5.23)$$

The vanishing quench effect in this limit of very large matrix particle cannot be deduced by a straightforward inspection of the diagrams in eq.(5.10). We have not succeeded in finding a formal proof. Therefore, we consider this prediction of SPT for vanish quench effect in case of very large matrix particles as a conjecture and this deserves certainly further investigations.

Finally, it is worth to note also that R_0 appears in eq.(5.23) only in the form of R_0^3 but no linear term in R_0 neither terms involving R_0^2 are present. This implies that in the limit of $\tau \rightarrow 0$, the surface free energy between the fluid and the matrix does not contribute to the chemical potential.

B. Small quench effect

At the end of the last subsection, we have just seen that quench effect vanishes

when the matrix particles are much larger than the fluid particles, i.e., $\tau = R_1 / R_0 \rightarrow 0$. The extensive numerical calculations we have carried out show that for all the cases with matrix particles larger than fluid particles, i.e., $R_0 > R_1$, the quench effect remains always quite moderate. The results for $\tau = 0.5$ are presented in [Fig. 5.3](#). For the two matrix densities considered, the chemical potential of the confined fluid and that of the corresponding equilibrium mixture are nearly the same even at high fluid densities. The mathematical reason for the moderate values of the quench chemical potential in the region of $0 < \tau < 1$ becomes clear by examining eq.(5.20). We see readily that no value of τ in this region can induce large variations of the quench chemical potential for physically meaningful values of matrix and fluid densities ($0 < \rho_0^* < 0.5, 0 < \rho_1^* < 0.5$). It is to note also that for both densities, it is slightly more difficult to insert a particle of species 1 into the equilibrium binary mixture than into a matrix at high fluid density, i.e., $\mu_1^{Equil} > \mu_1^{QA}$. We carried out also MC simulations under the same conditions and the results are plotted also in [Fig. 5.3](#) along with the SPT ones. We see that there is a very good agreement between SPT and MC results for both quench-annealed and equilibrium binary systems.

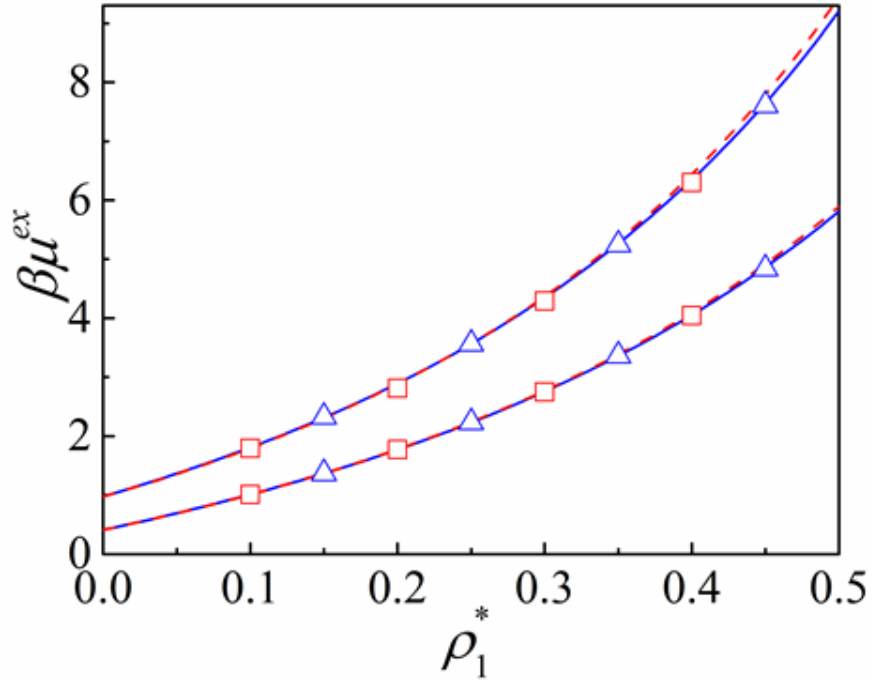


Figure 5.3. Comparison of the excess chemical potential as a function of fluid density [$\rho_1^* = \rho_1(2R_1)^3$] for a HS fluid in a HS matrix (SPT: curves with full line; MC: triangles) to that of a corresponding equilibrium system (SPT: curves with dash line; MC: squares) with $\tau = R_1 / R_0 = 0.5$ and matrix densities: a) $\rho_0^* = \rho_0(2R_0)^3 = 0.2$ (the four lower curves, overlapped together); b) $\rho_0^* = 0.5$ (the four upper curves, overlapped together).

C. Turning point for the change from small to large quench effects

The results for the case that the size of fluid and matrix particles is the same, i.e., $\tau = 1$, are presented in **Fig. 5.4**. When the matrix density is relatively low ($\rho_0^* = 0.2$), the quench effect remains small over the whole range of the considered fluid densities. Nevertheless, it is to note that the chemical potential of the quench-annealed system is higher than that of the corresponding equilibrium binary mixture, i.e., $\mu_1^{QA} > \mu_1^{Equil}$ (opposite to what is found for $\tau = 0.5$). The new feature shown by **Fig.5.4** is that at $\tau = 1$, the quench effect becomes significant when the matrix density is higher

($\rho_0^* = 0.5$) and again one observes $\mu_1^{QA} > \mu_1^{Equil}$. We will see in the next subsection that the quench effect becomes stronger in the region of $\tau > 1$. So, $\tau = 1$ is the turning point for the quench effect becoming significant and also the point at which the quench chemical potential changes sign, i.e., from $\mu_1^{Equil} > \mu_1^{QA}$ to $\mu_1^{QA} > \mu_1^{Equil}$. In **Fig.5.4**, the MC simulation results are also presented. For the equilibrium binary mixture, SPT gives always results in good agreement with the MC ones while it overestimates the fluid chemical potential of the quench-annealed system when the quench effect becomes significant.

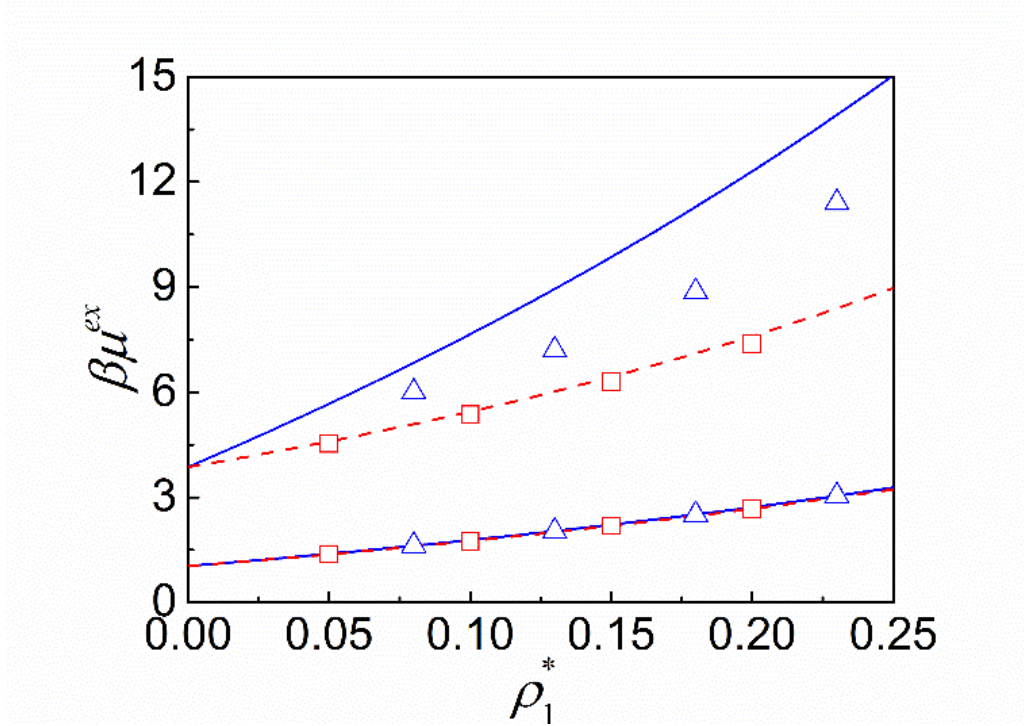


Figure 5.4. Comparison of the excess chemical potential as a function of fluid density [$\rho_1^* = \rho_1(2R_1)^3$] for a HS fluid in a HS matrix (SPT: curves with full line; MC: triangles) to that of a corresponding equilibrium system (SPT: curves with dash line; MC: squares) with $\tau = R_1/R_0 = 1$ and matrix densities: a) $\rho_0^* = \rho_0(2R_0)^3 = 0.2$ (the four lower curves, overlapped together); b) $\rho_0^* = 0.5$ (the four upper curves).

D. Strong quench effect

Now, we consider the case that matrix particles are smaller than the fluid particles, i.e., $\tau > 1$. The results for $\tau = 2$ and three matrix densities (ρ_0^* : 0.05, 0.2 and 0.3) are presented in **Fig. 5.5**. At very low matrix density ($\rho_0^* = 0.05$), the quench effect remains small (see **Fig. 5.5a**). As the matrix density increases, the quench effect becomes significant and increases with the fluid density (see **Fig. 5.5b** and **5c**). At high fluid densities, μ_1^{QA} is larger than μ_1^{Equil} (note that for $0 < \tau \leq 1$, $\mu_1^{Equil} > \mu_1^{QA}$ at high fluid densities). From **Fig. 5.5b** and **5c**, we see that the fluid chemical potential of the quench-annealed system is overestimated by SPT compared the MC simulation results. Nevertheless, the trend for the variation of the quench effect described by SPT is in agreement with that from MC simulations. It is to be pointed out that the accuracy of SPT for confined HS fluids has been checked previously only in the case of $\tau \leq 1$, i.e., the fluid particles being not smaller than the matrix particles. The present work confirms the good accuracy of SPT in this case but reveals that in the case of fluid particle smaller than the matrix particle, the accuracy of SPT deteriorates when fluid and matrix densities increase.

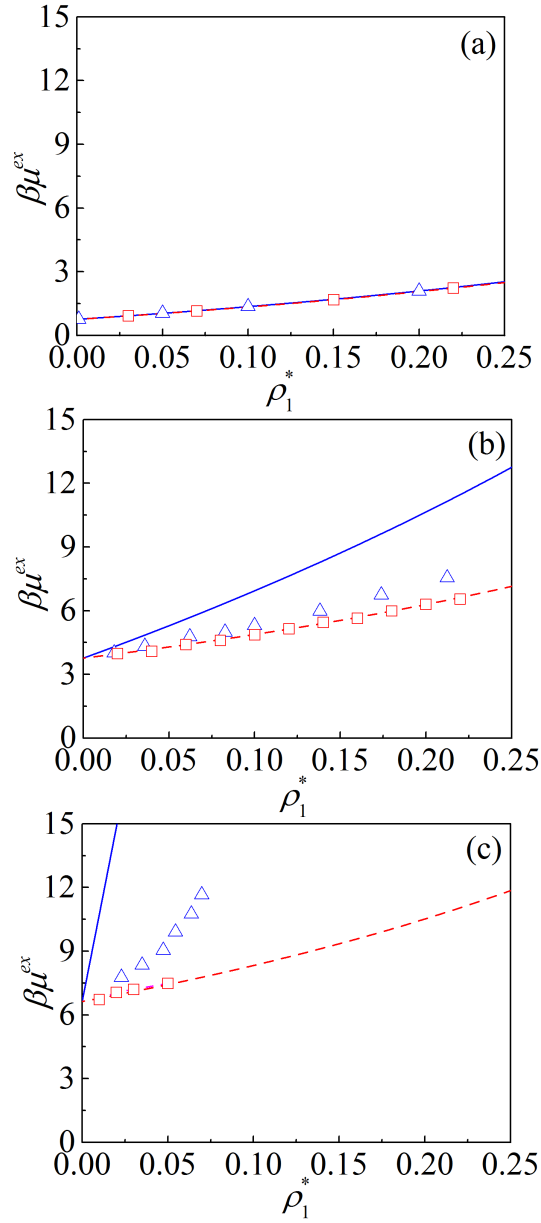


Figure 5.5. Comparison of the excess chemical potential as a function of fluid density $[\rho_1^* = \rho_1(2R_1)^3]$ for a HS fluid in a HS matrix (SPT: curves with full line; MC: triangles) to that of a corresponding equilibrium system (SPT: curves with dash line; MC: squares) with $\tau = R_1 / R_0 = 2$ and matrix densities: a) $\rho_0^* = \rho_0(2R_0)^3 = 0.05$; b) $\rho_0^* = 0.2$; c) $\rho_0^* = 0.3$.

In **Fig. 5.6**, the results for $\tau = 5$ and two matrix densities (ρ_0^* : 0.0384 and 0.05)

are presented. These results show that the quench effect becomes stronger when the size ratio of the fluid particle to the matrix particle increases.

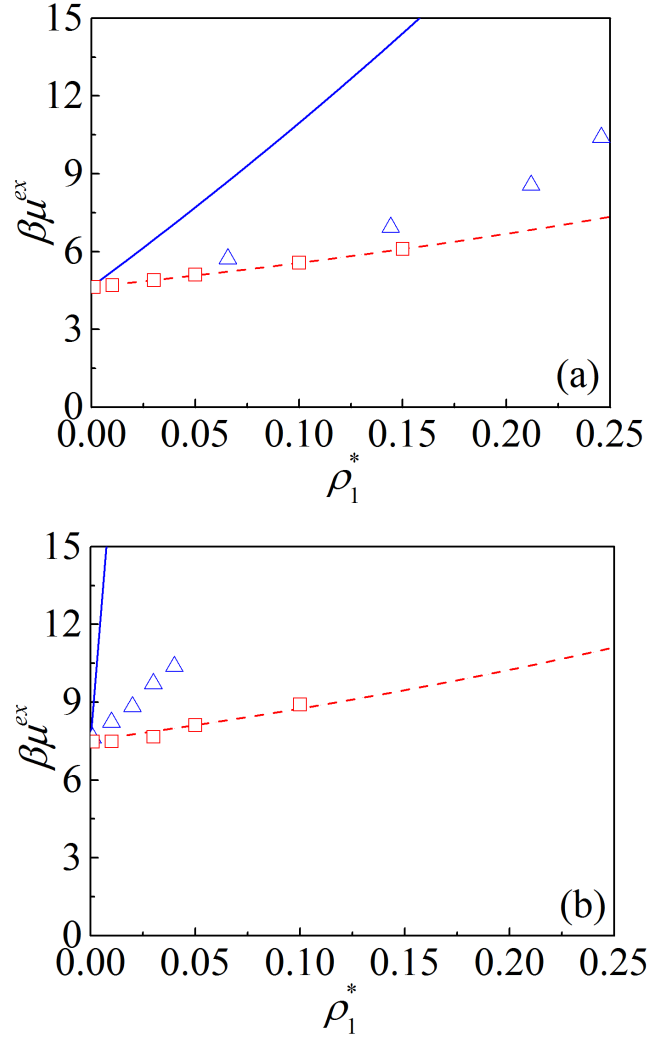


Figure 5.6. Comparison of the excess chemical potential as a function of fluid density [$\rho_1^* = \rho_1(2R_1)^3$] for a HS fluid in a HS matrix (SPT: curves with full line; MC: triangles) to that of a corresponding equilibrium system (SPT: curves with dash line; MC: squares) with $\tau = R_1 / R_0 = 5$ and matrix densities: a) $\rho_0^* = \rho_0(2R_0)^3 = 0.0384$; b) $\rho_0^* = 0.05$.

In order to understand the large quench effect found here, we consider the case of a matrix with point particles, i.e., $R_0 = 0$. Noting that in the limit $R_0 \rightarrow 0$ ($\tau \rightarrow \infty$), only $\tau^3\eta_0$ survive for the terms involving τ in eqs.(5.11), (5.12), and (5.14), we

obtain,

$$\beta\mu_1^{ex(QA)} = \frac{4\pi R_1^3 \rho_0}{3} - \ln(1-\eta_1) + \left[7 + e^{\frac{4\pi R_1^3 \rho_0}{3}} - 1 \right] \frac{\eta_1}{1-\eta_1}, \quad (5.24)$$

$$+ \frac{15}{2} \left(\frac{\eta_1}{1-\eta_1} \right)^2 + 3 \left(\frac{\eta_1}{1-\eta_1} \right)^3$$

and

$$\beta\mu_1^{ex(Equil)} = \frac{4\pi R_1^3 \rho_0}{3} - \ln(1-\eta_1) + \left[7 + \frac{4\pi R_1^3 \rho_0}{3} \right] \frac{\eta_1}{1-\eta_1}. \quad (5.25)$$

$$+ \frac{15}{2} \left(\frac{\eta_1}{1-\eta_1} \right)^2 + 3 \left(\frac{\eta_1}{1-\eta_1} \right)^3$$

We see now that μ_1^{QA} and μ_1^{Equil} are different only by the third terms on the RHS of eqs.(5.24) and (5.25). This third term for μ_1^{QA} increases exponentially with the matrix density while that for μ_1^{Equil} increases linearly. This explains why the difference between μ_1^{QA} and μ_1^{Equil} increases very quickly with the matrix density. The exponentially-increasing term comes from the term $(\phi_0 - \phi) / \phi$ in eq.(5.11). Numerical results for finite values of τ in the region of $1 < \tau < \infty$ show that the dominant contribution to quench chemical potential comes always from the term $(\phi_0 - \phi) / \phi$.

Moreover, it is worthwhile to note that eqs.(5.24) and (5.25) lead to a quite simple expression for the quench chemical potential, i.e.,

$$\beta\Delta\mu_1 = \left(e^{\frac{4\pi R_1^3 \rho_0}{3}} - 1 - \frac{4\pi R_1^3 \rho_0}{3} \right) \frac{\eta_1}{1-\eta_1}. \quad (5.26)$$

In the case of very large matrix particles, i.e., $\tau \rightarrow \infty$, the quench chemical potential varies linearly with $\eta_1 / (1-\eta_1)$ with a slope depending only on the matrix density, ρ_0 , and the fluid particle size, R_1 . It is also to note that the RHS of eq.(5.26) does not contain the contribution of the linear term in matrix density and this is in perfect

agreement with the general prediction from the diagrammatic expansion of quench chemical potential pointed out in section 5.3A.

5.4 Concluding remarks

In the present section, we studied in details the quench effect on the chemical potential of a hard-sphere fluid confined in a hard-sphere matrix. A quantitative measure is introduced which is the difference between the chemical potential of the confined fluid and that of the corresponding equilibrium binary mixture. From the diagrammatic expansion of quench chemical potential, we see that there is no quench effect at the linear order of matrix density. In some cases, e.g., one point fluid particle in an HS matrix or one finite size HS fluid particle in a matrix of point particles, both the chemical potential of the quench-annealed system and that of the corresponding equilibrium counterpart can be calculated exactly and analytically. In these cases of one single fluid particle, the quench effect vanishes strictly as well. Hence, the quench effect shows up only when fluid-fluid and matrix-matrix correlations are both present. Under more general conditions, we applied scaled particle theory for calculating the chemical potential of the quench-annealed system and that of its equilibrium counterpart. Thorough numerical investigations and analytical analysis allowed us to identify the parameter which controls the appearance of quench effect for the system considered here. When matrix particles are larger than fluid particles, quench effect is small for physically meaningful matrix and fluid densities and the equilibrium binary mixture appears slightly more crowded than the quench-annealed system. SPT predicts that in the limit of extremely large matrix particles, i.e., $\tau = R_1 / R_0 \rightarrow 0$, the quench effect vanishes. In the case of matrix particles smaller than fluid ones, the quench effect can become strong as matrix and fluid densities increase. In this case, the quench-annealed system can appear more crowded than the corresponding equilibrium binary mixture even when the density of each species is strictly the same in both systems respectively. The comparison between SPT and MC results show that the fluid chemical potential of

the quench-annealed system can be significantly overestimated by SPT in the case of fluid particles larger than the matrix particles. This is in sharp contrast with the excellent accuracy of SPT for confined HS fluid when the fluid particle is not larger than the matrix particle. For the moment, the origin of this inaccuracy does not appear clear and deserves certainly further investigations. Nevertheless, the trend for the variation of quench effect predicted by SPT is in agreement with that found from MC simulations.

Although the conclusions given above are obtained from the study of a simple model with only repulsions between hard cores, they should be general since the size effect exists for any real fluid and porous materials. Moreover, our results provide also some useful insights for the design of functionalized porous materials. For highly divided porous materials, i.e., those with its tiny solid constituents evenly distributed in space (e.g., aerogels), the quench effect is large and it can be hard to adsorb large fluid particles into such materials even when the porosity is high. For example, such a thumb rule can be useful for elaborating porous membrane for separation. Moreover, the findings of the present work should be useful also for assessing the quench effect on diffusion since the thermodynamics factor in an experimentally measured activity-based diffusion coefficient²⁶⁶ is directly related to chemical potential²⁶⁷. Nevertheless, a detailed discussion of this interesting topic is far beyond the scope of the present work.

6. Final remarks

Porous materials have important applications in both fundamental research and chemical industry, such as oil exploitation, catalysis, capturing Greenhouse gas, energy storage devices, and design of sensors. For instance, Aerogels with their highly macroscopic operability, extremely surface area, and recoverability, are widely used in photocatalysis. Many of those applications are based on the behavior of fluid adsorption in porous materials, such as the drug release, and gas separation. Thus a thorough understanding of the behavior of fluid confined in porous materials is necessary.

During the last few decades, a large number of theoretical and experimental investigations of fluids confined in different kinds of porous material had been made. The properties of confined fluid can be affected by the geometry of porous material, i.e., porosity, pore-connectivity, pore size distribution, pore shape, and disorder effect. Unfortunately, we still do not know the respective roles played by those geometric properties. Different from the bulk fluid, while the fluid particles adsorbed in porous material, the fluid particles feel not only the interaction from the surrounding fluid particles but also that from solid ones. This additional solid-fluid interaction can vary from very repulsive to very attractive ones. The different solid-fluid interaction can make the confined fluid exhibit very different behavior even materials with same geometry. Although confined fluid appears more complicated due to the presence of complex confining environment of adsorbent, one can wonder if there is any connection between confined and bulk fluids. To answer this question, in [Chapter 2](#), we derived a general scaling relation between the confined fluid and the corresponding bulk one-component fluid, which allows for connecting some thermodynamic properties of a confined fluid, i.e. chemical potential, Helmholtz free energy per particle, and grand potential per particle, to the bulk ones. The validity of this scaling relation is established with the help of a large number of simulation results, in a wide range of confining environments, from single isolated pore to random porous medium, and the fluid-fluid

and fluid-matrix pair interaction, from pure repulsive to repulsive plus attractive interaction. Since this scaling relation holds for chemical potential, Helmholtz free energy per particle, and grand potential per particle, one can immediately find that if Helmholtz free energy per particle and grand potential per particle are expressed as a function of chemical potential, the confined fluid will show the same behavior with the corresponding bulk one. This invariance implies the chemical potential should be considered as independent variable instead of fluid density, in the study of the confined or inhomogeneous fluids. Although a derivation of the scaling relation from the first-principles is currently unavailable, we have revealed its intimate connection with general theoretical frameworks like Gibbs theory for inhomogeneous fluids and morphological thermodynamics. We believe this is why the scaling relation works so well under wide conditions and for a large variety of confining environments. The scaling relation shows clearly that the porosity (space accessibility) and fluid-solid interaction (through the adsorption term) is of primary importance for determining the thermodynamics of confined fluids. The other characteristics, like pore-connectivity, pore-shape, pore-size distribution, etc., play less significant role. One potential application of our scaling relation is circumventing some experimental difficulty for direct measurement of some thermodynamic properties of confined fluid. In this work, the scaling relation was only used to study some thermodynamics properties of confined fluid. One nature extension is to see the scaling relation still holds for dynamics properties, such as diffusion coefficient. Another intuitive extension is to consider if the scaling relation holds also for the fluid adsorption in flexible porous materials, e.g. metal-organic frameworks (MOFs) or to find the modifications needed if necessary.

For fluid adsorption in a real porous material, the fluid-solid interfaces are generally curved ones. It might appear surprising that the thermodynamics for dealing with curved interfaces is not so well established although early investigations go back to Tolman. Thus a thorough understanding of the interfacial properties is necessary. Scaled particle theory is a powerful tool for studying the properties of fluid near to a

curved wall. The original motivation for scaled particle theory is to derive a simple equation of state for a bulk hard sphere fluid. Then, it was recognized that scaled particle theory provides not only the thermodynamic properties of a hard sphere fluid in bulk but also the surface tension of a hard sphere fluid near a spherical hard wall. However, the accuracy of its predictions is not as high as other recent equation of state like Carnahan-Starling equation of state. Mecke and co-workers have made efforts to develop a general framework, named as morphological thermodynamics, to account for more complex surface morphology. According to Hadwiger theorem in the integral geometry, the morphological thermodynamics assumes that the thermodynamic potential of an inhomogeneous system can be expressed as a linear combination, which only contains four terms, i.e., one bulk contribution proportional to system's volume and three surface contributions proportional respectively to surface area, mean and Gaussian curvatures of the interface. It is to be pointed out that in scaled particle theory, the chemical potential for creating a spherical cavity inside a fluid is assumed to have this form. The foundation of this method has been questioned recently. The contribution from the terms beyond the four Hadwiger's terms has been revealed from both diagrammatic expansion approach and molecular simulation. It is natural to ask that is it possible to include non-Hadwiger terms in scaled particle theory? To answer this question, in **Chapter 3**, two augmented scaled particle theory were proposed. The first one contains an adjustable parameter, and the second one uses two matching processes to circumvent the adjustable parameter. Both of them have simple analytical expressions. Also, both of them do not only significantly improve the accuracy of thermodynamic properties, i.e., pressure and chemical potential, but also improve the accuracy of surface properties, i.e., planar surface tension and Tolman length. Also, the same idea can be used to treat the multi-component hard sphere fluid system, and the improvement is significant. The success of our two augmented scaled particle theory indicates that the morphological thermodynamic is not an exact theory, it is only a very good approximation. One intuitive extension of this work is to consider if the more non-

Hadwiger terms are considered, will the higher accuracy of scaled particle be obtained?

For description of porous medium, many theoretical models for porous medium were carried out. Models with simple pore geometry, such as slit, cylinder pore, are widely studied. In such models, the pore-size distribution and pore connectivity are neglected. For ordered porous materials like MOF and ZIF, have been studied by molecular simulation and density functional theory. To consider the quench disorder effect, some random porous medium models have been carried out, i.e., Madden-Glandt matrix model, Van Tassel's templated matrix model, and hard sponge matrix model. The equation of state for confined fluid strongly depends on the model of porous medium. So, is it possible to derive a general equation of state which is irrelevant with the model of porous medium? In [Chapter 4](#), we derived a new general equation of state for describing the thermodynamic properties of fluids confined in different porous medium. To our best knowledge, this is the first equation of state for confined fluid that is irrelevant to the model of porous medium. In this general equation of state, the chemical potential is considered as the independent variable. In a large range, our new equation of state works well. Our new equation of state indicates that the porosity and other three geometric properties play the primary roles for the thermodynamic of confined fluid. All the other parameters, i.e., pore shape, pore connectivity, pore size distribution, and disorder effect, are much less important, which is similar to the results from our scaling relation. We also reported that even for an ideal gas fluid, in some cases, the morphological thermodynamic still does not hold, which means the morphological thermodynamics is only a good approximation. In this work, we only consider the hard sphere fluid. One nature extension of this work is to see if this equation of state still holds for other fluid, such as square-well fluid and Lennard-Jones fluid. An interesting application of this work is to consider if this equation of state can be used to describe the flexible porous materials.

The Madden-Glandt model is also called as a quench-annealed mixture with quenched species referring to the matrix and annealed species referring to the confined

fluid. Although many investigations have been devoted to study fluids confined in the random porous medium since Madden-Glandt model was proposed, no precise measure has ever been proposed to describe quantitatively the quench effect for the adsorption of a fluid in a random porous material. In **Chapter 5**, we introduced a quantitative measure of quench effect which is the difference between the chemical potential of the confined fluid and that of the corresponding equilibrium binary mixture. With the help of diagrammatic expansion, we revealed that this is no quench effect at the linear order of matrix density. Hence, the quench effect shows up only when fluid-fluid and matrix-matrix correlations are both present. With the help of scaled particle theory for confined fluid and the molecular simulation, we found that when matrix particles are larger than fluid particles, quench effect can be ignored. When the fluid particles are larger than matrix particles, the quench-annealed system can appear more crowded than the corresponding equilibrium binary mixture even when the density of each species is strictly the same in both systems. This indicates that the ratio of the radius of fluid particles to that of matrix ones plays the primary role for the quench effect. The comparison between scaled particle theory and molecular simulation results show that the fluid chemical potential of the quench-annealed system can be significantly overestimated by scaled particle theory in the case of fluid particles larger than the matrix particles. This is in sharp contrast with the excellent accuracy of scaled particle theory for confined hard sphere fluid when the fluid particle is not larger than the matrix particle. In my opinion, this is caused by the definition of porosity of porous materials. There are two porosities, geometric porosity, and probe particle porosity, in the scaled particle. By analyzing the contribution of each term, one can find that this overestimate comes from the probe particle porosity term. It means the probe particle porosity underestimated the fluid particle accessible volume of porous medium. If only the geometric porosity is used in scaled particle theory, SPT2a, the fluid chemical potential of the quench-annealed system will be underestimated. This can be explained by a simple example, consider fluids confined in a cubic lattice matrix which the distance

between two matrix particles is smaller than the diameter of fluid particle, in this system the fluid chemical potential is approach to infinity, but the prediction of chemical potential from SPT2a is same as the corresponding the bulk ones. This means the geometric porosity overestimated the fluid accessible volume of porous medium. Hence, how to find an appropriate porosity is the key to improve the accuracy of scaled particle theory for confined system. Our results provide some useful insights for the design of functionalized porous materials. For highly divided porous materials, i.e., those with its tiny solid constituents evenly distributed in space (e.g., aerogels), the quench effect is large and it can be hard to adsorb large fluid particles into such materials even when the porosity is high. For example, such a thumb rule can be useful for elaborating porous membrane for separation.

As a final remark, we would emphasize that with the help of theoretical approach and molecular simulation, this thesis studies the thermodynamics properties of confined fluid, clarifies the control variables of confined fluids, and discovers the common law of thermodynamics properties among different confined fluids. A scaling relation and two new equations of state were reported, they deepened the understanding of confined fluid, and advanced the development of the thermodynamics for confined fluid.

Appendix A. Some results for other versions of ASPT1

A.1. Single-point matching formulation with $n = 1$

Here we present the results of ASPT1 with a one order adjustable parameter. The excess chemical potential is described by a piecewise function,

$$\beta\mu_s^{ex}(R_s) = \begin{cases} -\ln\left[1-\eta\left(1+R_s/R\right)^3\right] & -R < R_s \leq 0 \\ \phi_{-1}\frac{\left(1-e^{-R_s/\delta}\right)}{R_s} + \phi_0 + \phi_1 R_s + \frac{1}{2}\phi_2 R_s^2 + \frac{4\pi R_s^3 \beta P}{3} & 0 < R_s \end{cases}. \quad (\text{A.1})$$

With the help of the following four conditions,

$$\beta\mu_s^{ex}(R_s = 0^-) = -\ln(1-\eta) = \beta\mu_s^{ex}(R_s = 0^+), \quad (\text{A.2})$$

$$\left.\frac{\partial\beta\mu_s^{ex}}{\partial R_s}\right|_{R_s=0^-} = \frac{1}{R} \frac{3\eta}{1-\eta} = \left.\frac{\partial\beta\mu_s^{ex}}{\partial R_s}\right|_{R_s=0^+}, \quad (\text{A.3})$$

$$\left.\frac{\partial^2\beta\mu_s^{ex}}{\partial R_s^2}\right|_{R_s=0^-} = \frac{1}{R^2} \frac{3\eta(2+\eta)}{(1-\eta)^2} = \left.\frac{\partial^2\beta\mu_s^{ex}}{\partial R_s^2}\right|_{R_s=0^+}, \quad (\text{A.4})$$

$$\left.\frac{\partial^3\beta\mu_s^{ex}}{\partial R_s^3}\right|_{R_s=0^-} = \frac{1}{R^3} \frac{6\eta(1+7\eta+\eta^2)}{(1-\eta)^3} + \frac{1}{R^3} \frac{9\eta(\beta P/\rho-1)}{(1-\eta)^3} = \left.\frac{\partial^3\beta\mu_s^{ex}}{\partial R_s^3}\right|_{R_s=0^+}. \quad (\text{A.5})$$

The four unknown ϕ_i ($i = -1, 0, 1, 2$) can be obtained as following.

$$\phi_0 = -\ln(1-\eta) - \frac{\phi_{-1}}{R} \frac{R}{\delta}, \quad (\text{A.6})$$

$$\phi_1 = \frac{1}{R} \left[\frac{3\eta}{1-\eta} + \frac{\phi_{-1}}{2R} \left(\frac{R}{\delta} \right)^2 \right], \quad (\text{A.7})$$

$$\phi_2 = \frac{1}{R^2} \left[\frac{3\eta}{1-\eta} \left(2 + \frac{3\eta}{1-\eta} \right) - \frac{\phi_{-1}}{3R} \left(\frac{R}{\delta} \right)^3 \right], \quad (\text{A.8})$$

$$\frac{\phi_{-1}}{R} = 24 \left(\frac{\delta}{R} \right)^4 \left[\frac{\eta(5-2\eta)}{2(1-\eta)} \frac{\beta P}{\rho} - \frac{5\eta}{2(1-\eta)} - 9 \left(\frac{\eta}{1-\eta} \right)^2 - 9 \left(\frac{\eta}{1-\eta} \right)^3 \right]. \quad (\text{A.9})$$

From eqs.(A.1)-(A.5), we obtain the following expression for the chemical potential,

$$\beta\mu = \beta\Phi(R_s = R) = \ln(\Lambda^3 \rho) - \ln(1-\eta) + \frac{6\eta}{1-\eta} + \frac{9}{2} \left(\frac{\eta}{1-\eta} \right)^2 + \eta \frac{\beta P}{\rho} + \frac{\phi_{-1}}{R} \left[1 - e^{-R/\delta} - \frac{R}{\delta} + \frac{1}{2} \left(\frac{R}{\delta} \right)^2 - \frac{1}{6} \left(\frac{R}{\delta} \right)^3 \right]. \quad (\text{A.10})$$

By using the same iterative procedure as presented in **Chapter 3**, the results of chemical potential and pressure can be obtained, named as ASPT11

$$\beta\mu^{ASPT11} = \beta\mu^{SPT} - a(\delta) \left(\frac{\eta}{1-\eta} \right)^3 \left(2 + \frac{3\eta}{1-\eta} \right), \quad (\text{A.11})$$

where

$$a(\delta) = \frac{6\delta}{R} \left[1 - \frac{3\delta}{R} + 6 \left(\frac{\delta}{R} \right)^2 - 6 \left(\frac{\delta}{R} \right)^3 (1 - e^{R/\delta}) \right]. \quad (\text{A.12})$$

By considering Gibbs-Duhem equation, the result for pressure is

$$\frac{\beta P^{ASPT11}}{\rho} = \frac{\beta P^{SPT}}{\rho} - 6a(\delta) \left\{ \frac{1}{2} \frac{\eta}{1-\eta} \left[\left(\frac{\eta}{1-\eta} \right)^3 + \frac{1}{3} \left(\frac{\eta}{1-\eta} \right)^2 + \frac{1}{3} \frac{\eta}{1-\eta} - 1 \right] - 1 - \frac{1}{\eta} \ln(1-\eta) \right\}. \quad (\text{A.13})$$

The surface tension near a spherical hard wall is given by

$$\tilde{\gamma}^{ASPT11}(R_s) = 4\pi R^2 \beta \gamma^{ASPT11}(R_s) = \tilde{\gamma}_0^{ASPT11} + \tilde{\gamma}_{-1}^{ASPT11} \frac{R}{R_s} + \tilde{\gamma}_{-2}^{ASPT11} \left(\frac{R}{R_s} \right)^2 + \tilde{\gamma}_{-3}^{ASPT11} \left(\frac{R}{R_s} \right)^3 (1 - e^{-R_s/\delta}), \quad (\text{A.14})$$

where

$$\tilde{\gamma}_0^{ASPT11} = \frac{\phi_2 R^2}{2} = \tilde{\gamma}_0^{SPT} - \frac{\tilde{\gamma}_{-3}^{ASPT11}}{6} \left(\frac{R}{\delta} \right)^3, \quad (\text{A.15})$$

$$\tilde{\gamma}_{-1}^{ASPT11} = \phi_1 R = \tilde{\gamma}_{-1}^{SPT} + \frac{\tilde{\gamma}_{-3}^{ASPT11}}{2} \left(\frac{R}{\delta} \right)^2, \quad (\text{A.16})$$

$$\tilde{\gamma}_{-2}^{ASPT11} = \phi_0 = \tilde{\gamma}_{-2}^{SPT} - \tilde{\gamma}_{-3}^{ASPT11} \frac{R}{\delta}, \quad (\text{A.17})$$

$$\tilde{\gamma}_{-3}^{ASPT11} = \frac{\phi_{-1}}{R} = 36 \left(\frac{\eta}{1-\eta} \right)^3 \left(2 + \frac{3\eta}{1-\eta} \right) \left(\frac{\delta}{R} \right)^4. \quad (\text{A.18})$$

By using the same way as presented in [Chapter 3](#), the adjustable parameter is obtained as $\delta/R=0.0438954$. Then we presented the numerical results of APST11 below. Following Figures show that ASPT11 significantly improved the accuracy of both bulk properties and interfacial properties. However, for non-Hadwiger term, the prediction of ASPT11 underestimated it.

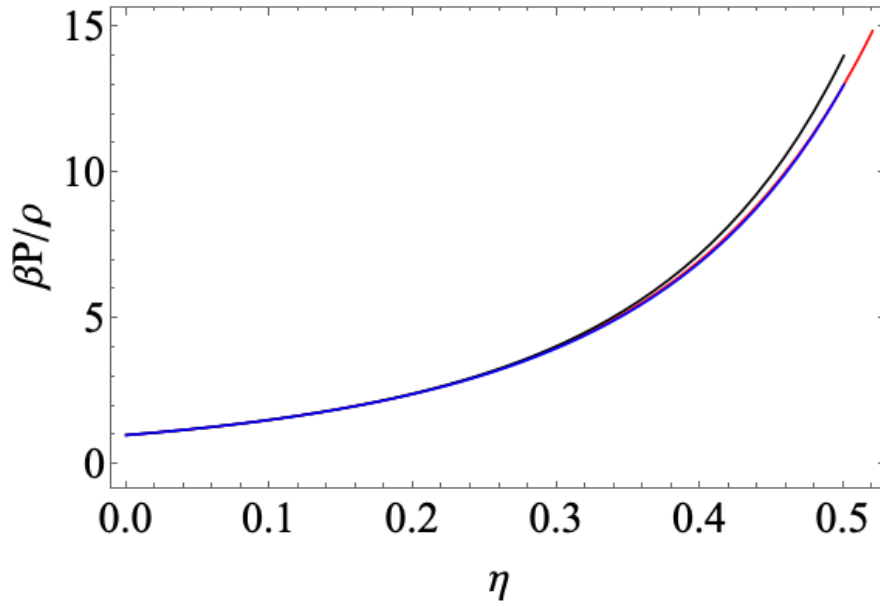


Figure A.1. Comparison of pressure of a hard sphere fluid. The simulation results are presented by the blue line, the black line is original SPT, and the red line is ASPT11

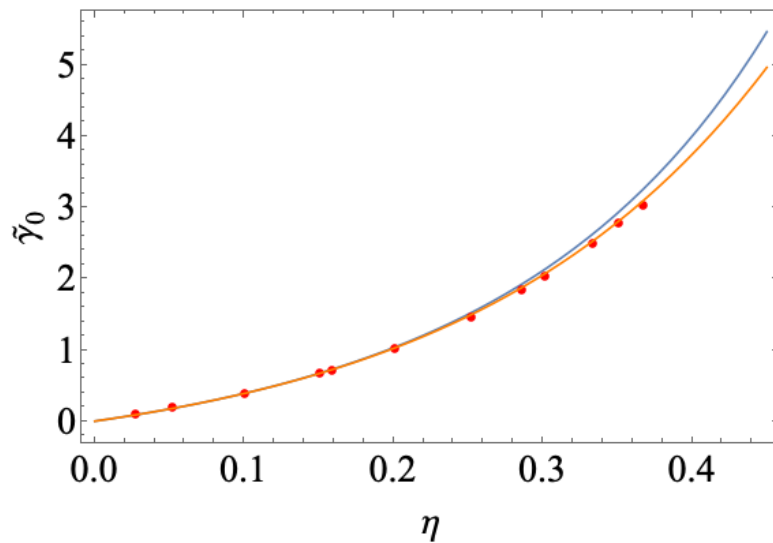


Figure A.2. Comparison of surface tension of a hard sphere fluid. The simulation results are presented by red circles, the blue line is original SPT, and the orange line is ASPT11

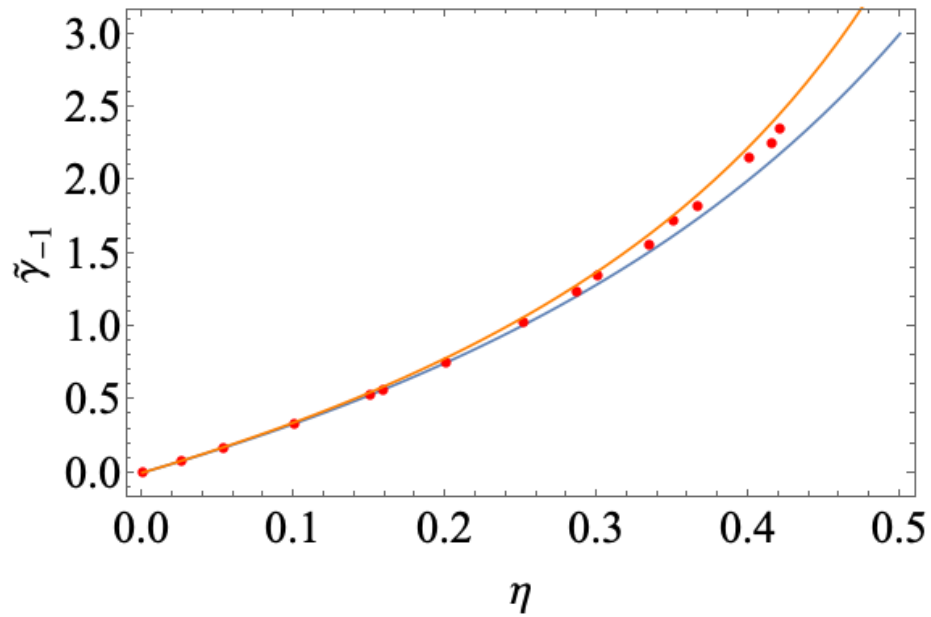


Figure A.3. Comparison of $\tilde{\gamma}_{-1}$ of a hard sphere fluid. The simulation results are presented by red circles, the blue line is original SPT, and the orange line is ASPT11

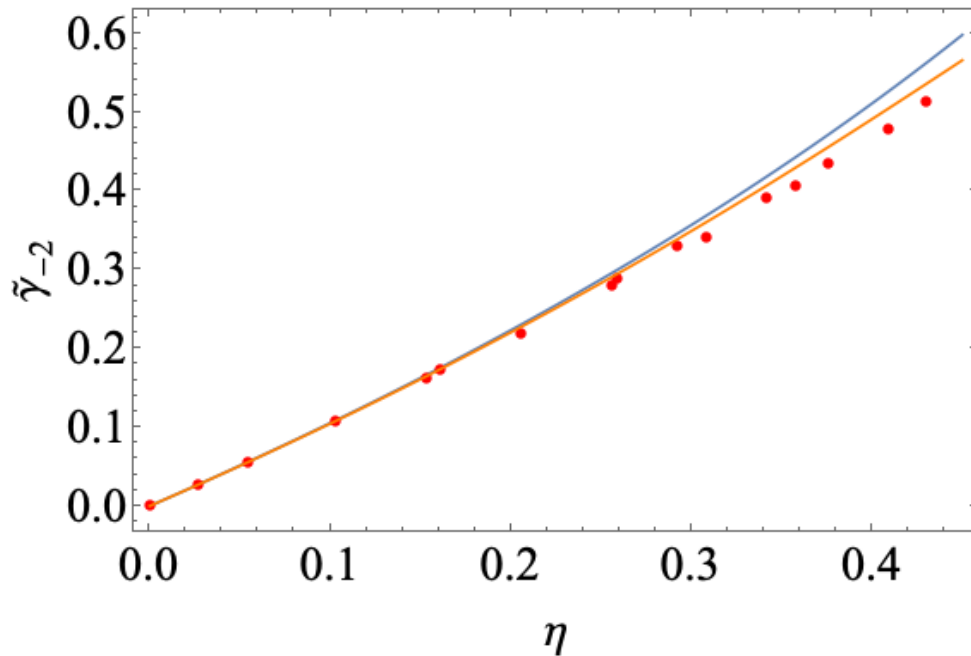


Figure A.4. Comparison of $\tilde{\gamma}_{-2}$ of a hard sphere fluid. The simulation results are presented by red circles, the blue line is original SPT, and the orange line is ASPT11

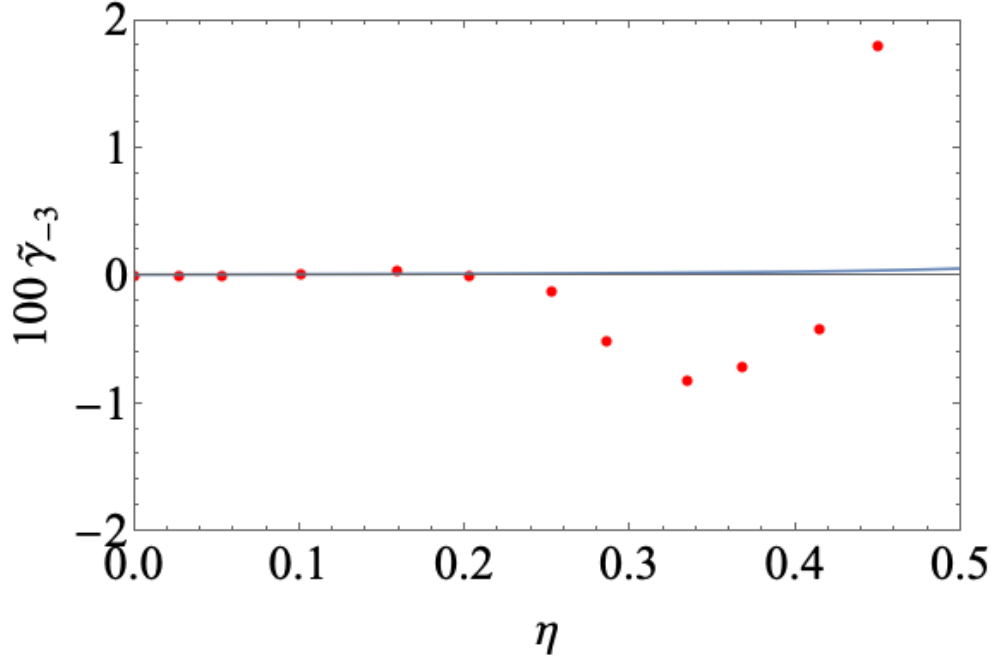


Figure A.5. Comparison of $\tilde{\gamma}_{-3}$ of a hard sphere fluid. The simulation results are presented by red circles, and the blue line is ASPT11

A.2. Single-point matching formulation with $n = 2$

Here we present the results of ASPT1 with a two order adjustable parameter. The excess chemical potential is described by a piecewise function,

$$\beta\mu_s^{\text{ex}}(R_s) = \begin{cases} -\ln\left[1 - \eta\left(1 + R_s/R\right)^3\right] & -R < R_s \leq 0 \\ \phi_{-1}\frac{\left(1 - e^{-R_s/\delta}\right)^2}{R_s} + \phi_0 + \phi_1 R_s + \frac{1}{2}\phi_2 R_s^2 + \frac{4\pi R_s^3 \beta P}{3} & 0 < R_s \end{cases}, \quad (\text{A.19})$$

With the help of eqs.(A.2)-(A.5), the four parameters ϕ_i ($i = -1, 0, 1, 2$) are

$$\phi_0 = -\ln(1 - \eta) \quad (\text{A.20})$$

$$\phi_1 = \frac{1}{R} \left[\frac{3\eta}{1 - \eta} - \frac{\phi_{-1}}{R} \left(\frac{R}{\delta} \right)^2 \right], \quad (\text{A.21})$$

$$\phi_2 = \frac{1}{R^2} \left[\frac{3\eta}{1 - \eta} \left(2 + \frac{3\eta}{1 - \eta} \right) + \frac{2\phi_{-1}}{R} \left(\frac{R}{\delta} \right)^3 \right], \quad (\text{A.22})$$

$$\frac{\phi_{-1}}{R} = -\frac{6}{7} \left(\frac{\delta}{R} \right)^4 \left[\frac{\eta(5-2\eta)}{2(1-\eta)} \frac{\beta P}{\rho} - \frac{5\eta}{2(1-\eta)} - 9 \left(\frac{\eta}{1-\eta} \right)^2 - 9 \left(\frac{\eta}{1-\eta} \right)^3 \right]. \quad (\text{A.23})$$

It should be noted that the sign of ϕ_{-1} is different from the ones when n is an odd number and ϕ_0 is same as the original SPT ones. From eqs.(A.20)-(A.23), we obtain the following expression for the chemical potential,

$$\begin{aligned} \beta\mu = \beta\Phi(R_s = R) = \ln(\Lambda^3 \rho) - \ln(1-\eta) + \frac{6\eta}{1-\eta} + \frac{9}{2} \left(\frac{\eta}{1-\eta} \right)^2 + \eta \frac{\beta P}{\rho} \\ + \frac{\phi_{-1}}{R} \left[\left(1 - e^{-R/\delta} \right)^2 - \left(\frac{R}{\delta} \right)^2 + \left(\frac{R}{\delta} \right)^3 \right]. \end{aligned} \quad (\text{A.24})$$

By using the same iterative procedure as presented in **Chapter 3**, the results of chemical potential and pressure can be obtained, named as ASPT12

$$\beta\mu^{ASPT12} = \beta\mu^{SPT} - a(\delta) \left(\frac{\eta}{1-\eta} \right)^3 \left(2 + \frac{3\eta}{1-\eta} \right), \quad (\text{A.25})$$

where

$$a(\delta) = \frac{18}{7} \frac{\delta}{R} \left[1 - \frac{\delta}{R} + \left(\frac{\delta}{R} \right)^3 \left(1 - e^{R/\delta} \right)^2 \right]. \quad (\text{A.26})$$

By considering Gibbs-Duhem equation, the result for pressure is

$$\begin{aligned} \frac{\beta P^{ASPT12}}{\rho} = \frac{\beta P^{SPT}}{\rho} - 6a(\delta) \left\{ \frac{1}{2} \frac{\eta}{1-\eta} \left[\left(\frac{\eta}{1-\eta} \right)^3 + \frac{1}{3} \left(\frac{\eta}{1-\eta} \right)^2 + \frac{1}{3} \frac{\eta}{1-\eta} - 1 \right] \right. \\ \left. - 1 - \frac{1}{\eta} \ln(1-\eta) \right\}. \end{aligned} \quad (\text{A.27})$$

The surface tension near a spherical hard wall is given by

$$\begin{aligned} \tilde{\gamma}^{ASPT12}(R_s) = 4\pi R^2 \beta \gamma^{ASPT12}(R_s) = \tilde{\gamma}_0^{ASPT12} + \tilde{\gamma}_{-1}^{ASPT12} \frac{R}{R_s} + \tilde{\gamma}_{-2}^{ASPT12} \left(\frac{R}{R_s} \right)^2 \\ + \tilde{\gamma}_{-3}^{ASPT12} \left(\frac{R}{R_s} \right)^3 \left(1 - e^{-R_s/\delta} \right)^2 \end{aligned}, \quad (\text{A.28})$$

where

$$\tilde{\gamma}_0^{ASPT11} = \frac{\phi_2 R^2}{2} = \tilde{\gamma}_0^{SPT} + \tilde{\gamma}_{-3}^{ASPT12} \left(\frac{R}{\delta} \right)^3, \quad (\text{A.29})$$

$$\tilde{\gamma}_{-1}^{ASPT12} = \phi_1 R = \tilde{\gamma}_{-1}^{SPT} - \tilde{\gamma}_{-3}^{ASPT12} \left(\frac{R}{\delta} \right)^2, \quad (\text{A.30})$$

$$\tilde{\gamma}_{-2}^{ASPT12} = \phi_0 = \tilde{\gamma}_{-2}^{SPT}, \quad (\text{A.31})$$

$$\tilde{\gamma}_{-3}^{ASPT11} = \frac{\phi_{-1}}{R} = 36 \left(\frac{\eta}{1-\eta} \right)^3 \left(2 + \frac{3\eta}{1-\eta} \right) \left(\frac{\delta}{R} \right)^4. \quad (\text{A.32})$$

By using the same way as presented in [Chapter 3](#), the adjustable parameter is obtained as $\delta/R = 0.0499796$. Then we presented the numerical results of APST12 below. Since the results of ϕ_0 in ASPT12 is same as the original ones, we only presented the numerical results of P and $\tilde{\gamma}_i$ ($i = 0, -1, -3$). One interesting find is the prediction of the non-Hadwiger term has a different sign with the result with an odd n . This indicates a potential form for describing non-Hadwiger terms, i.e., $(1 - e^{-\delta_1/R})^1 + (1 - e^{-\delta_2/R})^2$. With the suitable parameters, δ_1 and δ_2 , the prediction of non-Hadwiger term might have the same trend as the ones from molecular simulation.

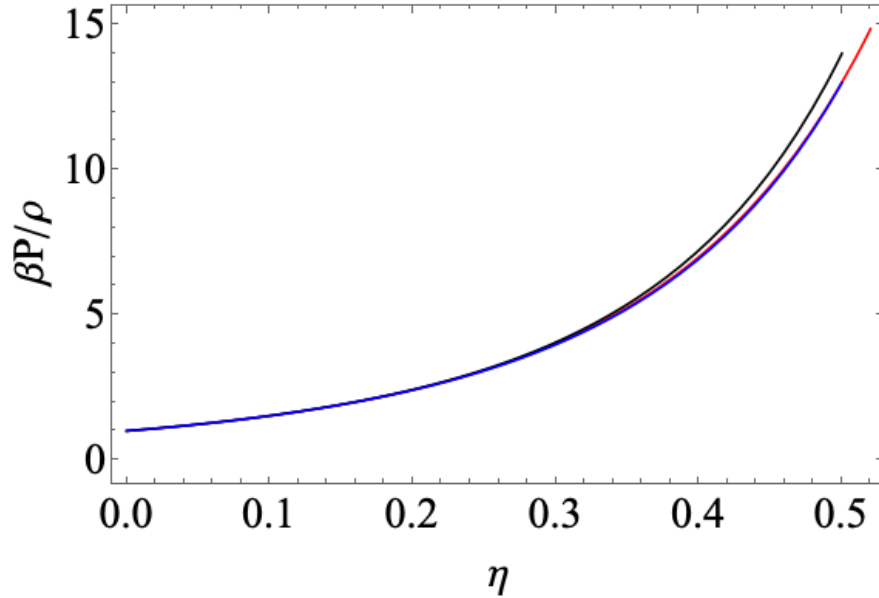


Figure A.6. Comparison of pressure of a hard sphere fluid. The simulation results are presented by the blue line, the black line is original SPT, and the red line is ASPT12

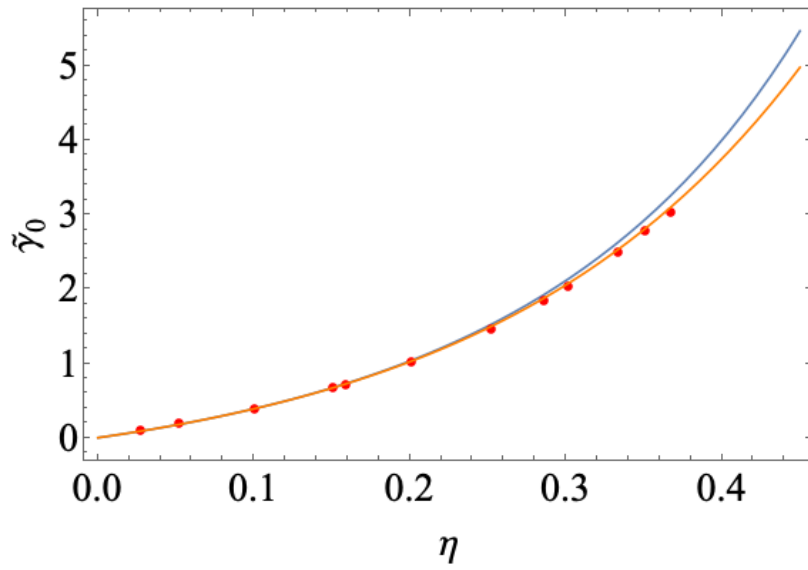


Figure A.7. Comparison of surface tension of a hard sphere fluid. The simulation results are presented by red circles, the blue line is original SPT, and the orange line is ASPT12

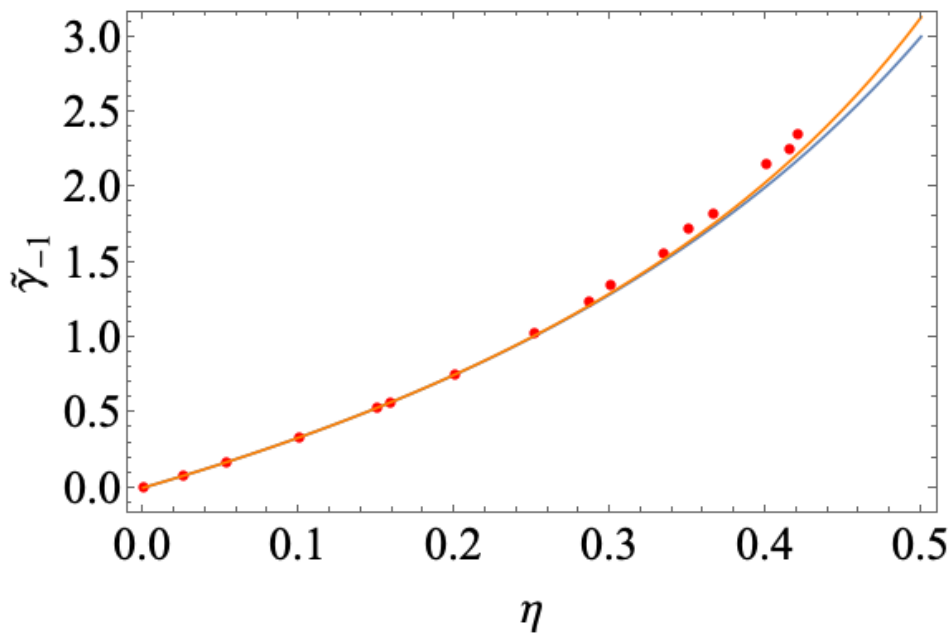


Figure A.8. Comparison of $\tilde{\gamma}_{-1}$ of a hard sphere fluid. The simulation results are presented by red circles, the blue line is original SPT, and the orange line is ASPT12.

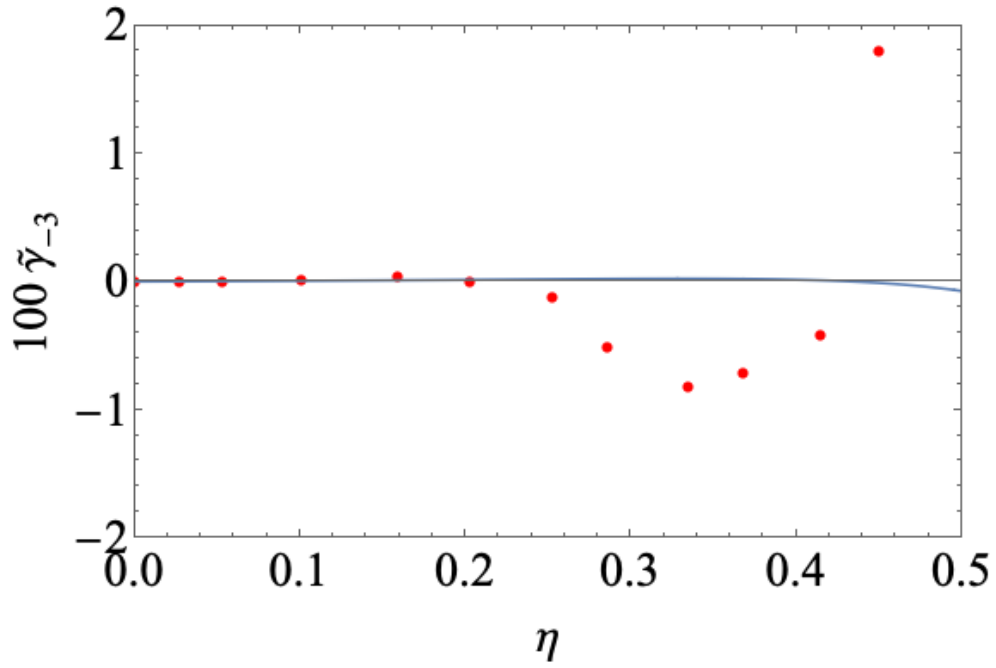


Figure A.9. Comparison of $\tilde{\gamma}_{-3}$ of a hard sphere fluid. The simulation results are presented by red circles, and the blue line is ASPT12

Appendix B. Invalidation of morphological thermodynamics

B.1. Fluid around two spherical solutes

Here, we consider an ideal gas fluid around two spherical solutes, as illustrated in **Fig. B.1**. The interaction between fluid and solutes is square well potential and the distance between two solutes is smaller than $2d$, which means some fluid particles suffered interaction from both two solutes. The grand partition function is

$$\Xi = \sum_{N=0}^{\infty} \frac{z^N}{N!} \int \exp[-\beta u_{01}(\mathbf{r})] d\mathbf{r}, \quad (\text{B.1})$$

The integrate above can be divided into two parts. Part 1 is the region suffered interaction from both two solutes, and part 2 is the remaining region. The integrate of part 1 is

$$V_1 = 2 \int_{L/2}^{R_0+d} \pi[(R_0+d)^2 - r^2] dr = \frac{4}{3} \pi (R_0+d)^3 - \frac{2\pi}{2} (R_0+d)^2 L + \frac{2\pi}{3} \left(\frac{L}{2}\right)^3, \quad (\text{B.2})$$

and the integrate of part 2 is

$$V_2 = \left[V - \frac{8\pi}{3} (R_0+d)^3 + V_1 \right] + e^{-\beta \varepsilon} \left[\frac{8\pi}{3} (R_0+d)^3 - \frac{8\pi}{3} R_0^3 - 2V_1 \right]. \quad (\text{B.3})$$

where V is system volume, and the grand potential is equal to

$$\beta \Omega = -z \left(V - \frac{8}{3} \pi R_0^3 \right) - z(e^{-\beta \varepsilon} - 1) \frac{8\pi}{3} (3R_0d + 3R_0d^2 + d^3) - z(e^{-\beta \varepsilon} - 1)V_1. \quad (\text{B.4})$$

From morphological thermodynamic, the grand potential of this system can be expressed as eq. (4.11) with same parameters, which all same as expression above but the last term. The last term of expression above denotes the contribution of the region suffered interaction from both two solutes. This calculation proves morphological thermodynamic cannot use for when such overlapping part appears. The future study of morphological thermodynamic and Hadwiger's volume theorem is still needed.

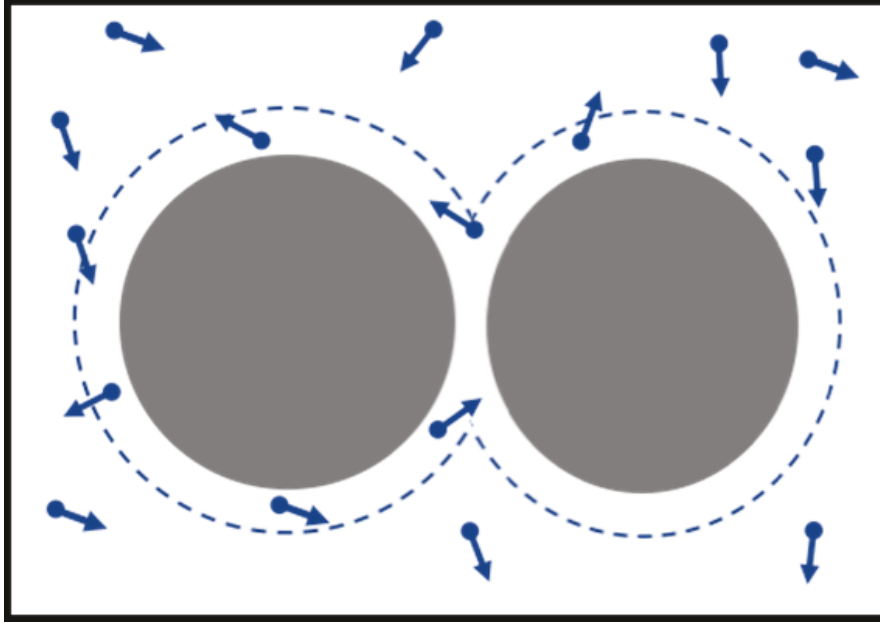


Figure B.1. Schematic presentation of an ideal gas fluid around two spherical matrix particles with square well potential.

B.2 Non-Hadwiger term

A. A brief review of Hansen-Goos' work

Firstly, we will quickly recall Hansen-Goos' work, the system in his work is a hard sphere fluid around a big hard sphere spherical solute. The interfacial tension and solvation free energy can be obtained from following equations:

$$\gamma = \frac{\Omega - p(V_{tot} - V)}{A}, \quad (\text{B.5})$$

$$F_{sol} = \frac{\Omega - pV_{tot}}{A}, \quad (\text{B.6})$$

where Ω is the grand potential, p is the solvent pressure, V_{tot} and V are the system and solute volume respectively. So, the interfacial tension can be calculated from solvation free energy,

$$\gamma = \frac{F_{sol} - pV}{A}. \quad (\text{B.7})$$

The solvation free energy F_{sol} can be obtained from the so-called binary mixture route.

Consider a binary mixture system, l and 0 are used to represent two components. ρ_0 and ρ_1 are the density of component 0 and component l . ρ_i and R_i are the density and radius of component i ($i = 0, 1$), the solvation free energy can be obtained as the excess chemical potential $\beta\mu_0^{ex}$ in the limit $\rho_0 \rightarrow 0$, i.e.,

$$\beta F_{sol} = \beta\mu_0^{ex} = \left. \frac{\partial \beta\Phi}{\partial \rho_0} \right|_{\rho_0 \rightarrow 0}, \quad (\text{B.8})$$

where Φ is the excess free energy density of the bulk binary mixture, and $\beta = 1/(k_B T)$ (k_B is the Boltzmann constant, T is the temperature). As we know Φ can be written as a Virial expansion:

$$\Phi = \sum_{n=2}^{\infty} \sum_{j=0}^n \frac{1}{n-1} \binom{n}{j} B_n^{[l]}(R') \rho_1^{n-j} \rho_0^j, \quad (\text{B.9})$$

$$\begin{aligned} \left. \frac{\partial \beta\Phi}{\partial \rho_0} \right|_{\rho_0 \rightarrow 0} &= \sum_{n=2}^{\infty} \frac{n}{n-1} B_n^{[l]} \rho_1^{n-1} \\ &= 2B_2^{[l]} \rho_1 + \frac{3}{2} B_3^{[l]} \rho_1^2 + \frac{4}{3} B_4^{[l]} \rho_1^3 + O(\rho_1^4) \end{aligned}, \quad (\text{B.10})$$

$B_n^{[l]}$ is the Virial coefficient, $R' = (R_1 + R_0)/R_1$. So far, the solvation free energy is obtained, and the solvent pressure is given as following:

$$\frac{\beta p}{\rho_1} = 1 + \sum_{i=2}^{\infty} B_i \rho_1^{i-1}. \quad (\text{B.11})$$

Now, the solute-solvent interfacial tension is given as a series of ρ_1 :

$$\beta\gamma_{exact} = \sum_{i=1}^{\infty} c_i \rho_1^i. \quad (\text{B.12})$$

Since exact $B_n^{[l]}$ for $n \leq 4$ are known from previous work. For a low-density fluid, the first three terms in eq. (B.12) can be given as

$$\frac{\beta\gamma_{exact}}{\rho_1 R_1} = c_2(R') \eta_1 + c_3(R') \eta_1^2 + O(\eta_1^3), \quad (\text{B.13})$$

where

$$c_2(R') = -\frac{3}{2} + \frac{1}{3R'^2}, \quad (\text{B.14})$$

$$\begin{aligned} c_3(R') = & -\frac{183}{35} + \frac{3}{R'} + \frac{67}{63R'^2} - \left(\frac{81}{35} + \frac{27}{7R'^2} \right) \frac{X}{\pi} \\ & - \left(\frac{R'^7}{14} - \frac{18R'^5}{35} + \frac{3R'^3}{2} - 2R' + \frac{3}{R'} \right) \frac{Y}{\pi}, \\ & + \left(\frac{R'^4}{28} - \frac{57R'^2}{280} + \frac{61}{140} + \frac{13}{21R'^2} \right) \frac{Q}{\pi} \end{aligned} \quad (\text{B.15})$$

with

$$X = \arctan(Q), \quad (\text{B.16})$$

$$y = \pi - 3 \arctan\left(\frac{Q}{R'}\right), \quad (\text{B.17})$$

$$Q = \sqrt{3R'^2 - 4}, \quad (\text{B.18})$$

where η_1 is the solvent packing fraction $\eta_1 = 4\pi\rho_1 R_1^3 / 3$ and from eq. 1, the solute-solvent interfacial tension can be given as a series of R'

$$\gamma = (F_{sol} - pV) / A = \sigma + \kappa_1 C / A + \kappa_2 X / A = \sigma + \sum_{i=1}^{\infty} \frac{\kappa_i R^{-i}}{R'^i}. \quad (\text{B.19})$$

From the Hadwiger's theorem, κ_i should be equal to 0 for $i > 2$. It means that if $c_3(R')$ is expanded in powers of $1/R'$, $1/R'^3$ and higher orders terms will not exist.

The expansion of $c_3(R')$ as following,

$$c_3(R') = \sum_{i=0}^{\infty} \frac{c_{3i}}{R'^i} = -\frac{447}{70} + \left(3 + \frac{27\sqrt{3}}{16\pi} \right) \frac{1}{R} - \frac{109}{126} \frac{1}{R'^2} + \frac{3\sqrt{3}}{20\pi} \frac{1}{R'^3} + O\left(\frac{1}{R'^5}\right), \quad (\text{B.20})$$

It is found that the $1/R'^3$ and higher order terms still exist. This proves that morphological thermodynamics is not an exact method and can only serve as an approximation. It should be pointed out that the interface between fluid and the solute particle is a concave interface from fluid view in Hansen-Goos' work, and from Hadwiger's theorem, the interface must be a convex one. In the follow section, we will study a system in which the interface is a convex one from fluid view.

B. Non-Hadwiger coefficient in convex system

The system is a hard sphere fluid confined in a spherical hard sphere cavity, and the interaction potentials in this system are described as following,

$$u_{11}(|\mathbf{r}_i - \mathbf{r}_j|) = \begin{cases} \infty, & |\mathbf{r}_i - \mathbf{r}_j| < 2R_1 \\ 0, & |\mathbf{r}_i - \mathbf{r}_j| \geq 2R_1 \end{cases}, \quad (\text{B.21})$$

$$u_{10}(|\mathbf{r}_i - \mathbf{q}_0|) = \begin{cases} 0, & |\mathbf{r}_i - \mathbf{q}_0| < R_1 + R_0 \\ \infty, & |\mathbf{r}_i - \mathbf{q}_0| \geq R_1 + R_0 \end{cases}, \quad (\text{B.22})$$

where R_1 and R_0 are the radius of fluid particles and cavity. r_i and r_j are the position vectors of the i th and the j th particle. q_0 is the position vectors of the cavity, it is fixed in the center of this system.

We start from the usual Gibbs adsorption equation

$$\left(\frac{\partial \gamma}{\partial \mu} \right)_T = \Gamma_N, \quad (\text{B.23})$$

where Γ_N is the excess interfacial number of particles per unit area at the interface. It can be obtained as

$$\Gamma_N = \frac{1}{4\pi R_0^2} \int_0^{R_0+R_1} [\rho(r) - \rho(0)] 4\pi r^2 dr. \quad (\text{B.24})$$

From diagrammatic expansion $\rho(r)$ and $\rho(0)$ can be given as:

$$\rho(r) = Z \{ \text{sum of all the connected diagrams which are composed of one white fluid point, some or no black fluid point, wighted by } Z, \text{ one white cavity point connect with each fluid point, some or } , \text{ (B.25)} \\ \text{no } f_{11} \text{ bonds between pairs of fluid points, some } f_{10} \text{ bonds between pairs of cavity and fluid points } \}$$

$$\rho(0) = Z \{ \text{sum of all the connected diagrams which are composed of one white fluid point, some or no black fluid point, wighted by } Z, , \text{ (B.26)} \\ \text{some or no } f_{11} \text{ bonds between pairs of fluid points} \}$$

where Z is the activity of fluid

$$Z = \frac{e^{-\beta\mu_1}}{\Lambda_1^3}, \quad (\text{B.27})$$

where μ_1 is the bulk chemical potential, Λ_1 is the thermal wave-length of fluid particles and Mayer functions are defined as,

$$f_{11}(|\mathbf{r}_i - \mathbf{r}_j|) = e^{-\beta u_{11}(|\mathbf{r}_i - \mathbf{r}_j|)} - 1, \quad (\text{B.28})$$

$$f_{10}(|\mathbf{r}_i - \mathbf{q}_0|) = e^{-\beta u_{10}(|\mathbf{r}_i - \mathbf{q}_0|)}. \quad (\text{B.29})$$

The Γ_N is obtained as following:

$$\Gamma_N = \frac{\pi}{36s^2} (7 + 18s + 9s^2) z^2 \sigma_1^4 - \frac{4\Delta}{\pi s^2} z^3 \sigma_1^7 + \frac{\pi^2 (1+s)^3}{432s^2}, \quad (\text{B.30})$$

$$(s^6 + 6s^5 + 15s^4 - 4s^3 - 30s^2 - 12s - 164) z^3 \sigma_1^7 + O(z)$$

where

$$\Delta = \frac{\pi^2 \sigma_1^9}{2240} [-18(3s^2 + 6s + 8)X + (s+1)(5s^8 + 40s^7 + 104s^6$$

$$+ 64s^5 - 85s^4 - 20s^3 + 90s^2 - 36s + 144)Y + \frac{Q}{36}(30s^6$$

$$+ 180s^5 + 279s^4 - 84s^3 - 210s^2 + 228s + 745)] \quad (\text{B.31})$$

with

$$X = \arctan(Q), \quad (\text{B.32})$$

$$Y = \arctan\left(\frac{Q}{s+1}\right), \quad (\text{B.33})$$

$$Q = \sqrt{3s^2 + 6s - 1}, \quad (\text{B.34})$$

$$s = \frac{\sigma_0}{\sigma_1}, \quad (\text{B.35})$$

where σ_1 and σ_0 are the diameter of fluid particles and cavity. The interfacial tension can be obtained as following,

$$\beta\gamma = \int \Gamma_N d\beta\mu_1 = \int \Gamma_N \frac{\partial\beta\mu_1}{\partial Z} = \int -\Gamma_N / Z dZ, \quad (\text{B.36})$$

$$\beta\gamma = C_2(s)Z^2 \sigma_1^4 + C_3(s)Z^3 \sigma_1^7 + O(Z^4), \quad (\text{B.37})$$

where

$$C_2(s) = \frac{-\pi}{72s^2}(7 + 18s + 9s^2), \quad (\text{B.38})$$

$$C_3(s) = -\frac{\pi^2(1+s)^3}{1296s^2}(s^6 + 6s^5 + 15s^4 - 4s^3 - 30s^2 - 12s - 164) + \frac{4\Delta}{3\pi s^2 \sigma_1^9}, \quad (\text{B.39})$$

For large s , $C_3(s)$ can be expanded in powers of s , it can be obtained as,

$$\begin{aligned} c_3(s) = & \frac{\pi^2 s^7}{4536} + \frac{\pi^2 s^6}{504} + \frac{\pi^2 s^5}{1260} - \frac{7\pi^2 s^4}{540} - \frac{\pi^2 s^3}{90} + \frac{\pi^2 s^2}{18} + \frac{13\pi^2 s}{54} \\ & + \frac{2143\pi^2}{5040} + \left(\frac{3\sqrt{3}\pi}{128} + \frac{1273\pi^2}{11340} \right) \frac{1}{s^2} + \frac{\pi}{160\sqrt{3}s^3} + O\left(\frac{1}{s^4}\right). \end{aligned} \quad (\text{B.40})$$

Clearly, the non-Hadwiger terms ($1/s^3$ and higher orders) still exist in this convex system. This proves that morphological thermodynamics is not an exact method and can only serve as a good approximation. This result shows that we still don't understand Hadwiger's volume theorem, we need come back to the theorem and find out where is the morphological thermodynamics violate the restriction of this theorem.

Appendix C. The summary of dissertation in Chinese

高性能功能性材料在多种社会问题中起着战略性的作用，例如，基于新型清洁能源的可持续性发展。氢是一种未来清洁能源，近来的科学研究已经在努力发展可靠的储氢材料¹。在 20 世纪末期，碳纳米管材料成为了一种最具吸引力的储氢材料。然而在后续研究中发现，该材料仍没有达到可工业应用所需的吸附能力（储氢质量超过系统总质量的 6%）。目前，对于这种多孔材料的搜索主要集中在新的合成多孔材料上²。除了流体吸附，多孔材料也在其他方面有着广泛应用。沸石材料被广泛的应用在气体分离，反应催化等方面。由于多孔材料具有特定的孔径大小和特殊的拓扑结构，基于沸石材料的催化剂通常具有极高的选择性。这种高选择性催化剂被广泛的应用于各种化工过程。例如石油化工中的催化裂解。当手性结构单元应用在中孔材料时，将选择性推向了更高水平，因此合成了对映选择性多孔材料，这种材料在制药工业中具有重要的应用³。目前材料工程允许我们在多孔材料上赋予各种有趣的特性。例如，目前已经合成出了具有磁性的多孔材料⁴，其中一些磁性多孔材料可以使得流体的转变温度高于室温⁵。由于它们的可调性以及掺入各种金属离子和有机配体发色团的可能性，对一些多孔材料的光学性质也有相当大的兴趣。这些材料可能作为荧光粉或荧光探针应用，特别是在化学传感器中。多孔材料的另一个非常重要的应用是药物释控²⁵。随着现代医学对于药物释放时间和药物精准释放要求的不断增加，开发更有效的控制药物释控的新方法成为了研究热点。连续稳定的药物递送能力在特定情况下可确保治疗效率，并大幅提高慢性病患者的生活质量，例如，糖尿病，癌症，艾滋病等。长时间连续稳定的药物递送能力需要一种新型的大容量载体去储存药物分子，同时，可控药物释放要求根据药物含量和性质对多孔材料进行改性。目前，新的混合多孔材料为药物释控提供了新途径。受控递送需要根据内部的药物含量对多孔材料进行一些适应性。新的混合柔性多孔材料为受控药物输送提供了有吸引力的新视角。

上述例子显示了多孔材料在催化，分离，传感器技术和制药工业等多种领域中所起的战略作用。据估计，与多孔材料相关的工业占据国家国内生产总值的 20%

以上²⁷。目前,对于多孔材料中受限流体的热力学性质的研究大多数是实验研究,而理论研究远远落后,特别是大多数的模拟与理论研究都是具有某种特定的材料模型,对于是否存在一种普适的状态方程或者理论可以应用在不同多孔材料上我们仍不知晓。

流体在多孔材料中存在着不可忽略的固液界面,导致了受限流体的性质可以显著的区别于均相流体。流体在多孔材料中的吸附行为是一个长期存在的问题,该问题具广泛的工业应用,如催化,过滤等。在过去的几十年里,大量的实验和理论工作研究了在多孔材料中流体的吸附行为以及各种热力学性质。但由于多孔材料种类丰富,受限流体性质还受孔径大小、孔隙率、流体与材料间的相互作用、流体密度、温度、压强等诸多因素影响,且这些因素之间往往还相互关联,因此目前对于受限流体的理论研究仍然处于逐案分析 (case-by-case) 的方法。在研究流体在多孔材料中的性质时,不仅需要考虑到流体的非均匀性,流体与多孔材料表面之间的相互作用同样十分重要。对于真实系统而言,当流体受限与多孔材料中时,其与多孔材料所形成的界面往往是一个弯曲表面,而对于流体在弯曲表面的性质的热力学性质研究目前仍然非常有限,尽管这一问题的研究可以追溯到 Tolman 的工作²³³。

近年来,大量关于受限流体的热力学性质的实验和理论工作被报道。孤立孔道模型被广泛的应用与研究受限流体性质,在该模型中,孔径分布和孔-孔关联被忽略。分子模拟被应用与研究流体在有序多孔材料中的扩散。为了研究多孔材料的无序性对于流体性质的影响,许多描述随机多孔材料模型被提出,例如, Madden-Glandt 模型及其变种类。在均相流体中,流体粒子被其周围的其他流体粒子所围绕。然而当流体受限与多孔材料时,大量的流体粒子是处于液体与多孔材料所形成的固液界面周围。这些粒子不仅受到周围粒子的相互作用,同时也受到多孔材料表面对其的影响。流体与固体之间的相互作用变化很大,既可以是极强的排斥作用也可以是极强的吸引作用。这个固液相互作用可以使受限流体展现出与均相流体截然不同的热力学行为。尽管复杂的受限环境可以使流体展现出不同的热力学性质,但是我们依然希望知道是否受限流体与均相流体之间是否存在关系,不同的受限流体之间是否存在某种关联。尽管大量关于受限流体的研究被

报导，然而目前对于受限流体在各种多孔材料中的普适规律仍然尚不明确。

在第二章中，通过分析一些具有严格解析结果的模型，例如，理想气体受限于多种受限环境，并参考具有不同相互作用的流体在不同多孔材料中的模拟结果。我们提出了以下的对应态原理，

$$\beta\mu(\chi\rho,T) = \beta\mu^{bulk}(\rho,T), \quad (C.1)$$

$$\beta f(\chi\rho,T) = \beta f^{bulk}(\rho,T), \quad (C.2)$$

$$\beta f(\chi\rho,T) = \beta f^{bulk}(\rho,T). \quad (C.3)$$

其中 $\beta=1/k_B T$ (k_B : 玻尔兹曼因子, T : 温度), μ 和 μ^{bulk} 分别表示受限流体和与之平衡的均相流体的化学势, ρ 是平衡时均相流体的数密度, f 和 f 分别受限流体和均相流体的 Helmholtz 自由能密度。 ω 是受限流体巨势密度。 Z^{bulk} 是均相流体的压缩因子。 标度因子为

$$\chi = \phi_0 + \Gamma A / \beta P V, \quad (C.4)$$

其中 ϕ_0 为多孔材料的几何孔隙率, Γ 表示单位表面积上的吸附量, A 为固液界面的表面积。模拟结果表明该标度定律在各种不同条件下均具有很好的结果 (参见图 2.1-2.3)。由于该对应态原理适用于描述受限流体的多种热力学性质如, 化学势, 巨势密度, Helmholtz 自由能密度, 可以自然而然地认为如果将 Helmholtz 自由能密度及巨势密度表示为化学势的函数, 受限流体将会表现出与均相流体相同的行为 (参见图 2.4)。该种不变性暗示了在研究受限流体或者非均匀流体时, 相比于目前广泛使用的密度, 选择化学势作为自变量是一种更合理的选择。虽然目前为止对于该对应态原理的从第一性原理出发的理论推导仍然缺失, 我们给出了该对应态原理和一些目前存在的普适理论框架例如, 对于非均匀流体的 Gibbs 理论以及形态热力学 (Morphological Thermodynamic) 之间的关联。这些关联可以解释为何对应态原理在如此大的范围内均适用。标度关系表明孔隙率和流体-固体间的相互作用是影响受限流体热力学性质的首要因素。相比之下, 其他的一些变量如, 孔-孔之间的关联性, 孔的形状, 孔径分布等因素对于受限流体的热力学性质影响较小。对于标度定律的一个潜在的应用是用来测量一些在实验中难以测

定的热力学量，例如 Helmholtz 自由能和巨势密度。在本工作中，标度关系仅被用于研究受限流体的一些热力学性质。标度关系是否对于一些动力学性质例如，扩散系数，仍然成立目前仍未清楚，该问题需要在未来进行进一步的研究。另外一个值得关注的问题是对于流体在一些结构可变的弹性多孔材料，例如，金属有机框架（MOFs）的吸附行为是否仍然可以用该种标度定律来关联。

对于真实系统，流体与多孔材料之间的固液界面一般为弯曲表面。然而目前为止，我们对于流体在弯曲表面的热力学性质然而所知甚少。因此对于流体在弯曲表面热力学性质的系统研究仍然是十分重要的。定标粒子理论^{205,268}（Scaled Particle Theory, SPT）是一个研究流体在弯曲表面热力学性质的强有力的方法。最初提出 SPT 的动机是为了提出一个具有简洁形式的，可以用来描述均相硬球（Hard Sphere, HS）流体的状态方程。之后研究者们意识到 SPT 并不仅仅可以用于提供均相硬球流体的热力学性质，还能提供描述硬球流体在一个球形表面的界面张力的解析表达式。然而 SPT 的精度并不如一些最近提出的半经验状态方程例如，Carnahan-Starling 状态方程。近年来，Mecke 和其合作者发展了一个可以用来描述流体在复杂表面热力学行为的普适框架，并命名为形态热力学（Morphological Thermodynamic）^{209,210}。基于积分几何中的 Hadwiger 定理，形态热力学认为对于受限流体的热力学势可以写成一个仅含有 4 项的线性组合即，一个流体均相贡献项乘以体系的体积， V ，以及三个表面贡献项分别于体系固液表面积， A ，固液表面的平均曲率， C ，以及固液表面的高斯曲率， X ，其形式可描述如下，

$$\Omega = PV + \sigma A + \kappa_1 C + \kappa_2 X. \quad (\text{C.5})$$

需要注意的是上式中对于热力学势的描述与 SPT 中对于创造一个球型空腔所需做功的描述完全一致。在最初，Mecke 等人用该方法分析星系分布的空间格局。之后该方法被发现可以用于微乳液，复合材料，复杂分子体系的研究。而后该方法被推广到研究流体在弯曲表面的表面张力，溶解自由能，平均力势（potential mean force, PMF）。最近形态热力学的基础被广泛质疑。Laird²²³ 使用分子动力学模拟(Molecular Dynamics simulation, MD)计算了流体在球形和圆柱形表面的表面张力。通过使用多项式拟合 MD 结果发现不仅仅存在式(C.5)中的四项，还有关于

$1/R$ 项的存在,

$$\Omega = PV + \sigma A + \kappa_1 C + \kappa_2 X + \kappa_3 \frac{1}{R}. \quad (\text{C.6})$$

结果表明当体系处于一个低密度状态即敛集率(Packing fraction, η)小于 0.42 时, 形态热力学给出的结果十分精确。在高密度情况下, 第一项非形态热力学参数明显增大。Hansen-Goos²²¹ 等人使用维里展开(Virial Expansion)的方法得到了一个准确的表面张力表达式, 该表达式明确了非形态热力学项的存在。Laird 使用大量的模拟来量化第一阶非形态热力学参数。数值结果表明, 第一阶非形态热力学参数比形态热力学参数中最小的一项小一个数量级。值得注意的是在这些文章中, 他们没有证明高阶的非形态热力学参数同号。在这种情况下, 非形态热力学的所有项加和可能等于零, 虽然这种情况的可能性非常小。事实上, 这些研究工作都是考虑一个流体在球形或者圆柱表面, 这表明了实际上从流体的角度来看, 流体和固体的界面是一个凹表面, 而 Hadwiger 定理仅仅在凸表面时成立。那么自然而然可以提出以下问题: 是否可以通过将 non-Hadwiger 项加入到 SPT 理论中来进一步提升 SPT 理论的精度? 是否可以找到一个简单的方法来加入 non-Hadwiger 项, 来使得 SPT 的结果仍然具有完全解析和具有简单表达式的性质?

在第三章中, 提出了两种 SPT 的改进版本 (Augmented Scaled Particle Theory, ASPT)。在 ASPT1 中, 包含了一个可调参数, 插入粒子化学势的表达式可以表示为如下形式:

$$\beta\mu_s^{\text{ex}}(R_s) = \begin{cases} -\ln[1 - \eta(1 + R_s/R)] & R < R_s \leq 0 \\ \frac{4\pi}{3} \beta P R_s^3 + \phi_2 R_s^2 + \phi_1 R_s + \phi_0 + \phi_{-1} \frac{1 - e^{-\delta/R_s}}{R_s} & 0 < R_s \end{cases}, \quad (\text{C.7})$$

其中 δ 为可调参数, 通过过剩化学势及其前三阶导数在 $R_s = 0$ 处的连续性, 即可求解 ASPT1。在 ASPT2 中, 为了避免这一可调参数, 通过使用如下表达式来描述插入粒子的化学势,

$$\beta\mu_s^{ex}(R_s) = \begin{cases} -\ln[1-\eta(1+R_s/R)] & R < R_s \leq 0 \\ \frac{4\pi}{3}\beta PR_s^3 + u_2 R_s^2 + u_1 R_s + u_0 & 0 < R_s \leq d, \\ \frac{4\pi}{3}\beta P_1 R_s^3 + \phi_2 R_s^2 + \phi_1 R_s + \phi_0 + \phi_{-1} \frac{1}{R_s} & d < R_s \end{cases} \quad (C.8)$$

其中 $d = (2/\sqrt{3}-1)R$ 。通过考虑过剩化学势及其前三阶导数在 $R_s = 0$ 和 $R_s = d$ 两处的连续性，即可求解 ASPT2。ASPT1 和 ASPT2 的结果都具有简洁的表达式。这两种方法不仅能极大的提高 SPT 对于均相流体性质如，化学势，压强的预测精度，而且对于流体在固液表面的性质例如，平面的表面张力和 Tolman 长度等的预测精度也得到了显著的提升。同样的想法也被应用于处理多组分硬球流体体系，并明显的提高了 SPT 对于混合物的预测精度。这两种改进版 SPT 的成功指出了形态热力学并不是一个严格成立的理论，但可以将其视为一种优秀的近似方法。本工作促进了我们对于流体在弯曲表面性质的理解。在本工作中我们考虑了加入一项非形态热力学项来提升 SPT 的精度，那么是否可以通过加入更多的非形态热力学项来提升 SPT 的精度？

为了描述流体在多孔材料中的性质，各种各样的理论模型被提出。为了描述孔道的几何性质对于流体性质的影响一些孤立孔道模型例如，平行板模型和柱形孔道模型被广泛的应用在理论研究中。有序多孔材料例如 MOF 和 ZIF 可以通过描述单元结构和周期边界条件来使用分子模拟进行研究。为了描述随机多孔材料中的无序性，很多理论模型最近被报道。随机多孔材料的理论模型一般借助与将一些流体粒子设定为多孔材料中的障碍物来实现。最早的一个随机多孔材料模型是 Madden 和 Glandt 在 1988 年提出的⁴⁰，在这个模型中，随机多孔材料的构型是通过冻结一个处于平衡态的流体得到的。该组分流体粒子被视为多孔材料材料结构，而粒子之间的空间被认为是孔道。多孔材料组分的粒子之间的相互作用势可以为理想气体或者硬球势。当流体被吸附在多孔材料中时，流体和多孔材料之间的相互作用不会改变多孔材料的构型。在这个模型中多孔材料粒子具有和平衡态的均相流体相同的径向分布函数。近年来，Holovko 等人提出了一个基于 SPT 理论的解析的状态方程来描述流体在 Madden-Glandt 模型中的热力学性质^{66,195}。

对于一些真实的多孔材料例如，MCM41，其孔道为类海绵结构。其几何形态无法使用 Madden-Glandt 模型进行描述，于是 Zhao 等人提出了一个新的描述随机多孔材料的模型，硬海绵模型，在该模型中通过在连续介质中使用挖取球形空腔的方法来生成孔道，当挖取的球形空腔的数量足够多时，即可形成连续的海绵型孔道¹⁷¹。与 Madden-Glandt 模型相反，在该模型中流体与多孔材料之间形成的是凸曲面，而在 Madden-Glandt 模型中其为凹曲面。近年来，Holovko 等人⁷⁹给出了一个同样基于 SPT 理论的解析的状态方程来描述流体在硬海绵模型中的热力学性质，然而对于该状态方程的严格推导目前仍然欠缺。虽然许多基于上述模型的关于受限流体热力学性质的研究被报道，但是我们对于受限流体的理解仍处于逐案研究（case-by-case）的阶段。所以建立一个可以描述流体在不同多孔材料中热力学性质的统一框架目前仍是一个挑战。在上文中提到的形态热力学方法为研究受限流体的普适规律提供了一个潜在的框架。在第四章中提出了一个新的普适的状态方程来描述受限流体的热力学性质。该模型基于形态热力学，形态热力学认为对于受限流体的热力学势可以使用如下表达式来描述：

$$\beta\Omega = -p(\mu, T)V\phi_0 + \gamma(\mu, T)A + \kappa_1(\mu, T)C + \kappa_2(\mu, T)X, \quad (\text{C.9})$$

在上式中的自变量为化学势和温度，即在该状态方程中，我们选择化学势作为自变量而非像之前的工作一样选用密度作为自变量，其中的四个参数可以通过 SPT 得到。借助 Gibbs 吸附方程，化学势和受限流体的密度可以表示为下式，

$$\rho_c = \frac{\partial p(\mu, T)}{\partial \mu} \phi_0 - \frac{\partial \sigma(\mu, T)}{\partial \mu} \frac{A}{V} - \frac{\partial(\mu, T) C}{\partial \mu} \frac{C}{V} - \frac{\partial(\mu, T) X}{\partial \mu} \frac{X}{V}. \quad (\text{C.10})$$

在均相体系中，流体化学势和密度的关系已经有深入的研究，借助于链式规则和 Gibbs-Duhem 方程，可以得到关于受限流体的密度于与之平衡的均相流体密度之间的关系。通过与模拟结果对比，发现该普适状态方程可很好的描述流体在 Madden-Glandt 模型，硬海绵模型，有序多孔材料和平行板模型中的热力学性质。该方程是第一个不依赖于多孔材料理论模型的状态方程。该方程表明在描述流体在多孔材料中的热力学性质时，孔隙率及三个描述多孔材料表面性质的参量其主导作用，而其他的因素如，孔径分布，孔-孔关联性以及孔的形状对于受限流体的影响并不大。同时，在第四章中发现即使对于理想气体流体在一些情况下形态热

力学仍然不能精确的描述其热力学行为,说明了形态热力学仅为一种较为精确的近似方法而并非一个严格的理论。在第四章中仅考虑了硬球流体,对于该工作的一个自然的拓展是检验该状态方程是否可以拓展到一些更复杂流体中例如,方阱 (Square well) 流体和 LJ (Lennard-Jones) 流体。在未来的工作中,我们希望探究这一普适状态方程是否可以用来描述流体在弹性可压缩多孔材料中的热力学性质。

由于在 Madden-Glandt 模型中,流体和多孔材料组分与均相两组分混合物十分相似,唯一的区别是在 Madden-Glandt 模型中,多孔材料组分被“冻结”了,那么这种冻结效应会如何影响流体热力学性质?虽然大量对于 Madden-Glandt 模型的热力学研究被报道。然而目前对于如何定量的描述流体在 Madden-Glandt 模型中的冻结效应仍不清楚。在第五章中,我们使用流体在 Madden-Glandt 模型中和与之对应的两组分均相流体中化学势之差来描述冻结效应。

$$\beta\Delta\mu_1 = \beta\Delta\mu_1^{QA} - \beta\Delta\mu_1^{Equil} \quad (C.11)$$

借助于图展开 (Diagrammatic expansion),发现在冻结效应的图展开中,只有当多孔材料的密度大于一阶时出现。因此,冻结效应只有在流体-流体和多孔材料-多孔材料关联都存在的时候出现。借助于受限流体的 SPT 和分子模拟,发现当多孔材料粒子大于流体粒子时,冻结效应可以被忽略。当流体粒子大于多孔材料粒子时,受限流体会表现出比相对应的均相流体更拥挤的现象即使这两种体系中各组分具有相同的密度。通过对比 SPT 和分子模拟的结果可以发现当流体粒子大于多孔材料粒子时,SPT 严重高估了多孔材料中流体的化学势。然而当流体粒子小于多孔材料粒子时,SPT 的结果和模拟结果可以很好的吻合。SPT 在流体粒子大于多孔材料粒子时高估了受限流体的化学势可能是由于对于多孔材料中孔隙率的定义存在着一定的问题。在 SPT 中使用了两种孔隙率分别为几何孔隙率 (探针粒子为理想气体) 和探针孔隙率 (探针粒子为流体粒子)。通过分析在 SPT 中每一项的贡献,可以发现误差来自于含有探针孔隙率的项中,该结果说明了探针孔隙率低估计多孔材料中粒子的自由体积。如果仅仅使用几何孔隙率如 SPT2a,受限流体的化学势将会被低估,也就是说仅使用几何孔隙率会高估流体在多孔材料中的自由体积。因此找到一个合适的孔隙率定义是改进受限流体 SPT

的重点。在第五章中我们的研究为设计功能性多孔材料提供了一些新见解。对于高度分散的体系，即细小的固体组分平均分布在空间范围内（例如气凝胶），在该种体系中，冻结效应非常大，并且流体粒子很难吸附到多孔材料中，即使多孔材料具有极大的孔隙率。该规律可以应用于设计用于气体分离的新型多孔材料。

总而言之，借助于理论方法和分子模拟方法，本文分析了受限流体的热力学性质，明确了调控受限流体的关键变量，发现了不同受限流体热力学性质之间的共同规律，基于此，提出了一个对应态原理和两个状态方程，加深了对于受限流体的理解，推进了受限流体热力学的发展。

Appendix D. Publication during the doctoral study

1. **C. Z. Qiao**, S. L. Zhao, H. L. Liu, and W. Dong. “Connect the Thermodynamics of Bulk and Confined Fluids: Confinement-Adsorption Scaling”, *Langmuir*, **2019**, 35(10): 3840-3847. (Supplementary Cover)
2. **C. Z. Qiao**, S. L. Zhao, H. L. Liu, and W. Dong. “Fluids in porous media. IV. Quench effect on chemical potential”, *J. Chem. Phys.*, **2017**, 146(23): 234504.
3. **C. Z. Qiao**, J. Zhang, P. Jiang, S. L. Zhao, X. F. Song, and J. G. Yu. “A Molecular Approach for Predicting Phase Diagrams of Ternary Aqueous Saline Solutions”, *Chem. Eng. Sci.*, **2020**, 211:115278.
4. 乔崇智, 刘文君, 付林伟, 白志山, 赵双良, 刘洪来. “低浓度纳米颗粒在剪切流中扩散、吸附的简单模型”, *化工学报*, **2015**, 66(1): 132-141.
5. **C. Z. Qiao**, S. L. Zhao, H. L. Liu, and W. Dong. “Augmented Scaled Particle Theory”, *J. Phys. Chem. B*, under review.
6. **C. Z. Qiao**, S. L. Zhao, H. L. Liu, and W. Dong. “How to use morphological thermodynamics”. To be submitted.
7. **C. Z. Qiao**, S. L. Zhao, H. L. Liu, and W. Dong. “Virial Coefficient of a hard sphere fluid in random porous media”. To be submitted.
8. X. C. Yu, **C. Z. Qiao**, X. Y. Song, T. Zhao, S. L. Zhao, H. L. Liu. “Enhancing Gas Solubility in Nanopores: A Combined Classical DFT and Machine Learning Study”. To be submitted. (co-first author)
9. X. Y. Song, **C. Z. Qiao**, J. b. Tao, B. Bao, X. Han and S. L. Zhao. “Interfacial Engineering of Thermoresponsive Microgel Capsules: Polymeric Wetting vs Colloidal Adhesion”, *Macromolecules*, **2019**, 52(10): 3869-3880.
10. X. Y. Song, **C. Z. Qiao**, T. Zhao, B. Bao, S. L. Zhao, J. Xu, and H. L. Liu. “Membrane Wrapping Pathway of Injectable Hydrogels: From Vertical Capillary Adhesion to Lateral Compressed Wrapping”, *Langmuir*, **2019**, 35(32): 10631.

Bibliography

- (1) Schlapbach, L.; Zittel, A. Hydrogen-Storage Materials for Mobile Applications. In *Materials for sustainable energy: a collection of peer-reviewed research and review articles from nature publishing group*; World Scientific, 2011; pp 265–270.
- (2) Sanderson, K. *Materials Chemistry: Space Invaders*. Nature Publishing Group 2007.
- (3) Seo, J. S.; Whang, D.; Lee, H.; Im Jun, S.; Oh, J.; Jeon, Y. J.; Kim, K. A Homochiral Metal–Organic Porous Material for Enantioselective Separation and Catalysis. *Nature* **2000**, *404* (6781), 982.
- (4) Férey, G. Microporous Solids: From Organically Templated Inorganic Skeletons to Hybrid Frameworks... Ecumenism in Chemistry. *Chem. Mater.* **2001**, *13* (10), 3084–3098.
- (5) Jain, R.; Kabir, K.; Gilroy, J. B.; Mitchell, K. A. R.; Wong, K.; Hicks, R. G. High-Temperature Metal–Organic Magnets. *Nature* **2007**, *445* (7125), 291.
- (6) Wang, Z.; Zhang, B.; Fujiwara, H.; Kurmoo, M. $Mn_3(HCOO)_6$: A 3D Porous Magnet of Diamond Framework with Nodes of Mn-Centered $MnMn_4$ Tetrahedron and Guest-Modulated Ordering Temperature †. **2004**, *3*, 416–417.
- (7) Cheetham, A. K.; Rao, C. N. R. There's Room in the Middle. *Science* (80-). **2007**, *318* (5847), 58–59.
- (8) Moreno-Castilla, C.; Maldonado-Hódar, F. J. Carbon Aerogels for Catalysis Applications: An Overview. *Carbon N. Y.* **2005**, *43* (3), 455–465.
- (9) Hu, L.; He, R.; Lei, H.; Fang, D. Carbon Aerogel for Insulation Applications: A Review. *Int. J. Thermophys.* **2019**, *40* (4), 1–25.
- (10) Mecklenburg, M.; Schuchardt, A.; Mishra, Y. K.; Kaps, S.; Adelung, R.; Lotnyk, A.; Kienle, L.; Schulte, K. Aerographite: Ultra Lightweight, Flexible Nanowall, Carbon Microtube Material with Outstanding Mechanical Performance. *Adv.*

- Mater.* **2012**, *24* (26), 3486–3490.
- (11) Schneider, M.; Baiker, A. Aerogels in Catalysis. *Catal. Rev.* **1995**, *37* (4), 515–556.
- (12) Quignard, F.; Valentin, R.; Di Renzo, F. Aerogel Materials from Marine Polysaccharides. *New J. Chem.* **2008**, *32* (8), 1300–1310.
- (13) Maldonado-Hódar, F. J.; Moreno-Castilla, C.; Pérez-Cadenas, A. F. Catalytic Combustion of Toluene on Platinum-Containing Monolithic Carbon Aerogels. *Appl. Catal. B Environ.* **2004**, *54* (4), 217–224.
- (14) Young, K. M.; Miller, T. M.; Wrighton, M. S. Comparison of the Thermal and Photochemical Reactions of (η -1-Cyclopentadienyl) Rhenium Pentacarbonyl and (η -1-9-Fluorenyl) Rhenium Pentacarbonyl: Nonthermal Chemical Reactions from the Lowest Excited State. *J. Am. Chem. Soc.* **1990**, *112* (4), 1529–1537.
- (15) Fujita, M.; Kwon, Y. J.; Washizu, S.; Ogura, K. Preparation, Clathration Ability, and Catalysis of a Two-Dimensional Square Network Material Composed of Cadmium (II) and 4, 4'-Bipyridine. *J. Am. Chem. Soc.* **1994**, *116* (3), 1151–1152.
- (16) Venkataraman, D.; Gardner, G. B.; Lee, S.; Moore, J. S. Zeolite-like Behavior of a Coordination Network. *J. Am. Chem. Soc.* **1995**, *117* (46), 11600–11601.
- (17) Schneemann, A.; Bon, V.; Schwedler, I.; Senkovska, I.; Kaskel, S.; Fischer, R. A. Flexible Metal-Organic Frameworks. *Chem. Soc. Rev.* **2014**, *43* (16), 6062–6096.
- (18) Fortes, A. D.; Suard, E.; Knight, K. S. Negative Linear Compressibility and Massive Anisotropic Thermal Expansion in Methanol Monohydrate. *Science* (80-.). **2011**, *331* (6018), 742–746.
- (19) Hodgson, S. A.; Adamson, J.; Hunt, S. J.; Cliffe, M. J.; Cairns, A. B.; Thompson, A. L.; Tucker, M. G.; Funnell, N. P.; Goodwin, A. L. Negative Area Compressibility in Silver(I) Tricyanomethanide. *Chem. Commun.* **2014**, *50* (40), 5264–5266.

- (20) Bousquet, D.; Coudert, F.-X.; Fossati, A. G. J.; Neimark, A. V.; Fuchs, A. H.; Boutin, A. Adsorption Induced Transitions in Soft Porous Crystals: An Osmotic Potential Approach to Multistability and Intermediate Structures. *J. Chem. Phys.* **2013**, *138* (17), 174706.
- (21) Coudert, F.-X.; Boutin, A.; Fuchs, A. H.; Neimark, A. V. Adsorption Deformation and Structural Transitions in Metal–Organic Frameworks: From the Unit Cell to the Crystal. *J. Phys. Chem. Lett.* **2013**, *4* (19), 3198–3205.
- (22) Krause, S.; Bon, V.; Senkovska, I.; Stoeck, U.; Wallacher, D.; Töbrens, D. M.; Zander, S.; Pillai, R. S.; Maurin, G.; Coudert, F. X.; et al. A Pressure-Amplifying Framework Material with Negative Gas Adsorption Transitions. *Nature* **2016**, *532* (7599), 348–352.
- (23) Yanai, N.; Kitayama, K.; Hijikata, Y.; Sato, H.; Matsuda, R.; Kubota, Y.; Takata, M.; Mizuno, M.; Uemura, T.; Kitagawa, S. Gas Detection by Structural Variations of Fluorescent Guest Molecules in a Flexible Porous Coordination Polymer. *Nat. Mater.* **2011**, *10* (10), 787.
- (24) Klein, N.; Herzog, C.; Sabo, M.; Senkovska, I.; Getzschmann, J.; Paasch, S.; Lohe, M. R.; Brunner, E.; Kaskel, S. Monitoring Adsorption-Induced Switching by ¹²⁹Xe NMR Spectroscopy in a New Metal–Organic Framework Ni₂(2,6-Ndc)₂ (Dabco). *Phys. Chem. Chem. Phys.* **2010**, *12* (37), 11778–11784.
- (25) Koutsopoulos, S.; Unsworth, L. D.; Nagai, Y.; Zhang, S. Controlled Release of Functional Proteins through Designer Self-Assembling Peptide Nanofiber Hydrogel Scaffold. **2009**, *106* (12).
- (26) Horcajada, P.; Serre, C.; Vallet-regí, M.; Sebban, M.; Taulelle, F.; Førey, G. *Zuschriften*. **2006**, 6120–6124.
- (27) Brinker, C. J. Porous Inorganic Materials. *Curr. Opin. Solid State Mater. Sci.* **1996**, *1* (6), 798–805.
- (28) Zhao, X. S.; Su, F.; Yan, Q.; Guo, W.; Bao, X. Y.; Lv, L.; Zhou, Z. Templating Methods for Preparation of Porous Structures. *J. Mater. Chem.* **2006**, *16* (7),

- 637–648.
- (29) Raman, N. K.; Anderson, M. T.; Brinker, C. J. Template-Based Approaches to the Preparation of Amorphous, Nanoporous Silicas. *Chem. Mater.* **1996**, *8* (8), 1682–1701.
- (30) Yuan, Z.-Y.; Su, B.-L. Insights into Hierarchically Meso–Macroporous Structured Materials. *J. Mater. Chem.* **2006**, *16* (7), 663–677.
- (31) Ma, Y.; Tong, W.; Zhou, H.; Suib, S. L. A Review of Zeolite-like Porous Materials. *Microporous mesoporous Mater.* **2000**, *37* (1–2), 243–252.
- (32) Adebajo, M. O.; Frost, R. L.; Klopogge, J. T.; Carmody, O.; Kokot, S. Porous Materials for Oil Spill Cleanup: A Review of Synthesis and Absorbing Properties. *J. Porous Mater.* **2003**, *10* (3), 159–170.
- (33) Hilfer, R. Review on Scale Dependent Characterization of the Microstructure of Porous Media. *Transp. Porous Media* **2002**, *46* (2–3), 373–390.
- (34) Adler, P. M.; Thovert, J.-F. Real Porous Media: Local Geometry and Macroscopic Properties. *Appl. Mech. Rev.* **1998**, *51* (9), 537–585.
- (35) Shih, F. Y. *Image Processing and Mathematical Morphology: Fundamentals and Applications*; CRC press, 2017.
- (36) Roberts, A. P. Statistical Reconstruction of Three-Dimensional Porous Media from Two-Dimensional Images. *Phys. Rev. E* **1997**, *56* (3), 3203.
- (37) Yeong, C. L. Y.; Torquato, S. Reconstructing Random Media. *Phys. Rev. E* **1998**, *57* (1), 495.
- (38) Adler, P. M.; Jacquin, C. G.; Quiblier, J. A. Flow in Simulated Porous Media. *Int. J. Multiph. Flow* **1990**, *16* (4), 691–712.
- (39) Adler, P. M.; Jacquin, C. G.; Thovert, J. The Formation Factor of Reconstructed Porous Media. *Water Resour. Res.* **1992**, *28* (6), 1571–1576.
- (40) Madden, W. G.; Glandt, E. D. Distribution Functions for Fluids in Random Media. *J. Stat. Phys.* **1988**, *51* (3–4), 537–558.
- (41) Fanti, L. A.; Glandt, E. D.; Madden, W. G. Fluids in Equilibrium with Disordered

- Porous Materials. Integral Equation Theory. *J. Chem. Phys.* **1990**, *93* (8), 5945–5953.
- (42) Vega, C.; Kaminsky, R. D.; Monson, P. a. Adsorption of Fluids in Disordered Porous Media from Integral Equation Theory. *J. Chem. Phys.* **1993**, *99* (4), 3003.
- (43) Vakarin, E. V.; Dong, W.; Badiali, J. P. On the Double Phase-Transition of Fluids Adsorbed in Disordered Porous Media. *Phys. A Stat. Mech. its Appl.* **2007**, *379* (2), 389–400.
- (44) Danwanichakul, P.; Charinpanitkul, T. Random Sequential Adsorption of Polydisperse Spherical Particles: An Integral-Equation Theory. *Phys. A Stat. Mech. its Appl.* **2007**, *377* (1), 102–114.
- (45) Sarkisov, L.; Van Tassel, P. R. Integral Equation Theory of Adsorption in Templated Materials: Influence of Molecular Attraction. *J. Phys. Chem. C* **2007**, *111* (43), 15726–15735.
- (46) Dong, W.; Krakoviack, V.; Zhao, S. L. Fluids Confined in Porous Media: A Soft-Sponge Model. *J. Phys. Chem. C* **2007**, *111* (43), 15910–15923.
- (47) Krakoviack, V. Mode-Coupling Theory for the Slow Collective Dynamics of Fluids Adsorbed in Disordered Porous Media. *Phys. Rev. E* **2007**, *75* (3), 031503.
- (48) Chávez-Rojo, M. A.; Juárez-Maldonado, R.; Medina-Noyola, M. Diffusion of Colloidal Fluids in Random Porous Media. *Phys. Rev. E* **2008**, *77* (4), 040401.
- (49) Kumar, A. N.; Singh, J. K. The Effects of Interaction Range , Porosity and Molecular Association on the Phase Equilibrium of a Fluid Confined in a Disordered Porous Media. *Mol. Phys.* **2008**, *106* (19), 2277–2288.
- (50) Sarkisov, L.; Van Tassel, P. R. Theories of Molecular Fluids Confined in Disordered Porous Materials. *J. Phys. Condens. Matter* **2008**, *20* (33), 333101.
- (51) Sarkisov, L. Theory of Pair Connectedness in Templated Quenched-Annealed Systems. *J. Chem. Phys.* **2008**, *128* (4), 044707.
- (52) Schwanzer, D. F.; Coslovich, D.; Kurzidim, J.; Kahl, G. Effects of Porous Confinement on the Structural Properties of the Gaussian Core Model. *Mol. Phys.*

- 2009**, *107* (4–6), 433–441.
- (53) Rosinberg, M. L.; Tarjus, G.; Stell, G. Thermodynamics of Fluids in Quenched Disordered Matrices. *J. Chem. Phys.* **1994**, *100* (7), 5172.
- (54) Schmidt, M. Test Particle Limit for the Pair Structure of Quenched-Annealed Fluid Mixtures. *Phys. Rev. E* **2009**, *79* (3), 031405.
- (55) Krakoviack, V. Tagged-Particle Dynamics in a Fluid Adsorbed in a Disordered Porous Solid: Interplay between the Diffusion-Localization and Liquid-Glass Transitions. *Phys. Rev. E* **2009**, *79* (6), 061501.
- (56) Almarza, N. G.; Gallardo, A.; Martín, C.; Guil, J. M.; Lomba, E. Topological Considerations on Microporous Adsorption Processes in Simple Models for Pillared Interlayered Clays. *J. Chem. Phys.* **2009**, *131* (24), 244701.
- (57) Pizio, O.; Dominguez, H.; Pusztai, L.; Sokolowski, S. A Core-Softened Fluid Model in Disordered Porous Media. Grand Canonical Monte Carlo Simulation and Integral Equations. *Phys. A Stat. Mech. its Appl.* **2009**, *388* (12), 2278–2288.
- (58) Holovko, M.; Dong, W. A Highly Accurate and Analytic Equation of State for a Hard Sphere Fluid in Random Porous Media. *J. Phys. Chem. B* **2009**, *113* (18), 6360–6365.
- (59) Vink, R. L. C. Critical Behavior of Soft Matter Fluids in Bulk and in Random Porous Media: From Ising to Random-Field Ising Universality. *Soft Matter* **2009**, *5*, 4388.
- (60) Cheung, D. L.; Schmidt, M. Quenched-Annealed Density Functional Theory for Interfacial Behavior of Hard Rods at a Hard Rod Matrix. *J. Chem. Phys.* **2009**, *131* (21), 214705.
- (61) Chen, W.; Dong, W.; Holovko, M.; Chen, X. S. Comment on “A Highly Accurate and Analytic Equation of State for a Hard Sphere Fluid in Random Porous Media.” *J. Phys. Chem. B* **2010**, *114* (2), 1225–1225.
- (62) Lomba, E.; Weis, J.-J. A Computational Study of Electrolyte Adsorption in a Simple Model for Intercalated Clays. *J. Chem. Phys.* **2010**, *132* (10), 104705.

- (63) Krakoviack, V. Statistical Mechanics of Homogeneous Partly Pinned Fluid Systems. *Phys. Rev. E* **2010**, *82* (6), 061501.
- (64) Kaminsky, R. D.; Monson, P. A. A Simple Mean Field Theory of Adsorption in Disordered Porous Materials. *Chem. Eng. Sci.* **1994**, *49* (17), 2967–2977.
- (65) Kurzidim, J.; Coslovich, D.; Kahl, G. Impact of Random Obstacles on the Dynamics of a Dense Colloidal Fluid. *Phys. Rev. E* **2010**, *82* (4), 041505.
- (66) Patsahan, T.; Holovko, M.; Dong, W. Fluids in Porous Media. III. Scaled Particle Theory. *J. Chem. Phys.* **2011**, *134* (7), 074503.
- (67) Gallo, P.; Rovere, M. Lennard-Jones Binary Mixture in Disordered Matrices: Exploring the Mode Coupling Scenario at Increasing Confinement. *J. Phys. Condens. Matter* **2011**, *23* (23), 234118.
- (68) Lukšič, M.; Hribar-Lee, B.; Tochimani, S. B.; Pizio, O. Solvent Primitive Model for Electrolyte Solutions in Disordered Porous Matrices of Charged Species. Replica Ornstein-Zernike Theory and Grand Canonical Monte Carlo Simulations. *Mol. Phys.* **2011**, *110* (1), 17–30.
- (69) Krakoviack, V. Mode-Coupling Theory Predictions for the Dynamical Transitions of Partly Pinned Fluid Systems. *Phys. Rev. E - Stat. Nonlinear, Soft Matter Phys.* **2011**, *84* (5), 050501.
- (70) Tarjus, G.; Rosinberg, M.; Kierlik, E. Hierarchical Reference Theory of Critical Fluids in Disordered Porous Media. *Mol. Phys.* **2011**, *109* (November 2014), 2863.
- (71) Kurzidim, J.; Kahl, G. Accessible Volume in Quenched-Annealed Mixtures of Hard Spheres: A Geometric Decomposition. *Mol. Phys.* **2011**, *109* (7–10), 1331–1342.
- (72) Fischer, T.; Vink, R. L. C. Domain Formation in Membranes with Quenched Protein Obstacles: Lateral Heterogeneity and the Connection to Universality Classes. *J. Chem. Phys.* **2011**, *134* (5), 055106.
- (73) Fischer, T.; Vink, R. L. C. Fluids with Quenched Disorder: Scaling of the Free

- Energy Barrier near Critical Points. *J. Phys. Condens. Matter* **2011**, *23* (23), 234117.
- (74) Schultz, A. J.; Barlow, N. S.; Chaudhary, V.; Kofke, D. A. Mayer Sampling Monte Carlo Calculation of Virial Coefficients on Graphics Processors. *Mol. Phys.* **2013**, *111* (4), 535–543.
- (75) Given, J. A.; Stell, G. R. The Replica Ornstein-Zernike Equations and the Structure of Partly Quenched Media. *Phys. A Stat. Mech. its Appl.* **1994**, *209* (3–4), 495–510.
- (76) Links, D. A.; Fischer, T.; Risselada, H. J.; Vink, R. L. C. Membrane Lateral Structure : The Influence of Immobilized Particles on Domain Size. *Phys. Chem. Chem. Phys.* **2012**, *14* (42), 14500–14508.
- (77) Holovko; Patsahan; Dong. One-Dimensional Hard Rod Fluid in a Disordered Porous Medium: Scaled Particle Theory. *Condens. Matter Phys.* **2012**, *15* (2), 23607.
- (78) Pellicane, G.; Vink, R. L. C.; Russo, B.; Giaquinta, P. V. Fluids in Porous Media: The Case of Neutral Walls. *Phys. Rev. E* **2013**, *88* (4), 042131.
- (79) Holovko, M.; Patsahan, T.; Dong, W. Fluids in Random Porous Media: Scaled Particle Theory. *Pure Appl. Chem.* **2013**, *85* (1), 115–133.
- (80) Kalyuzhnyi, Y. V.; Holovko, M.; Patsahan, T.; Cummings, P. T. Phase Behavior and Percolation Properties of the Patchy Colloidal Fluids in the Random Porous Media. *J. Phys. Chem. Lett.* **2014**, *5* (24), 4260–4264.
- (81) Krakoviack, V. Simple Physics of the Partly Pinned Fluid Systems. *J. Chem. Phys.* **2014**, *141* (10), 104504.
- (82) Lomba, E.; Bores, C.; Sánchez-Gil, V.; Noya, E. G. A Three Dimensional Integral Equation Approach for Fluids under Confinement: Argon in Zeolites. *J. Chem. Phys.* **2015**, *143* (16), 164703.
- (83) Bores, C.; Almarza, N. G.; Lomba, E.; Kahl, G. Inclusions of a Two Dimensional Fluid with Competing Interactions in a Disordered, Porous Matrix. *J. Phys.*

- Condens. Matter* **2015**, 27 (19), 194127.
- (84) Chen, W.; Zhao, S. L.; Holovko, M.; Chen, X. S.; Dong, W. Scaled Particle Theory for Multicomponent Hard Sphere Fluids Confined in Random Porous Media. *J. Phys. Chem. B* **2016**, 120 (24), 5491–5504.
- (85) Dong, W.; Kierlik, E.; Rosinberg, M. L. Integral Equations for a Fluid near a Random Substrate. *Phys. Rev. E* **1994**, 50 (6), 4750–4753.
- (86) Ford, D. M.; Glandt, E. Compressibility Equation for Fluids in Random Microporous Materials. *J. Chem. Phys.* **1994**, 100 (1994), 2391–2393.
- (87) Ford, D. M.; Glandt, E. D. Vapor-Liquid Phase Equilibrium in Random Microporous Matrices. *Phys. Rev. E* **1994**, 50 (2), 1280–1286.
- (88) Given, J. A. On the Thermodynamics of Fluids Adsorbed in Porous Media. *J. Chem. Phys.* **1995**, 102 (7), 2934.
- (89) Dong, W. Mechanical Route to the Pressure of a Fluid Adsorbed in a Random Porous Medium. *J. Chem. Phys.* **1995**, 102 (16), 6570–6573.
- (90) Madden, W. G. Some Integral Relationships for Distribution Functions of Fluids in Disordered Media. *J. Chem. Phys.* **1995**, 103 (18), 8156–8165.
- (91) Chandler, D. RISM Equations for Fluids in Quenched Amorphous Materials. *J. Phys. Condens. Matter* **1991**, 3 (42), F1–F8.
- (92) Ford, D. M.; Thompson, A. P.; Glandt, E. D. Thermodynamics of Fluids in Random Microporous Materials from Scaled Particle Theory. *J. Chem. Phys.* **1995**, 103 (3), 1099–1105.
- (93) Pitard, E.; Rosinberg, M. L.; Stell, G.; Tarjus, G. Critical Behavior of a Fluid in a Disordered Porous Matrix: An Ornstein-Zernike Approach. *Phys. Rev. Lett.* **1995**, 74 (22), 4361–4364.
- (94) Trokhymchuk, A.; Pizio, O.; Sokołowski, S.; Henderson, D. Density Profiles of Chemically Reacting Fluids in Slit-like Pores. *Mol. Phys.* **1995**, 86 (1), 53–71.
- (95) Kierlik, E.; Rosinberg, M. L.; Tarjus, G.; Monson, P. The Pressure of a Fluid Confined in a Disordered Porous Material. *J. Chem. Phys.* **1995**, 103 (10), 4256.

- (96) Page, K.; Monson, P. Phase Equilibrium in a Molecular Model of a Fluid Confined in a Disordered Porous Material. *Phys. Rev. E* **1996**, *54* (1), R29–R32.
- (97) Trokhymchuk, A.; Pizio, O.; Holovko, M.; Sokolowski, S. Adsorption of Fluids in Disordered Porous Media from the Multidensity Integral Equation Theory. Associative Analogue of the Madden–Glandt Ornstein–Zernike Approximation. *J. Phys. Chem.* **1996**, *100* (42), 17004–17010.
- (98) Pitard, E.; Rosinberg, M.; Tarjus, G. Thermodynamics of Fluids in Disordered Porous Materials. *Mol. Simul.* **1996**, No. July 2011, 37–41.
- (99) Meroni, A.; Levesque, D.; Weis, J. J. Correlation Functions of Hard Sphere Fluids Adsorbed in Porous Media. *J. Chem. Phys.* **1996**, *105* (3), 1101.
- (100) Henderson, D.; Patrykiewicz, A.; Pizio, O.; Sokołowski, S. Adsorption of Dimerizing Fluids in Disordered Porous Networks. *Phys. A Stat. Mech. its Appl.* **1996**, *233* (1–2), 67–76.
- (101) Page, K. S.; Monson, P. A. Monte Carlo Calculations of Phase Diagrams for a Fluid Confined in a Disordered Porous Material. *Phys. Rev. E* **1996**, *54* (6), 6557–6564.
- (102) Kaminsky, R. D.; Monson, P. a. The Influence of Adsorbent Microstructure upon Adsorption Equilibria: Investigations of a Model System. *J. Chem. Phys.* **1991**, *95* (4), 2936.
- (103) Thompson, A. P.; Glandt, E. D. Polymers in Random Porous Materials: Structure, Thermodynamics, and Concentration Effects. *Macromolecules* **1996**, *29* (12), 4314–4323.
- (104) Pizio, O.; Sokolowski, S. Adsorption of Fluids in Confined Disordered Media from Inhomogeneous Replica Ornstein-Zernike Equations. *Phys. Rev. E* **1997**, *56* (1), R63–R66.
- (105) Padilla, P.; Vega, C. Adsorption Isotherm for Flexible Molecules in Random Porous Media. Can We Regard the System as a Binary Mixture? *J. Chem. Phys.* **1997**, *106* (5), 1997–2011.

- (106) Kierlik, E.; Rosinberg, M. L.; Tarjus, G.; Monson, P. a. Phase Diagrams of Single-Component Fluids in Disordered Porous Materials: Predictions from Integral-Equation Theory. *J. Chem. Phys.* **1997**, *106* (1), 264–279.
- (107) Orozco, G. A.; Pizio, O.; Sokolowski, S.; Trokhymchuk, A. Replica Ornstein-Zernike Theory for Chemically Associating Fluids with Directional Forces in Disordered Porous Media: Smith-Nezbeda Model in a Hard Sphere Matrix. *Mol. Phys.* **1997**, *91* (4), 625–634.
- (108) Van Tassel, P. R. Theoretical Studies of the Available Volume for Adsorption in a Random Quenched and Depleted Disordered Medium. *J. Chem. Phys.* **1997**, *107* (1997), 9530.
- (109) Trokhymchuk, A.; Pizio, O.; Holovko, M.; Sokolowski, S. Associative Replica Ornstein–Zernike Equations and the Structure of Chemically Reacting Fluids in Porous Media. *J. Chem. Phys.* **1997**, *106* (1), 200–209.
- (110) Padilla, P.; Pizio, O.; Trokhymchuk, A.; Vega, C. Adsorption of Dimerizing and Dimer Fluids in Disordered Porous Media. *J. Phys. Chem. B* **1998**, *102* (16), 3012–3017.
- (111) Duda, Y.; Sokolowski, S.; Bryk, P.; Pizio, O. Structure and Adsorption of a Hard Sphere Fluid in a Cylindrical and Spherical Pore Filled by a Disordered Matrix: A Monte Carlo Study. *J. Phys. Chem. B* **1998**, *102* (28), 5490–5494.
- (112) Padilla, P.; Vega, C.; Pizio, O. and Trokhymchuk, A. The Structure and Adsorption of Diatomic Fluids in Disordered Porous Media. A Monte Carlo Simulation Study. *Mol. Phys.* **1998**, *95* (4), 701–712.
- (113) Madden, W. G. Fluid Distributions in Random Media: Arbitrary Matrices. *J. Chem. Phys.* **1992**, *96* (7), 5422–5432.
- (114) Duda, Y.; Henderson, D.; Pizio, O.; Wasan, D. Replica Ornstein-Zernike Equations and the Structure of a Simple Fluid Mixture in Disordered Porous Media: Application to a Composite Monomolecular Adlayer. *Mol. Phys.* **1998**, *94* (2), 341–348.

- (115) Pérez, L.; Sokołowski, S.; Pizio, O. Capillary Condensation of Lennard-Jones Fluid in a Slitlike Pore Filled with Quenched Disordered Matrix. *J. Chem. Phys.* **1998**, *109* (3), 1147–1151.
- (116) Kovalenko, A.; Sokołowski, S.; Henderson, D.; Pizio, O. Adsorption of a Hard Sphere Fluid in a Slitlike Pore Filled with a Disordered Matrix by the Inhomogeneous Replica Ornstein-Zernike Equations. *Phys. Rev. E* **1998**, *57* (2), 1824–1831.
- (117) Hribar, B.; Pizio, O.; Trokhymchuk, A.; Vlachy, V. Ion-Ion Correlations in Electrolyte Solutions Adsorbed in Disordered Electroneutral Charged Matrices from Replica Ornstein-Zernike Equations. *J. Chem. Phys.* **1998**, *109* (6), 2480–2489.
- (118) Bryk, P.; Pizio, O.; Sokolowski, S. A Hard Sphere Fluid in Equilibrium with Microporous Membranes. Inhomogeneous Replica Ornstein–Zernike Equations and Grand Canonical Monte Carlo Simulations. *Mol. Phys.* **1998**, *95* (2), 311–317.
- (119) Kovalenko, A.; Pizio, O. The Structure and Adsorption of the Four Bonding Sites Model for Associating Fluids in Disordered Porous Media from Replica Ornstein–Zernike Integral Equation Theory. *J. Chem. Phys.* **1998**, *108* (20), 8651–8661.
- (120) Hribar, B.; Vlachy, V.; Trokhymchuk, A.; Pizio, O. Structure and Thermodynamics of Asymmetric Electrolytes Adsorbed in Disordered Electroneutral Charged Matrices from Replica Ornstein–Zernike Equations. *J. Phys. Chem. B* **1999**, *103* (25), 5361–5369.
- (121) Van Tassel, P. R. Theoretical Model of Adsorption in a Templated Porous Material. *Phys. Rev. E* **1999**, *60* (1), R25–R28.
- (122) Ilnytsky, J.; Patrykiewicz, A.; Sokołowski, S.; Pizio, O. Replica Ornstein-Zernike Equations for Polydisperse Quenched-Annealed Fluids. Hard Spheres in a Polydisperse Disordered Hard Sphere Matrix. *J. Phys. Chem. B* **1999**, *103* (5),

- 868–871.
- (123) Fernaud, M. J.; Lomba, E.; Lee, L. L. Chemical Potentials and Potential Distributions of Inclusion Gas in Quenched-Annealed Random Porous Media. *J. Chem. Phys.* **1999**, *111* (22), 10275–10286.
- (124) Duda, Y.; Patrykiewicz, A.; Pizio, O.; Sokołowski, S. Density Profiles of Hard Spheres in a Cylinder Filled with Disordered Matrix: Application of the Born–Green–Yvon Equation. *Phys. A Stat. Mech. its Appl.* **1999**, *265* (3–4), 424–431.
- (125) Rzysko, W.; Pizio, O.; Sokolowski, S. Structural Properties of a Two-Dimensional Model for Partly Quenched Colloidal Dispersions. *Phys. A Stat. Mech. its Appl.* **1999**, *273* (3–4), 241–247.
- (126) Alvarez, M.; Levesque, D.; Weis, J. J. Monte Carlo Approach to the Gas-Liquid Transition in Porous Materials. *Phys. Rev. E. Stat. Phys. Plasmas. Fluids. Relat. Interdiscip. Topics* **1999**, *60* (5), 5495–5504.
- (127) Bracamontes, L. I.; Pizio, O.; Sokolowski, S.; Trokhymchuk, A. Adsorption and the Structure of a Hard Sphere Fluid in Disordered Quenched Microporous Matrices of Permeable Species. *Mol. Phys.* **1999**, *96* (9), 1341–1348.
- (128) Hribar, B.; Vlachy, V.; Pizio, O. Structural and Thermodynamic Properties of Electrolyte Solutions in Hard-Sphere Confinement: Predictions of the Replica Integral Equation Theory. *J. Phys. Chem. B* **2000**, *104* (18), 4479–4488.
- (129) Sarkisov, L.; Monson, P. A. Hysteresis in Monte Carlo and Molecular Dynamics Simulations of Adsorption in Porous Materials. *Langmuir* **2000**, *16* (25), 9857–9860.
- (130) Wang, Q.; Danwanichakul, P.; Glandt, E. D. Sequential Addition of Particles: Integral Equations. *J. Chem. Phys.* **2000**, *112* (15), 6733–6738.
- (131) Zhang, L.; Van Tassel, P. R. Configurational Effects of Templating on the Adsorption Isotherms of Templated Porous Materials. *Mol. Phys.* **2000**, *98* (19), 1521–1527.
- (132) Rzysko, W.; De Pablo, J. J.; Sokolowski, S. Critical Behavior of Simple Fluids

- Confined by Microporous Materials. *J. Chem. Phys.* **2000**, *113* (21), 9772–9777.
- (133) Given, J. A. Liquid-State Methods for Random Media: Random Sequential Adsorption. *Phys. Rev. A* **1992**, *45* (2), 816–824.
- (134) Gelb, L. D.; Gubbins, K. E.; Radhakrishnan, R.; Sliwinski-Bartkowiak, M. Phase Separation in Confined Systems. *Reports Prog. Phys.* **2000**, *63* (4), 727–727.
- (135) Sarkisov, L.; Monson, P. A. Computer Simulations of Phase Equilibrium for a Fluid Confined in a Disordered Porous Structure. *Phys. Rev. E - Stat. Physics, Plasmas, Fluids, Relat. Interdiscip. Top.* **2000**, *61* (6), 7231–7234.
- (136) Zhang, L.; Van Tassel, P. R. Theory and Simulation of Adsorption in a Templated Porous Material: Hard Sphere Systems. *J. Chem. Phys.* **2000**, *112* (6), 3006–3013.
- (137) Cheng, S.; Van Tassel, P. R. Theory and Simulation of the Available Volume for Adsorption in a Chain Molecule Templated Porous Material. *J. Chem. Phys.* **2001**, *114* (11), 4974–4981.
- (138) Fernaud, M. J.; Lomba, E.; Weis, J. J. Adsorption of a Diatomic Molecular Fluid into Random Porous Media. *Phys. Rev. E* **2001**, *64* (5 I), 051501.
- (139) Krakoviack, V.; Kierlik, E.; Rosinberg, M. L.; Tarjus, G. Adsorption of a Fluid in an Aerogel: Integral Equation Approach. *J. Chem. Phys.* **2001**, *115* (24), 11289–11298.
- (140) Sierra, O.; Duda, Y. Fluid–Fluid Phase Equilibria in Disordered Porous Media. Nonadditive Hard Sphere Mixture. *Phys. Lett. A* **2001**, *280* (3), 146–152.
- (141) Kovalenko, A.; Hirata, F. A Replica Reference Interaction Site Model Theory for a Polar Molecular Liquid Sorbed in a Disordered Microporous Material with Polar Chemical Groups. *J. Chem. Phys.* **2001**, *115* (18), 8620–8633.
- (142) Hribar, B.; Vlachy, V.; Pizio, O. Equilibrium Properties of a Model Electrolyte Adsorbed in Quenched Disordered Charged Media: The ROZ Theory and GCMC Simulations. *J. Phys. Chem. B* **2001**, *105* (20), 4727–4734.

- (143) Danwanichakul, P.; Glandt, E. D. Sequential Quenching of Square-Well Particles. *J. Chem. Phys.* **2001**, *114* (4), 1785–1790.
- (144) Thompson, A. P.; Glandt, E. D. Adsorption of Polymeric Fluids in Microporous Materials. I. Ideal Freely Jointed Chains. *J. Chem. Phys.* **1993**, *99* (10), 8325–8329.
- (145) Schöll-Paschinger, E.; Levesque, D.; Weis, J.-J.; Kahl, G. Phase Diagram of a Symmetric Binary Fluid in a Porous Matrix. *Phys. Rev. E* **2001**, *64* (1), 011502.
- (146) Reszko-zygmunt, J.; Patrykiewicz, A.; Sokolowska, S. Phase Coexistence and Interface Structure of a Two-Component Lennard-Jones Fluid in Porous Media: Application of Born—Green—Yvon Equation. *Mol. Phys.* **2002**, *100* (12), 1905–1910.
- (147) Reszko-Zygmunt, J.; Patrykiewicz, A.; Sokolowski, S.; Sokolowska, Z. Phase Coexistence and Interface Structure of a Two-Component Lennard-Jones Fluid in Porous Media: Application of Born—Green—Yvon Equation. *Mol. Phys.* **2002**, *100* (12), 1905–1910.
- (148) Hribar, B.; Vlachy, V.; Pizio, O. Chemical Potential of Electrolytes Adsorbed in Porous Media with Charged Obstacles: Application of the Continuum Replica Methodology. *Mol. Phys.* **2002**, *100* (19), 3093–3103.
- (149) Yethiraj, A. Integral Equations for Polymers in Quenched Random Media. *J. Chem. Phys.* **2002**, *116* (13), 25–26.
- (150) Brennan, J. K.; Dong, W. Phase Transitions of One-Component Fluids Adsorbed in Random Porous Media: Monte Carlo Simulations. *J. Chem. Phys.* **2002**, *116* (20), 8948–8958.
- (151) Schmidt, M. Density-Functional Theory for Fluids in Porous Media. *Phys. Rev. E* **2002**, *66* (4), 041108.
- (152) Wessels, P. P. F.; Schmidt, M.; Löwen, H. Capillary Condensation and Interface Structure of a Model Colloid-Polymer Mixture in a Porous Medium. *Phys. Rev. E* **2003**, *68* (6), 061404.

- (153) Brennan, J. K.; Dong, W. Molecular Simulation of the Vapor-Liquid Phase Behavior of Lennard-Jones Mixtures in Porous Solids. *Phys. Rev. E* **2003**, *67* (3), 031503.
- (154) Fernaud, M. J.; Lomba, E.; Martín, C.; Levesque, D.; Weis, J.-J. Study of Dipolar Fluid Inclusions in Charged Random Matrices. *J. Chem. Phys.* **2003**, *119* (1), 364–372.
- (155) Kaminsky, R. D.; Monson, P. A. Physical Adsorption in Heterogeneous Porous Materials - an Analytical Study of a One-Dimensional Model. *Langmuir* **1993**, *9* (2), 561–567.
- (156) De Grandis, V.; Gallo, P.; Rovere, M. Computer Simulation of the Phase Diagram for a Fluid Confined in a Fractal and Disordered Porous Material. *Phys. Rev. E* **2004**, *70* (6), 061505.
- (157) Pellicane, G.; Caccamo, C.; Wilson, D. S.; Lee, L. L. Replica Ornstein-Zernike Self-Consistent Theory for Mixtures in Random Pores. *Phys. Rev. E* **2004**, *69* (6 1), 1–10.
- (158) Chang, R.; Jagannathan, K.; Yethiraj, A. Diffusion of Hard Sphere Fluids in Disordered Media: A Molecular Dynamics Simulation Study. *Phys. Rev. E* **2004**, *69* (5), 051101.
- (159) Vlachy, V.; Dominguez, H.; Pizio, O. Temperature Effects in Adsorption of a Primitive Model Electrolyte in Disordered Quenched Media: Predictions of the Replica OZ/HNC Approximation. *J. Phys. Chem. B* **2004**, *108*, 1046–1055.
- (160) Duda, Y.; Pizio, O.; Sokolowski, S. Nonadditive Binary Hard Sphere Mixture in Disordered Hard Sphere Matrices: Integral Equations and Computer Simulation. *J. Phys. Chem. B* **2004**, *108* (50), 19442–19450.
- (161) Reich, H.; Schmidt, M. Replica Density Functional Study of One-Dimensional Hard Core Fluids in Porous Media. *J. Stat. Phys.* **2004**, *116* (5/6), 1683–1702.
- (162) Krakoviack, V. Liquid-Glass Transition of a Fluid Confined in a Disordered Porous Matrix: A Mode-Coupling Theory. *Phys. Rev. Lett.* **2005**, *94* (6), 065703.

- (163) Sarkisov, L.; Van Tassel, P. R. Replica Ornstein-Zernike Theory of Adsorption in a Templated Porous Material: Interaction Site Systems. *J. Chem. Phys.* **2005**, *123* (16), 164706.
- (164) Dong, W.; Chen, X. S.; Zheng, W. M. Thermodynamic Pressure of a Fluid Confined in a Random Porous Medium. *Phys. Rev. E* **2005**, *72* (1), 012201.
- (165) Sung, B. J.; Yethiraj, A. Monte Carlo Simulation and Self-Consistent Integral Equation Theory for Polymers in Quenched Random Media. *J. Chem. Phys.* **2005**, *123* (7), 074909.
- (166) Lomba, E.; Given, J. A.; Stell, G.; Weis, J. J.; Levesque, D. Ornstein-Zernike Equations and Simulation Results for Hard-Sphere Fluids Adsorbed in Porous Media. *Phys. Rev. E* **1993**, *48* (1), 233–244.
- (167) Schmidt, M. Replica Density Functional Theory: An Overview. *J. Phys. Condens. Matter* **2005**, *17* (45), S3481–S3486.
- (168) Mittal, J.; Errington, J. R.; Truskett, T. M. Using Available Volume to Predict Fluid Diffusivity in Random Media. *Phys. Rev. E - Stat. Nonlinear, Soft Matter Phys.* **2006**, *74* (4), 040102.
- (169) Lafuente, L.; Cuesta, J. A. First-Principles Derivation of Density-Functional Formalism for Quenched-Annealed Systems. *Phys. Rev. E - Stat. Nonlinear, Soft Matter Phys.* **2006**, *74* (4), 041502.
- (170) Archer, A. J.; Schmidt, M.; Evans, R. Soft Core Fluid in a Quenched Matrix of Soft Core Particles: A Mobile Mixture in a Model Gel. *Phys. Rev. E - Stat. Nonlinear, Soft Matter Phys.* **2006**, *73* (1), 011506.
- (171) Zhao, S. L.; Dong, W.; Liu, Q. H. Fluids in Porous Media. I. A Hard Sponge Model. *J. Chem. Phys.* **2006**, *125* (24), 244703.
- (172) Ravikovitch, P. I.; Neimark, A. V. Density Functional Theory Model of Adsorption Deformation. *Langmuir* **2006**, *22* (26), 10864–10868.
- (173) Dong, W. Fluids Confined in Porous Media: An Ideal Gas in Different Matrices. *Condens. Matter Phys.* **2007**, *10* (4), 509–537.

- (174) Lukšič, M.; Hribar-Lee, B.; Vlachy, V. Electrolyte Exclusion from Charged Adsorbent: Replica Ornstein-Zernike Theory and Simulations. *J. Phys. Chem. B* **2007**, *111* (21), 5966–5975.
- (175) Zhao, S. L.; Dong, W.; Liu, Q. H. A New Model of Templated Porous Materials. *J. Mol. Liq.* **2007**, *136* (3), 241–248.
- (176) Weeks, J. D.; Chandler, D.; Andersen, H. C. Role of Repulsive Forces in Determining the Equilibrium Structure of Simple Liquids. *J. Chem. Phys.* **1971**, *54* (12), 5237–5247.
- (177) Barker, J. A.; Henderson, D. Perturbation Theory and Equation of State for Fluids. II. A Successful Theory of Liquids. *J. Chem. Phys.* **1967**, *47* (11), 4714–4721.
- (178) Spencer, E. C.; Kiran, M. S. R. N.; Li, W.; Ramamurty, U.; Ross, N. L.; Cheetham, A. K. Pressure-Induced Bond Rearrangement and Reversible Phase Transformation in a Metal-Organic Framework. *Angew. Chemie - Int. Ed.* **2014**, *53* (22), 5583–5586.
- (179) Devic, T.; Horcajada, P.; Serre, C.; Salles, F.; Maurin, G.; Moulin, B.; Heurtaux, D.; Clet, G.; Vimont, A.; Grenéche, J. M.; et al. Functionalization in Flexible Porous Solids: Effects on the Pore Opening and the Host-Guest Interactions. *J. Am. Chem. Soc.* **2010**, *132* (3), 1127–1136.
- (180) Baughman, R. H.; Stafström, S.; Cui, C.; Dantas, S. O. Materials with Negative Compressibilities in One or More Dimensions. *Science* (80-.). **1998**, *279* (5356), 1522–1524.
- (181) Pauling, L.; Pauling, P. A. Trireticulate Crystal Structure: Trihydrogen Cobalticyanide and Trisilver Cobalticyanide. *Proc. Natl. Acad. Sci.* **1968**, *60* (2), 362–367.
- (182) Cairns, A. B.; Catafesta, J.; Levelut, C.; Rouquette, J.; Van Der Lee, A.; Peters, L.; Thompson, A. L.; Dmitriev, V.; Haines, J.; Goodwin, A. L. Giant Negative Linear Compressibility in Zinc Dicyanoaurate. *Nat. Mater.* **2013**, *12* (3), 212–

- (183) Gagnon, K. J.; Beavers, C. M.; Clearfield, A. MOFs under Pressure: The Reversible Compression of a Single Crystal. *J. Am. Chem. Soc.* **2013**, *135* (4), 1252–1255.
- (184) Kondo, M.; Furukawa, S.; Hirai, K.; Tsuruoka, T.; Reboul, J.; Uehara, H.; Diring, S.; Sakata, Y.; Sakata, O.; Kitagawa, S. Trapping of a Spatial Transient State during the Framework Transformation of a Porous Coordination Polymer. *J. Am. Chem. Soc.* **2014**, *136* (13), 4938–4944.
- (185) Ceppatelli, M.; Scelta, D.; Tuci, G.; Giambastiani, G.; Hanfland, M.; Bini, R. Lattice Expansion of Graphite Oxide by Pressure Induced Insertion of Liquid Ammonia. *Carbon N. Y.* **2015**, *93*, 484–491.
- (186) Dyer, T.; Thamwattana, N.; Jalili, R. Modelling the Interaction of Graphene Oxide Using an Atomistic-Continuum Model. *RSC Adv.* **2015**, *5* (94), 77062–77070.
- (187) Odriozola, G.; Aguilar, J. F. Stability of Ca-Montmorillonite Hydrates: A Computer Simulation Study. *J. Chem. Phys.* **2005**, *123* (17), 174708.
- (188) Han, S. S.; Goddard, W. A. Metal-Organic Frameworks Provide Large Negative Thermal Expansion Behavior. *J. Phys. Chem. C* **2007**, *111* (42), 15185–15191.
- (189) Gatt, R.; Grima, J. N. Negative Compressibility. *Phys. Status Solidi - Rapid Res. Lett.* **2008**, *2* (5), 236–238.
- (190) Li, W.; Probert, M. R.; Kosa, M.; Bennett, T. D.; Thirumurugan, A.; Burwood, R. P.; Parinello, M.; Howard, J. A. K.; Cheetham, A. K. Negative Linear Compressibility of a Metal-Organic Framework. *J. Am. Chem. Soc.* **2012**, *134* (29), 11940–11943.
- (191) Barnes, D. L.; Miller, W.; Evans, K. E.; Marmier, A. Modelling Negative Linear Compressibility in Tetragonal Beam Structures. *Mech. Mater.* **2012**, *46*, 123–128.
- (192) Coudert, F. X. Systematic Investigation of the Mechanical Properties of Pure

- Silica Zeolites: Stiffness, Anisotropy, and Negative Linear Compressibility. *Phys. Chem. Chem. Phys.* **2013**, *15* (38), 16012–16018.
- (193) Dong, W.; Chen, X. Scaled Particle Theory for Bulk and Confined Fluids: A Review. *Sci. China Physics, Mech. Astron.* **2018**, *61* (7), 70501.
- (194) Hvozď, M.; Patsahan, T.; Holovko, M. Isotropic-Nematic Transition and Demixing Behavior in Binary Mixtures of Hard Spheres and Hard Spherocylinders Confined in a Disordered Porous Medium: Scaled Particle Theory. *J. Phys. Chem. B* **2018**, *122* (21), 5534–5546.
- (195) Holovko, M.; Dong, W. A Highly Accurate and Analytic Equation of State for a Hard Sphere Fluid in Random Porous Media. *J. Phys. Chem. B* **2009**, *113* (18), 6360–6365.
- (196) Holovko, M.; Shmotolokha, V.; Patsahan, T. Hard Convex Body Fluids in Random Porous Media: Scaled Particle Theory. *J. Mol. Liq.* **2014**, *189*, 30–38.
- (197) Holovko, M. F.; Patsahan, T. M.; Shmotolokha, V. I. What Is Liquid in Random Porous Media: The Barker-Henderson Perturbation Theory. *Condens. Matter Phys.* **2015**, *18* (1), 1–17.
- (198) Holovko, M. F.; Patsahan, O.; Patsahan, T. Vapour-Liquid Phase Diagram for an Ionic Fluid in a Random Porous Medium. *J. Phys. Condens. Matter* **2016**, *28* (41), 414003.
- (199) Holovko, M. F.; Patsahan, T. M.; Patsahan, O. V. Application of the Ionic Association Concept to the Study of the Phase Behaviour of Size-Asymmetric Ionic Fluids in Disordered Porous Media. *J. Mol. Liq.* **2017**, *235*, 53–59.
- (200) González-Tovar; Lozada-Cassou. Model Charged Cylindrical Nanopore in a Colloidal Dispersion: Charge Reversal, Overcharging and Double Overcharging. *Condens. Matter Phys.* **2017**, *20* (3), 33604.
- (201) Patsahan, O.; Patsahan, T.; Holovko, M. Vapour-Liquid Critical Parameters of a 2:1 Primitive Model of Ionic Fluids Confined in Disordered Porous Media. *J. Mol. Liq.* **2018**, *270*, 97–105.

- (202) Holovko, M. F.; Shmotolokha, V. I. Scaled Particle Theory for a Hard Spherocylinder Fluid in a Disordered Porous Medium: Carnahan-Starling and Parsons-Lee Corrections. *Condens. Matter Phys.* **2018**, *21* (1), 1–13.
- (203) Neimark, A.; Ravikovitch, P.; Grün, M.; Schuth, F.; Unger, K. Pore Size Analysis of MCM-41 Type Adsorbents by Means of Nitrogen and Argon Adsorption. *J. Colloid Interface Sci.* **1998**, *207*, 159–169.
- (204) Reiss, H.; Frisch, H. L.; Lebowitz, J. L. Statistical Mechanics of Rigid Spheres. *J. Chem. Phys.* **1959**, *31* (2), 369–380.
- (205) Reiss, H.; Frisch, H. L.; Helfand, E.; Lebowitz, J. L. Aspects of the Statistical Thermodynamics of Real Fluids. *J. Chem. Phys.* **1960**, *32* (1), 119–124.
- (206) Kalyuzhnyi, Y. V.; Holovko, M.; Patsahan, T.; Cummings, P. T. Phase Behavior and Percolation Properties of the Patchy Colloidal Fluids in the Random Porous Media. *J. Phys. Chem. Lett.* **2014**, *5* (24), 4260–4264.
- (207) Mecke, K. R. A Morphological Model for Complex Fluids. *J. Phys. Condens. Matter* **1996**, *8* (47), 9663–9667.
- (208) Mecke, K. R. Morphological Thermodynamics of Composite Media. *Fluid Phase Equilib.* **1998**, *150–151*, 591–598.
- (209) König, P.-M.; Roth, R.; Mecke, K. R. Morphological Thermodynamics of Fluids: Shape Dependence of Free Energies. *Phys. Rev. Lett.* **2004**, *93* (16), 160601.
- (210) Mecke, K.; Arns, C. H. Fluids in Porous Media: A Morphometric Approach. *J. Phys. Condens. Matter* **2005**, *17* (9), S503–S534.
- (211) Klain, D. A. A Short Proof of Hadwiger’s Characterization Theorem. *Mathematika* **1995**, *42* (02), 329.
- (212) Chen, B. A Simplified Elementary Proof of Hadwiger’s Volume Theorem. *Geom. Dedicata* **2004**, *105* (1), 107–120.
- (213) Mecke, K. R.; Wagner, H. Euler Characteristic and Related Measures for Random Geometric Sets. *J. Stat. Phys.* **1991**, *64* (3–4), 843–850.
- (214) Likos, C. N.; Mecke, K. R.; Wagner, H. Statistical Morphology of Random

- Interfaces in Microemulsions. *J. Chem. Phys.* **1995**, *102* (23), 9350–9361.
- (215) Mecke, K. R. Bending Rigidity of Fluctuating Membranes. *Zeitschrift fur Phys. B Condens. Matter* **1995**, *97* (2), 379–387.
- (216) Roth, R.; Harano, Y.; Kinoshita, M. Morphometric Approach to the Solvation Free Energy of Complex Molecules. *Phys. Rev. Lett.* **2006**, *97* (7), 078101.
- (217) Bryk, P.; Roth, R.; Mecke, K. R.; Dietrich, S. Hard-Sphere Fluids in Contact with Curved Substrates. *Phys. Rev. E* **2003**, *68* (3), 031602.
- (218) Oettel, M.; Hansen-Goos, H.; Bryk, P.; Roth, R. Depletion Interaction of Two Spheres —Full Density Functional Theory vs. Morphometric Results. *EPL (Europhysics Lett.)* **2009**, *85* (3), 36003.
- (219) Jin, Z.; Kim, J.; Wu, J. Shape Effect on Nanoparticle Solvation: A Comparison of Morphometric Thermodynamics and Microscopic Theories. *Langmuir* **2012**, *28* (17), 6997–7006.
- (220) Reindl, A.; Bier, M.; Dietrich, S. Implications of Interface Conventions for Morphometric Thermodynamics. *Phys. Rev. E* **2015**, *91* (2), 022406.
- (221) Hansen-Goos, H. Communication: Non-Hadwiger Terms in Morphological Thermodynamics of Fluids. *J. Chem. Phys.* **2014**, *141* (17), 171101.
- (222) Blokhuis, E. M. Existence of a Bending Rigidity for a Hard-Sphere Liquid near a Curved Hard Wall: Validity of the Hadwiger Theorem. *Phys. Rev. E* **2013**, *87* (2), 022401.
- (223) Laird, B. B.; Hunter, A.; Davidchack, R. L. Interfacial Free Energy of a Hard-Sphere Fluid in Contact with Curved Hard Surfaces. *Phys. Rev. E* **2012**, *86* (6), 060602.
- (224) Urrutia, I. Bending Rigidity and Higher-Order Curvature Terms for the Hard-Sphere Fluid near a Curved Wall. *Phys. Rev. E* **2014**, *89* (3), 032122.
- (225) Liu, Y.; Zhao, S.; Liu, H.; Hu, Y. High-Throughput and Comprehensive Prediction of H₂ Adsorption in Metal-Organic Frameworks Under Various Conditions. **2015**, *61* (9), 2951–2957.

- (226) Allen, M. P.; Tildesley, D. J. *Computer Simulation of Liquids*; Oxford university press, 2017.
- (227) Hansen, J.-P.; McDonald, I. R. *Theory of Simple Liquids*; Elsevier, 1990.
- (228) Frenkel, D.; Smit, B. *Understanding Molecular Simulation: From Algorithms to Applications*; Elsevier, 2001; Vol. 1.
- (229) Turner, C. H.; Johnson, J. K.; Gubbins, K. E. Effect of Confinement on Chemical Reaction Equilibria: The Reactions $2\text{NO} \rightleftharpoons (\text{NO})_2$ and $\text{N}_2 + 3\text{H}_2 \rightleftharpoons 2\text{NH}_3$ in Carbon Micropores. *J. Chem. Phys.* **2001**, *114* (2001), 1851.
- (230) Turner, C. H.; Brennan, J. K.; Pikunic, J.; Gubbins, K. E. Simulation of Chemical Reaction Equilibria and Kinetics in Heterogeneous Carbon Micropores. *Appl. Surf. Sci.* **2002**, *196*, 366–374.
- (231) Santiso, E. E.; George, A. M.; Turner, C. H.; Kostov, M. K.; Gubbins, K. E.; Buongiorno-Nardelli, M.; Sliwinska-Bartkowiak, M. Adsorption and Catalysis: The Effect of Confinement on Chemical Reactions. *Appl. Surf. Sci.* **2005**, *252*, 766–777.
- (232) Santiso, E. E.; Kostov, M. K.; George, A. M.; Nardelli, M. B.; Gubbins, K. E. Confinement Effects on Chemical Reactions-Toward an Integrated Rational Catalyst Design. *Appl. Surf. Sci.* **2007**, *253*, 5570–5579.
- (233) Tolman, R. C. The Effect of Droplet Size on Surface Tension. *J. Chem. Phys.* **1949**, *17* (3), 333–337.
- (234) Hansen-Goos, H.; Roth, R.; Mecke, K.; Dietrich, S. Solvation of Proteins: Linking Thermodynamics to Geometry. *Phys. Rev. Lett.* **2007**, *99* (12), 128101.
- (235) Johnson, J. K.; Zollweg, J. A.; Gubbins, K. E. The Lennard-Jones Equation of State Revisited. *Mol. Phys.* **1993**, *78* (3), 591–618.
- (236) Gibbs, J. W. The Collected Works of JW Gibbs, Vol. 1. *Lonmans, Green, New York, NY* **1931**.
- (237) Rowlinson, J. S.; Widom, B. *Molecular Theory of Capillarity*, Oxford University Press. Chap 1982.

- (238) Hansen-Goos, H.; Mecke, K. Fundamental Measure Theory for Inhomogeneous Fluids of Nonspherical Hard Particles. *Phys. Rev. Lett.* **2009**, *102* (1), 018302.
- (239) Mittal, J.; Errington, J. R.; Truskett, T. M. Does Confining the Hard-Sphere Fluid between Hard Walls Change Its Average Properties? *J. Chem. Phys.* **2007**, *126* (24), 244708.
- (240) Mittal, J. Using Compressibility Factor as a Predictor of Confined Hard-Sphere Fluid Dynamics. *J. Phys. Chem. B* **2009**, *113* (42), 13800–13804.
- (241) Borah, B. J.; Maiti, P. K.; Chakravarty, C.; Yashonath, S. Transport in Nanoporous Zeolites: Relationships between Sorbate Size, Entropy, and Diffusivity. *J. Chem. Phys.* **2012**, *136* (17), 174510.
- (242) Ingebrigtsen, T. S.; Errington, J. R.; Truskett, T. M.; Dyre, J. C. Predicting How Nanoconfinement Changes the Relaxation Time of a Supercooled Liquid. *Phys. Rev. Lett.* **2013**, *111* (23), 235901.
- (243) Reiss, H.; Frisch, H. L.; Helfand, E.; Lebowitz, J. L. Aspects of the Statistical Thermodynamics of Real Fluids. *J. Chem. Phys.* **1960**, *32* (1), 119–124.
- (244) Holovko, M. F.; Shmotolokha, V. I.; Dong, W. Analytical Theory of One- and Two-Dimensional Hard Sphere Fluids in Random Porous Media. **2010**, *13* (2), 1–7.
- (245) Lebowitz, J. L.; Helfand, E.; Praestgaard, E. Scaled Particle Theory of Fluid Mixtures. *J. Chem. Phys.* **1965**, *43* (3), 774–779.
- (246) Siderius, D. W.; Corti, D. S. On the Use of Multiple Interpolation Functions in Scaled Particle Theory to Improve the Predictions of the Properties of the Hard-Sphere Fluid. *J. Chem. Phys.* **2007**, *127* (14), 144502.
- (247) Tully-Smith, D. M.; Reiss, H. Further Development of Scaled Particle Theory of Rigid Sphere Fluids. *J. Chem. Phys.* **2004**, *53* (10), 4015–4025.
- (248) Stillinger, F. H. Structure in Aqueous Solutions of Nonpolar Solutes from the Standpoint of Scaled-Particle Theory. In *The Physical Chemistry of Aqueous System*; Springer, 1973; pp 43–60.

- (249) Mandell, M. J.; Reiss, H. Scaled Particle Theory: Solution to the Complete Set of Scaled Particle Theory Conditions: Applications to Surface Structure and Dilute Mixtures. *J. Stat. Phys.* **1975**, *13* (2), 113–128.
- (250) Heying, M.; Corti, D. S. Scaled Particle Theory Revisited: New Conditions and Improved Predictions of the Properties of the Hard Sphere Fluid. *J. Phys. Chem. B* **2004**, *108* (51), 19756–19768.
- (251) Siderius, D. W.; Corti, D. S. Extension of Scaled Particle Theory to Inhomogeneous Hard Particle Fluids. I. Cavity Growth at a Hard Wall. *Phys. Rev. E* **2005**, *71* (3), 036141.
- (252) Stillinger, F. H.; Debenedetti, P. G.; Chatterjee, S. Scaled Particle Theory for Hard Sphere Pairs. I. Mathematical Structure. *J. Chem. Phys.* **2006**, *125* (20), 204504.
- (253) Chatterjee, S.; Debenedetti, P. G.; Stillinger, F. H. Scaled Particle Theory for Hard Sphere Pairs. II. Numerical Analysis. *J. Chem. Phys.* **2006**, *125* (20), 204505.
- (254) Ashbaugh, H. S.; Pratt, L. R. Colloquium: Scaled Particle Theory and the Length Scales of Hydrophobicity. *Rev. Mod. Phys.* **2006**, *78* (1), 159–178.
- (255) Carnahan, N. F.; Starling, K. E. Equation of State for Nonattracting Rigid Spheres. *J. Chem. Phys.* **1969**, *51* (2), 635–636.
- (256) Heying, M.; Corti, D. S. On the Use of Multiple Interpolation Series in Scaled Particle Theory: Improved Predictions and Limitations. *Mol. Phys.* **2014**, *112* (16), 2160–2175.
- (257) Buchert, T. Robust Morphological Measures for Large-Scale Structure. *Astron. Astrophys.* **1994**, *288*, 697–704.
- (258) Siderius, D. W.; Corti, D. S. Thermodynamically Consistent Adaptation of Scaled Particle Theory to an Arbitrary Hard-Sphere Equation of State. *Ind. Eng. Chem. Res.* **2006**, *45* (16), 5489–5500.
- (259) Hansen-Goos, H.; Roth, R. Density Functional Theory for Hard-Sphere Mixtures:

- The White Bear Version Mark II. *J. physics. Condens. matter* **2006**, *18* (37), 8413–8425.
- (260) Mansoori, G. a.; Carnahan, N. F.; Starling, K. E.; Leland, T. W. J. Equilibrium Thermodynamic Properties of the Mixture of Hard Spheres. *J. Chem. Phys.* **1971**, *54* (1971), 1523.
- (261) Scholz, C.; Wirner, F.; Gotz, J.; Rude, U.; Schroder-Turk, G. E.; Mecke, K.; Bechinger, C. Permeability of Porous Materials Determined from the Euler Characteristic. *Phys. Rev. Lett.* **2012**, *109* (26), 264504.
- (262) Morita, T.; Hiroike, K. A New Approach to the Theory of Classical Fluids. I. *Prog. Theor. Phys.* **1960**, *23* (6), 1003–1027.
- (263) Morita, T.; Hiroike, K. A New Approach to the Theory of Classical Fluids. II. *Prog. Theor. Phys.* **1960**, *24* (2), 317–330.
- (264) Morita, T.; Hiroike, K. A New Approach to the Theory of Classical Fluids. III. *Prog. Theor. Phys.* **1961**, *25* (4), 537–578.
- (265) Hansen, J.-P.; McDonald, I. R. *Theory of Simple Liquids: With Applications to Soft Matter*; Academic Press, 2013.
- (266) Dullien, F. A. L.; Shemilt, L. W. Activity-Based Diffusion Coefficients for Liquid Solutions. *Nature* **1961**, *190* (4775), 526.
- (267) Kärger, J.; Ruthven, D. M. *Diffusion in Zeolites and Other Microporous Solids* John Wiley & Sons. Inc., USA, New York **1992**.
- (268) Reiss, H.; Frisch, H. L.; Lebowitz, J. L. Statistical Mechanics of Rigid Spheres. *J. Chem. Phys.* **1959**, *31* (2), 369–380.